Nonlinear Optics

Manfred Wöhlecke **Klaus Betzler** **Mirco Imlau**

University of Osnabrück

Summer Term 2003, rev. 2005

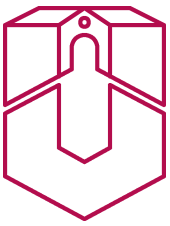

"Physics would be dull and life most unfulfilling if all physical phenomena around us were linear. Fortunately, we are living in a nonlinear world. While linearization beautifies physics, nonlinearity provides excitement in physics."

Y. R. Shen in *The Principles of Nonlinear Optics*

apl. Prof. Dr. Manfred Wöhlecke
http://www.physik.uni-osnabrueck.de/optmat
mailto:Manfred.Woehlecke@uos.de

apl. Prof. Dr. Klaus Betzler
http://www.physik.uni-osnabrueck.de/kbetzler
mailto:Klaus.Betzler@uos.de

Jun.-Prof. Dr. Mirco Imlau
http://www.physik.uni-osnabrueck.de/photonik
mailto:Mirco.Imlau@uos.de

Fachbereich Physik
Universität Osnabrück
Barbarastraße 7
49074 Osnabrück

http://www.physik.uni-osnabrueck.de

Contents

1 Introduction

Linearity is one of the basics of classical optics. Light waves usually do *not* interact. In other fields of electricity and magnetism, yet, *nonlinearities* are known since scientists have begun to study the phenomena in more detail. Saturation effects at high (static) electric or magnetic fields and nonlinear electrical characteristics of devices like vacuum tubes, semiconductor diodes, and even resistors are quite familiar examples. In the field of optics, however, nonlinear effects became a subject of interest only after the invention of the laser.

To measure the *nonlinear* response of matter to electromagnetic waves in the optical region, in general high fields are necessary, starting at about 1 kV/cm. The corresponding light intensities of some kW/cm^2 necessitate laser beams. As laser physics started with the ruby laser with its high pulse intensities, it took only few years after the invention of the laser [1] that many classical experiments in nonlinear optics were successfully performed. Among the first were the second order processes like the experiments on second harmonic generation by Franken et al. [2] in 1961, on sum frequency generation by Bass et al. [3] in 1962, and on optical rectification by Bass et al. [4] in 1962.

Since that time *Nonlinear Optics* has become a rapidly growing field in physics. Nonlinearities are found everywhere in optical applications. Presently, many optical materials are of special interest in information technologies, *photonics* as supplement and extension of *electronics* plays a steadily increasing role. Nonlinearities in the properties of these optical materials are often of significant relevance for the technological application – sometimes useful, sometimes hampering. To understand these nonlinearities – and to use them for new effects – will be of basic importance for the further development of photonic applications.

These lecture notes cover some basic topics in nonlinear optics, they accompany lectures held for the Ph. D. students in the graduate college *Nonlinearities of Optical Materials*.

The first part gives a short introduction to the physics of crystals and the treatment of symmetry-dependent properties. Then the nonlinear susceptibility is shortly discussed followed by a section about harmonic generation with an emphasis put on second-order and high-order processes. Thereafter various techniques for the measurement of nonlinear optical properties of crystals are described. A subsequent chapter deals with non-collinear harmonic generation processes and some of their applications.

References

[1] T. H. Maiman. *Stimulated Optical Radiation in Ruby*. Nature **187**, 493–494 (1960).

[2] P. A. Franken, A. E. Hill, C. W. Peters, G. Weinreich. *Generation of Optical Harmonics*. Phys. Rev. Lett. **7**, 118 (1961).

[3] M. Bass, P. A. Franken, A. E. Hill, C. W. Peters, G. Weinreich. *Optical Mixing*. Phys. Rev. Lett. **8**, 18 (1962).

[4] M. Bass, P. A. Franken, J. F. Ward, G. Weinreich. *Optical Rectification*. Phys. Rev. Lett. **9**, 446 (1962).

2 Tools to describe crystals

2.1 Two cubic crystals

Usually an introduction to point and space groups starts with a definition of symmetry elements and a lattice. We will begin with an inspection of two cubic crystals (see Figure 1) and ask the following question:

How can we describe the crystal structure in a simple and elegant way?

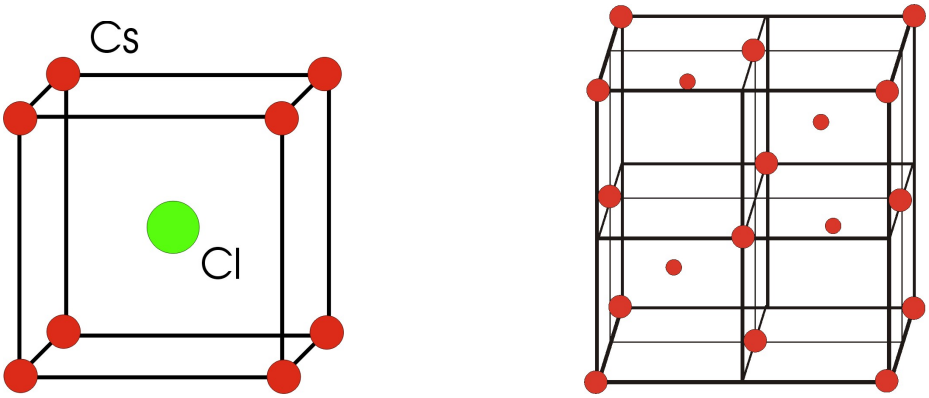

Figure 1: Crystal structure of CsCl (left), structure of diamond (right)

The CsCl crystal looks quite simple, eight Cs ions are at the corners and one Cl in the cube center. Diamond looks much more complicate and we hope that we do not have to write down the coordinates of ions in all these many positions. One solution would be to generate with some operator all ions in similar positions, simply by applying a translational operation. But what means similar position? In CsCl we may regard the Cs ions as being in a similar position. If we extend this to the Cl ions, then we have a procedure to describe the crystal. But this idea immediately fails or becomes very complicate in crystals like diamond, where we need four or five such sets of similar positions depending on the translational operations allowed. A much more clever approach uses a lattice and some basic pattern, often called the basis and sometimes motif. A lattice is related to our sets of similar positions, but not identical.

A **lattice** is a collection of mathematical points arranged in such a way that each lattice point has the same environment in the same orientation.

If we apply this idea to CsCl , we see that the centered Cl ion is not qualified as a lattice point, because a movement to the right brings us sooner or later to another Cl ion, but if we do the same starting from a Cs ion we meet another Cs, thus we have no equal environment moving in the same direction. Similar violations are faced with diamond. Here are some warnings:

(a) There are no constraints that ions have to be placed on lattice points!

(b) Ions may occupy positions which are not lattice points!

With respect to the warnings (a) and (b) we may collect some ions and regard them as belonging to *one* lattice point. Let us consider the Cs plus the Cl ion as one unit and regard them as a basis. Then the lattice points coincide with the positions of the Cs ions. With this choice everything looks fine, but what about the diamond? If we think of the same kind of lattice, fixed to one C ion in a cube corner, the basis grows up and consists of one C in the origin, three C in the center of the cube faces (squares) and four C in the octants. This looks quite complicate. An easier description is obtained if we construct a lattice with lattice points in the corner of the cube and the center of the faces. Then our basis reduces to C in the origin and one C in the octant at a position $(\frac{1}{4}, \frac{1}{4}, \frac{1}{4})$.

This finding can be generalized as follows:

A crystal structure is made up of a lattice and a basis.

To get an idea how many lattices exist in 3 dimensions we derive first the crystal systems and then the 14 Bravais lattices. For the first step we need the symmetry operations leaving one point fixed.

2.2 Point symmetry operations

A point-symmetry operation is a symmetry operation that keeps one point in space fixed. A set of such operations may form a group. For a mathematical description we take three vectors, $\mathbf{a}$, $\mathbf{b}$, and $\mathbf{c}$, measured from a common origin, in such a way that $\mathbf{a}$ and $\mathbf{b}$ are not collinear and $\mathbf{c}$ is not coplanar with the ab-plane. These three vectors act as axes of reference and need not be orthogonal. There are basically two ways of describing the effect of symmetry operations with an operator R. We can set up a symmetry operator which moves all points or position vectors of space with all vectors referred to a set of fixed axes. Alternatively, the symmetry operator can be made to move the axes of reference leaving all points in space, and hence position vectors, unmoved. The former type of operator is called an active operator R_{active}, and the latter, which is its inverse, is called a passive operator $R_{passive}$. We shall use only active operators here. The two conventions are linked by $R_{active} = R^{-1}_{passive}$, but do not forget the change of the multiplication order. In active mode we have $R_{active} \times T_{active} = S_{active}$ but in passive mode the order is reversed $T_{passive} \times R_{passive} = S_{passive}$.

Under a point-symmetry operation R a point P with position vector $\mathbf{r}$ will be moved to a point P' with position vector $\mathbf{r}'$ governed by an equation of the form

$$\mathbf{r}' = \mathbf{R}\,\mathbf{r} \quad \text{or} \quad \begin{pmatrix} x' \\ y' \\ z' \end{pmatrix} = \begin{pmatrix} r_{11} & r_{12} & r_{13} \\ r_{21} & r_{22} & r_{23} \\ r_{31} & r_{32} & r_{33} \end{pmatrix} \begin{pmatrix} x \\ y \\ z \end{pmatrix} \tag{2.1}$$

An alternative is the scheme x'_i and x_i with $(i = 1, 2, 3)$

$$\begin{pmatrix} x'_1 \\ x'_2 \\ x'_3 \end{pmatrix} = \begin{pmatrix} r_{11} & r_{12} & r_{13} \\ r_{21} & r_{22} & r_{23} \\ r_{31} & r_{32} & r_{33} \end{pmatrix} \begin{pmatrix} x_1 \\ x_2 \\ x_3 \end{pmatrix} \quad \text{or} \quad x'_i = \sum_{j=1}^{3} r_{ij} x_j \quad \text{or} \quad x'_i = r_{ij} x_j \tag{2.2}$$

and the Einstein convention of calculating the sum if a suffix occurs twice.

Besides the identity, that means do nothing with the object, there are two important point-symmetry operations, the inversion and the rotation. There are two types of notations for point-symmetry operations, the International System (preferred by crystallographers) and the Schönflies System (often used in Solid State Physics).

point-symmetry element	*International notation*	*Schönflies notation*	
identity	1	E	
inversion	$\bar{1}$	i	
rotation	$n[uvw]$	$C_n[uvw]$	
mirror reflection	m	σ	
		σ_h:	mirror reflection in the horizontal plane
		σ_v:	mirror reflection in the vertical plane
		σ_d:	mirror reflection in the vertical diagonal plane
rotation inversion	$\bar{n}$	S_n	

Table 1: Types of point-symmetry elements and the different notations

In Table 1 several entries have to be explained. We start with the elements n or $C_n[uvw]$ which describe a rotation by an amount $2\pi/n$, where n is called the order of the rotation, which is performed according to the counter-clockwise convention. In crystals we have only $n = 1, 2, 3, 4, 6$.

This rotation is often called a pure or proper rotation. Since rotations are taken about certain rotation axes we have to specify these axes. There is no generally accepted way of doing this, often the axis is described by a vector with components u, v, and w with respect to $\mathbf{a}$, $\mathbf{b}$, and $\mathbf{c}$. Usually crystallographers write brackets $[uvw]$, because parentheses are reserved for planes. We

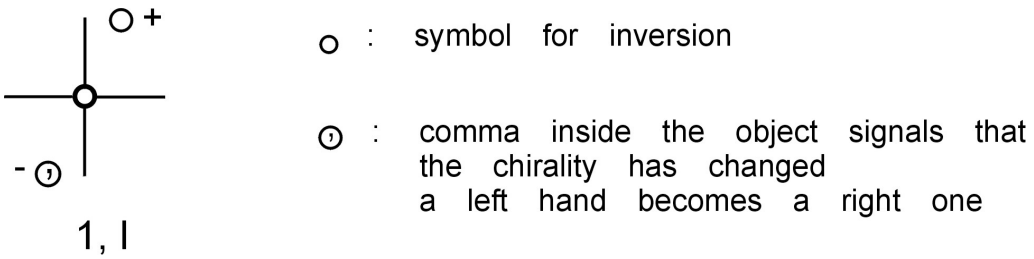

Figure 2: Inversion operation

point out a convention about the sequence of two operations: if two operations A B are applied to an object, the operation on the right B is considered to be applied first and A second. Finally we

emphasize that the inversion (inversion through a center) changes right hands to left hands and we illustrate this in Figure 2.

All the operations below the horizontal line in Table 1 consist of a rotation $n\,(C_n)$ followed by an inversion $\bar{1}\,(i)$ that means $\bar{1}\,n$ with the short-hand notation $\bar{n}$ and the special case $\bar{1}\,2 = \bar{2} = m\,(\sigma)$. The operations are called improper rotations . What about the notation of these point-symmetry elements in the Schönflies scheme? Its name is S_n, but we have to be very careful, because of the following property $\bar{n} \neq S_n$. The reason for this difference is the different approach in the two systems. As explained above the International System starts with a rotation followed by an inversion. The Schönflies system starts with a rotation, too, but then a horizontal mirror operation σ_h follows. Since $\sigma_h = i\,C_2$ we have $S_n = iC_2C_n = \bar{1}2n$ with one more 2-rotation than in the International System. For an illustration we use Figure 3

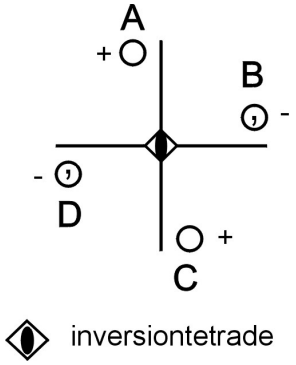

Figure 3: Illustration of the operation $\bar{4}$ and S_4. Multiple applications of $\bar{4}$ yields:
$A \overset{\bar{4}}{\Longrightarrow} B \overset{\bar{4}}{\Longrightarrow} C \overset{\bar{4}}{\Longrightarrow} D \overset{\bar{4}}{\Longrightarrow} A$
in analogy we find for S_4:
$A \overset{S_4}{\Longrightarrow} D \overset{S_4}{\Longrightarrow} C \overset{S_4}{\Longrightarrow} B \overset{S_4}{\Longrightarrow} A$

2.3 Crystal systems

Because of its translational invariance a lattice is generated by applying primitive translations T_n to an object. A primitive translation vector $\mathbf{t_n}$ is described by

$$\mathbf{t_n} = \mathbf{n_1 a} + \mathbf{n_2 b} + \mathbf{n_3 c} \tag{2.3}$$

where n_i is an integer and the vectors are those defined in section 2.2. If we construct a parallelepiped with the vectors $\mathbf{a}$, $\mathbf{b}$, and $\mathbf{c}$ according to $\mathbf{a} \cdot (\mathbf{b} \times \mathbf{c})$, the space is completely filled by translations $\mathbf{t}_n$ applied to this object. Such a volume $\mathbf{a} \cdot (\mathbf{b} \times \mathbf{c})$ is called a unit cell. If it only contains *one* lattice point, it is called a primitive unit cell. What means this last definition? If the origin of a unit cell is chosen on a lattice point, then there are eight lattice points involved (one at each corner). However, because each lattice point belongs to eight parallelepipeds, in one primitive cell there is only $8 \times \frac{1}{8} = 1$ lattice point. The message is even more obvious, if we do not put the origin in a lattice point. Thus the origin can arbitrarily be chosen anywhere and we add that all primitive unit cells have the same volume. For an illustration see Figure 4

With the demand that the lattice is invariant with respect to the translations *and* point-symmetry operations, relations hold between the vectors $\mathbf{a}$, $\mathbf{b}$, and $\mathbf{c}$ and the angles $\alpha(\mathbf{b}, \mathbf{c})$, $\beta(\mathbf{c}, \mathbf{a})$, $\gamma(\mathbf{a}, \mathbf{b})$ between them. The general procedure for deriving the relations is quite simple. One starts with

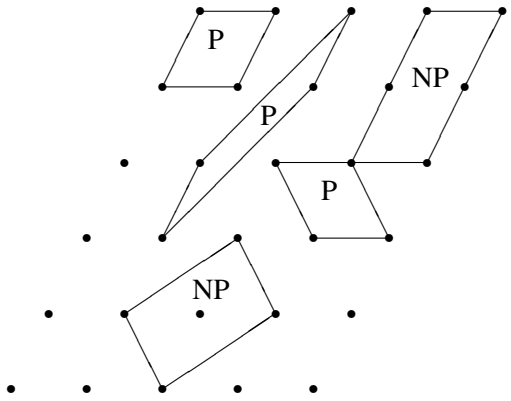

Figure 4: Examples for primitive and non-primitive unit cells

the most simple point-symmetry operations 1 and $\bar{1}$ and applies this to the vectors $\mathbf{a}$, $\mathbf{b}$, and $\mathbf{c}$ of a unit cell. We take the appropriate matrices from Appendix A and obtain the equations

$$\mathbf{r}' = \{1\}\mathbf{r} = \begin{pmatrix} 1 & 0 & 0 \\ 0 & 1 & 0 \\ 0 & 0 & 1 \end{pmatrix} \mathbf{r} = x'\mathbf{a} + y'\mathbf{b} + z'\mathbf{c} = x\mathbf{a} + y\mathbf{b} + z\mathbf{c} \tag{2.4}$$

$$\mathbf{r}' = \{\bar{1}\}\mathbf{r} = \begin{pmatrix} -1 & 0 & 0 \\ 0 & -1 & 0 \\ 0 & 0 & -1 \end{pmatrix} \mathbf{r} = -x'\mathbf{a} - y'\mathbf{b} - z'\mathbf{c} = -x\mathbf{a} - y\mathbf{b} - z\mathbf{c} \tag{2.5}$$

In both cases the coordinates x, y, z are attached to the same axes as before the symmetry operation. Thus no restrictions are put on the unit cell shape, we call this system triclinic , the relations can be read from Table 2.

In a next step we derive the relations for the monoclinic system. We add a rotation $2(C_2)$ and / or a mirror operation $\mathrm{m}(\sigma)$. In solid state physics the first setting is preferred ($2 \parallel \mathbf{c}$), while in crystallography $2 \parallel \mathbf{b}$ (second setting) is used. Let us rotate a point inside the unit cell with coordinates x, y, z by

$$\mathbf{r}\,' = \mathbf{2}[\mathbf{001}]\mathbf{r} = -\mathbf{x}\mathbf{a} - \mathbf{y}\mathbf{b} + \mathbf{z}\mathbf{c}.$$

The brackets after the 2 describes the orientation of the rotation axis. With $\mathbf{r}$ we obtain for the scalar product $xz\mathbf{a} \cdot \mathbf{c}$, while $\mathbf{r}\,'$ yields $-xz\mathbf{a} \cdot \mathbf{c}$. Because 2 is a symmetry operation, we have

$$xz|\mathbf{a}||\mathbf{c}| \cos\beta = -\mathbf{xz}|\mathbf{a}||\mathbf{c}| \cos\beta \quad \text{with} \quad \cos\beta = -\cos\beta \quad \text{and} \quad \beta = \mathbf{90}^\circ$$

which means $\mathbf{a} \perp \mathbf{c}$. In the same manner we find $\mathbf{b} \perp \mathbf{c}$. Thus the triclinic system requires

$$a \neq b \neq c, \alpha = \beta = 90^\circ \qquad \gamma \neq 90^\circ.$$

Often for the unit cell $\gamma > 90^\circ$ is taken, but this is simply a convention.

Next we add two more twofold rotations or mirror planes and apply them to $\mathbf{r}$

$$2[100]\mathbf{r} = x\mathbf{a} - \mathbf{y}\mathbf{b} - \mathbf{z}\mathbf{c} \tag{2.6}$$

$$2[010]\mathbf{r} = -x\mathbf{a} + \mathbf{y}\mathbf{b} - \mathbf{z}\mathbf{c} \tag{2.7}$$

$$2[001]\mathbf{r} = -x\mathbf{a} - \mathbf{y}\mathbf{b} + \mathbf{z}\mathbf{c} \tag{2.8}$$

With similar arguments as in the monoclinic system we deduce from equations (2.6 - 2.8) the relations for the orthorhombic system

$$\mathbf{a} \perp \mathbf{b} \quad \text{und} \quad \mathbf{a} \perp \mathbf{c} \quad \text{from (2.6)} \quad \mathbf{b} \perp \mathbf{a} \quad \text{and} \quad \mathbf{b} \perp \mathbf{c} \quad \text{from (2.7)}$$

Since no operation interchanges the components with respect to $\mathbf{a},\ \mathbf{b},\ \mathbf{c}$, we yield again for the unit vectors

$$a \neq b \neq c \quad \text{and} \quad \alpha = \beta = \gamma = 90^\circ \quad \text{because of (2.8)}$$

.

To derive the conditions for the tetragonal system one allows besides the identity or inversion the operations 4 or $\bar{4}$.

$$\mathbf{r}' = \{4\,[001]\}\mathbf{r} = -y\mathbf{a} + x\mathbf{b} + z\mathbf{c} \tag{2.9}$$

$$\mathbf{r}' = \{4^3\,[001]\}\mathbf{r} = y\mathbf{a} - x\mathbf{b} + z\mathbf{c} \tag{2.10}$$

Again, the opposite signs show that all axes are mutually perpendicular and x interchanges with y, thus $a = b$.

The hexagonal system will be skipped because of special problems, the reader should consult chapter 2 in the book of Burns and Glazer [1], where the following discussion of the cubic system is taken from. This crystal system is familiar to solid state physicists and chemists, and it is the system with the highest symmetry. However, despite its familiarity we need to be careful about how we define it; it is not sufficient to use the criterion that all axes are equal and all angles 90°. As we continue to emphasize, the symmetry is the important thing in determining the crystal system. The *symmetry* conditions our choice of axes, not the other way round. What, then, are the important symmetry elements in the cubic system? Surprisingly perhaps, they are not the three mutually perpendicular 4-fold axes so readily observed in a cube, but rather, the four 3-fold axes corresponding to the body-diagonals, $\langle 111 \rangle$, of the cubic unit cell. (Note that angular brackets signify the set of symmetry-equivalent directions. In this case $\langle 111 \rangle$ means the set $[111], [\bar{1}\bar{1}\bar{1}], [\bar{1}11], [1\bar{1}\bar{1}], [\bar{1}\bar{1}1], [11\bar{1}], [\bar{1}1\bar{1}]$, and $[1\bar{1}1]$.) It is possible to have a cubic crystal without any 4-fold axes of symmetry. It is also possible to prove either by group theory or by spherical trigonometry that if a crystal contains more than one 3-fold axis, then it must contain four altogether, each one making an angle of $109°28'$ with any other. The equal length of all axes follows from the fact that a $\{3\,[111]\}$ operation interchanges all axes.

2.4 The 14 Bravais Lattices

The seven crystal systems of Table 2 define six different parallelepipeds, because the conditions for the trigonal and the rhombohedral system are equal. These lattices are called **P-Lattices**, because they are based on primitive unit cells. But as we will see, there are more possibilities to fill the whole space by translational operations of some unit. To do this, one has to allow centering of a cell. Centering means that we put a lattice point somewhere into a cell or on one or more of its surfaces. After doing this we have to ask:

1 or $\bar{1}$	triclinic	$a \neq b \neq c$ $\alpha \neq \beta \neq \gamma$
2 or $\bar{2}$	monoclinic	$a \neq b \neq c$ $\alpha = \beta = 90^\circ \neq \gamma$ (1st setting) $\alpha = \gamma = 90^\circ \neq \beta$ (2nd setting)
two 2 or $\bar{2}$	orthorhombic	$a \neq b \neq c$ $\alpha = \beta = \gamma = 90^\circ$
4 or $\bar{4}$	tetragonal	$a = b \neq c$ $\alpha = \beta = \gamma = 90^\circ$
four 3 or $\bar{3}$	cubic	$a = b = c$ $\alpha = \beta = \gamma = 90^\circ$
6 or $\bar{6}$	hexagonal	$a = b \neq c$ $\alpha = \beta = 90^\circ;\ \gamma = 120^\circ$
3 or $\bar{3}$	trigonal	$a = b \neq c$ $\alpha = \beta = 90^\circ;\ \gamma = 120^\circ$
	(rhombohedral)	$a = b = c;\ \alpha = \beta = \gamma \neq 90^\circ$

Table 2: The seven crystal systems. The first column contains the generating point-symmetry operations. The last one gives the relations for the lengths of the axes and the angles.

a) Is this new arrangement of points really a lattice?
b) Have we produced a new lattice?

As a result of centering eight new lattices with new names show up.

I: body centering
F: face centering
A,B,C: one-face centering (base centering).

Of course, the corresponding centered parallelepipeds are not unit cells, but they have the advantage that they have the symmetry of the underlying P-cell and thus the same axes can be used.

Later we will see, that even for I, F, A, B, C cells primitive unit cells are possible, but with the disadvantage that they do not display the point symmetry.

Again we follow the book by Burns and Glazer [1] and discuss the idea of centering in some selected crystal systems.

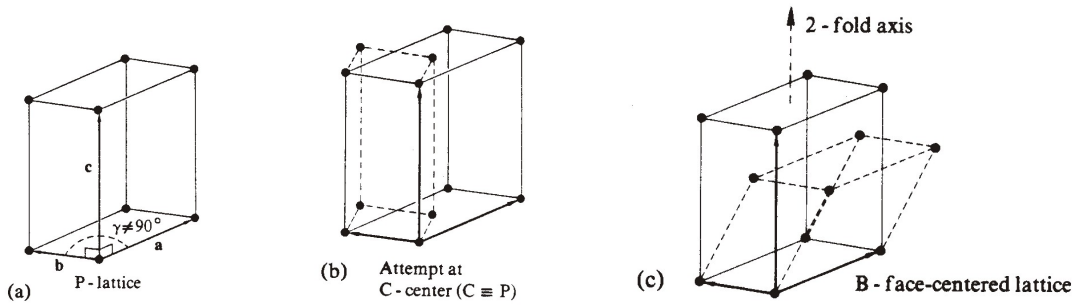

Figure 5: Different aspects of centering a monoclinic lattice. Taken from [1]

Figure 5 shows several trials for centering a monoclinic lattice. We put the 2-axis along **c** and from part (b) of this figure we conclude that a centering of the C-face (**a**, **b**-plane) does not produce a new lattice. If we introduce a new **a** and γ according to the dashed cell, we obtain again a primitive cell of the monoclinic system. But centering a B-face (**a**, **c**-plane) results in a *new* lattice. The dashed parallelepiped in part (c) does not fulfill the conditions (length and angle) for a monoclinic lattice, that means we have *no* primitive monoclinic lattice. A B-lattice occurred with unit cell vectors (bold arrows) as shown in part (c) of Figure 5. In the same manner an A-lattice can be formed, but the B-lattice is preferred. Our next example deals with the tetragonal system. The

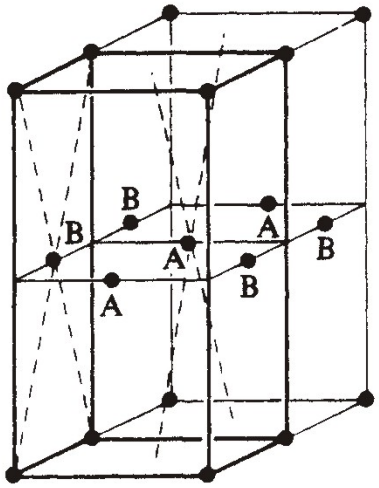

Figure 6: Centering of two independent faces can never form a lattice, since the environment of all points (as indicated, for example, by the dashed lines) is not the same no matter how one picks the translation vectors. Taken from [1].

existence of a fourfold axis requires a centering of both A- and B-planes, but as explained in the caption of Figure 6 this does not form a lattice, where each point has the same environment.

Next we try a centering of the C-face. An inspection of the left part of Figure 7 shows that we have produced a P-lattice, which is rotated by $45°$. With a body centering we have more luck and really obtain a new lattice, where each point has the same environment, see Figure 7 right side. A face centering is possible in the tetragonal system, too, but it turned out, that such a centering can be described by a rotated body-centered cell, see right part of Figure 7.

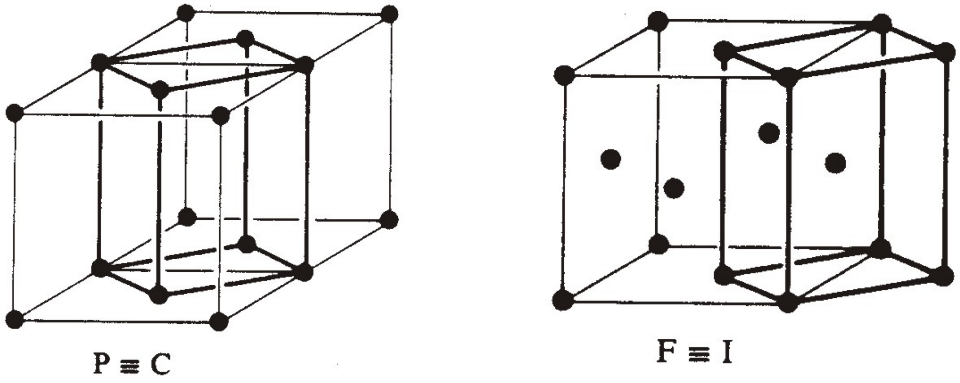

Figure 7: Trials of centering a tetragonal lattice

The remaining Bravais lattices are shown together with those just discussed in Figure 8. Again we skip the details of hexagonal and trigonal lattices, a detailed discussion is given in the book by Burns and Glazer [1]. For the cubic system often I-lattices are called bbc = body-centered cubic, while F-lattices are denoted by fcc = face-centered cubic.

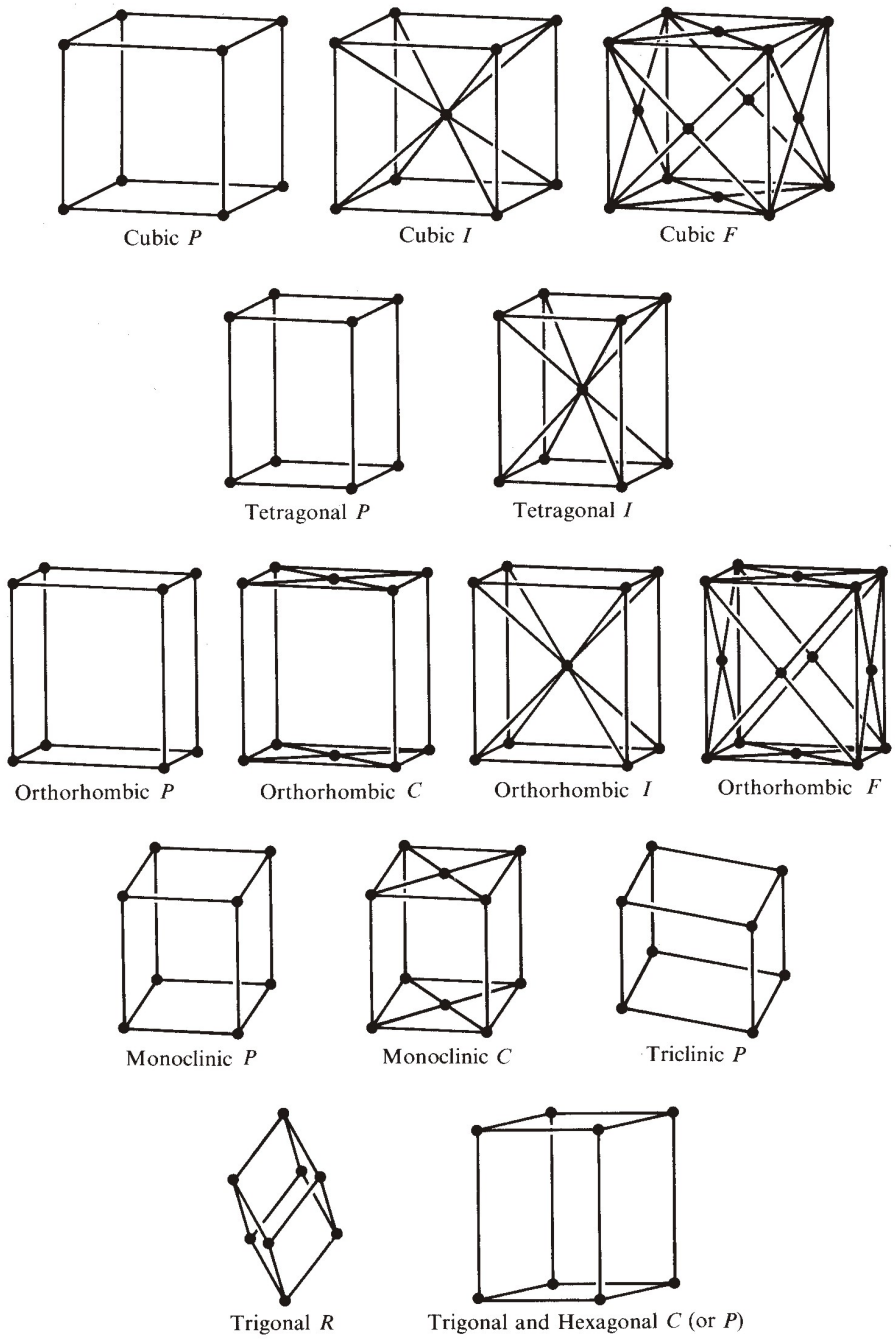

Figure 8: All 14 Bravais lattices, taken from [2].

Primitive unit cells of the Bravais lattices are discussed now. Such cells are of importance for calculations of electronic energy bands or the dispersion of lattice vibrations. The typical primitive unit cells for I, F, and C-lattices are shown in Figure 9.

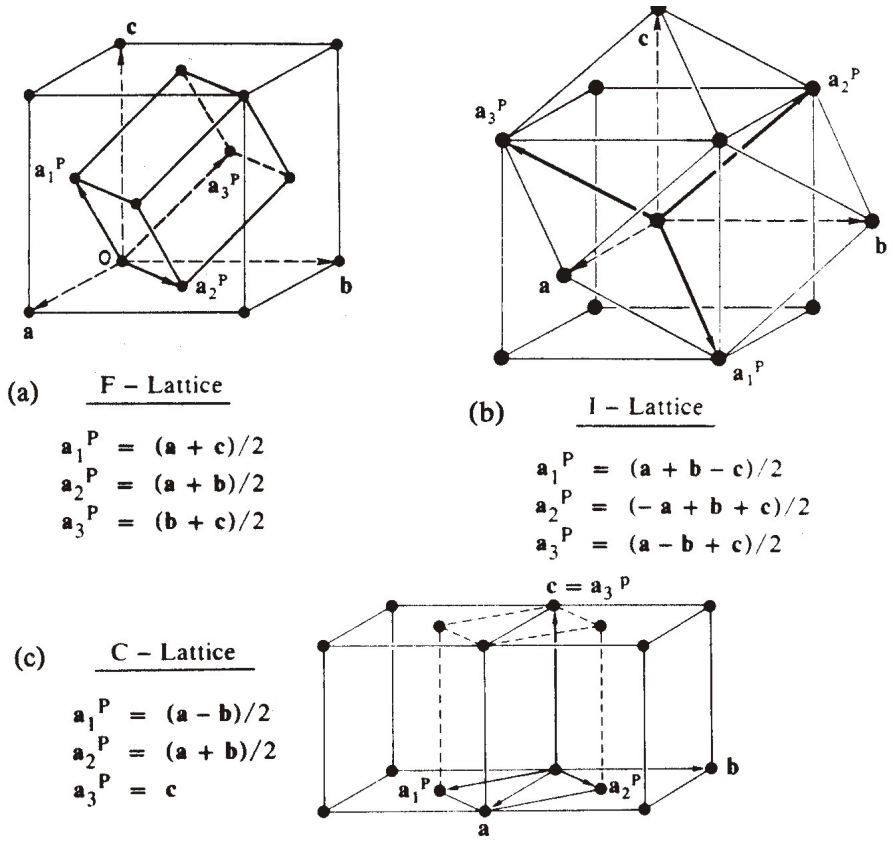

Figure 9: The conventional primitive unit cells for I, F, and C-lattices, taken from [1].

We proceed now with some general remarks on Wigner-Seitz unit cells, taken from Burns and Glazer [1]. Occasionally some special unit cell is chosen to emphasize certain special aspects of the crystal structure. For example, there might be a change of structure at some temperature (a phase transition) from a very simple high-temperature structure to a much more complicated low-temperature structure. The unit cell chosen in the simple structure could be relatively complicated (contain many lattice points centered at various positions), but might be picked to show how the low-temperature structure follows in a natural way from the high-temperature structure. Thus, the orientation of the axes in the high-temperature structure might be chosen so that the same orientation of axes above and below the phase transition is maintained. This choice would make visualization of the phase transition easy, although it may make the choice of the unit cell in the high-temperature structure unusual.

Besides this type of special choice of unit cell there is another primitive unit cell of more general use, particularly in electronic band theory. This is known as the Wigner-Seitz cell . This cell is

obtained by starting at any lattice point, called the origin, and drawing vectors to all neighboring lattice points. Planes are then constructed perpendicular to and passing through the midpoints of these vectors. The Wigner-Seitz cell is the smallest-volume cell about the origin bounded by these planes.

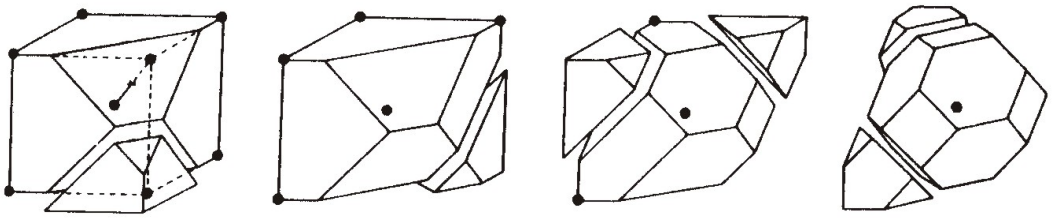

Figure 10: Some steps of constructing the Wigner-Seitz cell of a cubic I-lattice. The lattice points of the origin and the next nearest ones are shown.

Figure 10 shows a step-by-step construction of the Wigner-Seitz cell for a body-centered cubic (I-cubic) lattice. Note that the Wigner-Seitz cell contains just one lattice point and displays the full rotational symmetry of the crystal system as do the conventional unit cells of the 14 Bravais lattices (Fig. 8). Of course, the Wigner-Seitz cell does not form a parallelepiped but it is, nevertheless, a perfectly acceptable unit cell. Figures 11 (a) and (b) show the Wigner-Seitz cells for I- and F-

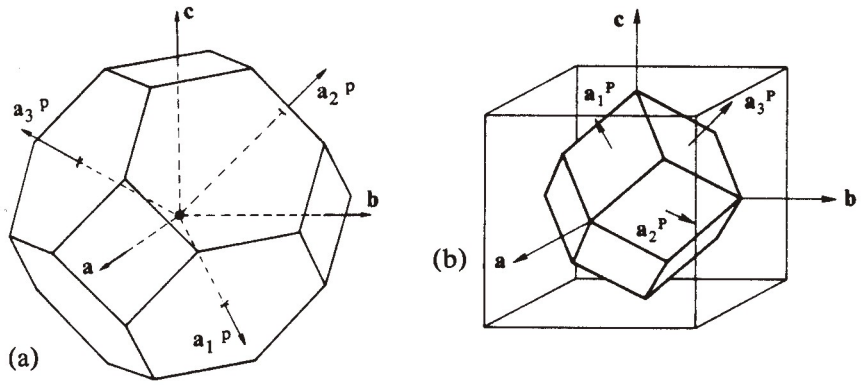

Figure 11: Wigner-Seitz cells of the cubic I- and F-lattices, taken from [1].

cubic lattices, where the full cubic symmetry is again obvious. The Wigner-Seitz cell construction is often used in reciprocal space, or k-space, where the resulting cell is given the name, the first Brillouin zone. Furthermore, to those readers who are familiar with Brillouin zones we remind them that an I-cubic lattice in space (direct space) has a reciprocal lattice that is an F-cubic lattice. Thus, the first Brillouin zone of an I-cubic lattice looks like the Wigner-Seitz cell a direct space F-cubic lattice and vice versa.

The Wigner-Seitz cell has been the last topic in our discussion of the lattices. Although there are still many details missing the present knowledge should be sufficient to understand the description of crystals.

2.5 Point groups and lattices

On page 3 we have learnt that a crystal is composed of a lattice and the basis. The symmetry induced properties of the lattice have been treated in the previous two sections. Now we investigate the influence of the symmetry on the basis. The same is meant, when we ask for point groups compatible with a given lattice.

To answer this question we give first a short derivation of the 32 point groups allowed in crystals. In principal there is no need to use group theoretical concepts for such a derivation, but first there is an intimate connection between these point groups and mathematical groups, and second the application of group theoretical methods allow a much deeper insight into the structure of point groups. The details of mathematical groups are considered in appendix B.

2.5.1 Notations of point groups

Schönflies Notation Like for point group symmetry elements, the notations are different for the groups, too.

C_n:	cyclic groups, $n = 1, 2, 3, 4, 6$
C_i:	group composed of inversion and identity
D_n:	C_n plus a two-fold rotation axis perpendicular to the main one
C_{nh}:	C_n enlarged by σ_h
D_{nh}:	D_n enlarged by σ_h
C_{nv}:	C_n enlarged by σ_v
D_{nd}:	D_n enlarged by σ_d
S_n:	n-fold rotary reflection n = 2,4,6
T, T_h, T_d, O, O_h:	cubic groups

Table 3: Schönflies notation for point groups

International Notation If we omit the cubic groups, three basic types of the labelling scheme are apparent.

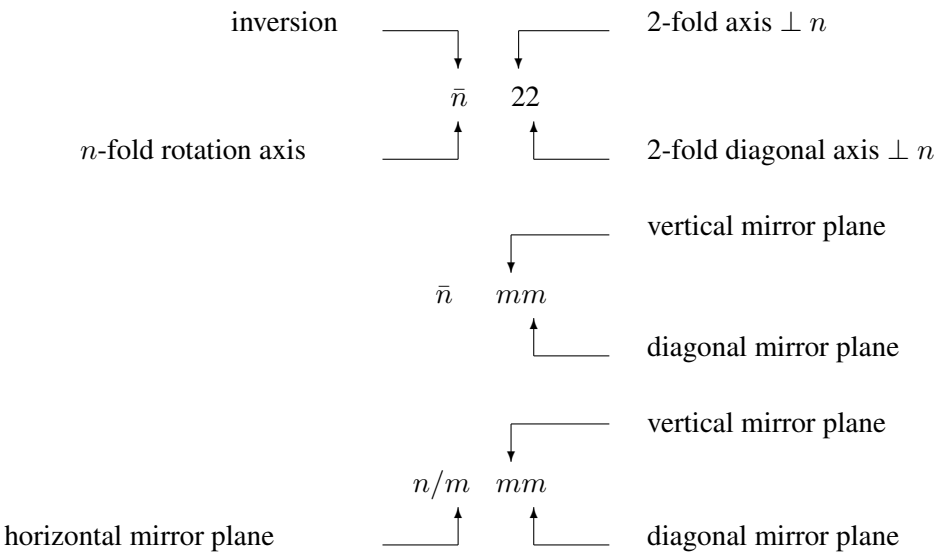

2.5.2 Cyclic point groups

Cyclic groups occur when there is only one axis of rotation. Because of n= 1,2,3,4,6 we obtain five groups, which are called according to their generators n; C_n. Do not be confused that here the labels stay for both the symmetry elements and the group.

2.5.3 Dihedral groups

We add now 2-fold rotation axes (to keep the principal axis) perpendicular to the principal axis. The direct product of $C_2 = \{E, C_2[100]\}$ and C_n = $\{E, C_n[001], ...\}$ yields the groups D_n

$$C_n \times \{E, C_2[100]\} = D_n.$$

Since C_2 contains two elements the order of D_n is twice of that of the cyclic subgroups C_n. We obtain four new groups (not five, because $C_1 \equiv$ E and $C_1 \times C_2 = C_2$ is already known).

Int. Not.:	1 2 3 4 6	222 32 422 622
	cyclic groups	dihedral groups
Schönflies Not.:	C_1 C_2 C_3 C_4 C_6	D_2 D_3 D_4 D_6

2.5.4 Cubic groups

A cubic group does not necessarily has a 4-fold axis as already discussed. Two symmetry elements are sufficient, a 3-fold rotation about a space diagonal and a 2-fold rotation. The products of these two generators produce altogether 12 rotations and we call the group 23 (T); please note: 23 (T) $\neq$ 32 (D_3).

Adding 4-fold axes to 23 (T) yields the group 432 (O). Besides $4, 4^3$ about [100], [010], and [001], six more twofold axes along $\langle 110 \rangle$ directions show up. The group order of 432 (O) is 24. All groups derived sofar consist of pure rotations and we have found altogether 11 of them.

2.5.5 Centrosymmetric groups

Eleven more groups are generated by the direct product with $\bar{1} = \{1, \bar{1}\} = \{E, I\}$. The order of these groups is twice as that of the subgroups of pure rotations.

International Notation

1	2	3	4	6	222	32	422	622	23	432
$\bar{1}$	2/m	$\bar{3}$	4/m	6/m	mmm	$\bar{3}m$	4/mmm	6/mmm	$m3$	$m\bar{3}m$

2.5.6 Subgroups of the centrosymmetric groups

The eleven centrosymmetric groups contain ten subgroups which are unknown to us. Below we list them together with their subgroups they originate from.

2/m	mmm	4/m	4/mmm	$\bar{3}m$	6/m	6/mmm	$m\bar{3}m$
m	$mm2$	$\bar{4}$	$42m$ $4mm$	$3m$	$\bar{6}$	$\bar{6}m2$ $6mm$	$\bar{4}3m$
C_{2h}	D_{2h}	C_{4h}	D_{4h}	D_{3d}	C_{6h}	D_{6h}	O_h
C_{1h}	C_{2v}	S_4	D_{2d} C_{4v}	C_{3v}	C_{3h}	D_{3h} C_{6v}	T_d

Thus all the 32 point groups have been introduced. ($C_{1h} \equiv C_s \equiv S_1$)

Remark: Laue pattern always appear to be centrosymmetric, even so the crystal has no inversion center. Thus we can determine by simple X-ray diffraction only 11 point groups, more details have to follow from other physical properties like polar axes.

For those who are more interested in the derivation of the 32 point groups we mention two other methods. Starting with a proper point group $\mathcal{P}$ one searches for an invariant subgroup $\mathcal{Q}$ of index 2. Then $\mathcal{P}$ can be written $\mathcal{P} = \mathcal{Q} + R\mathcal{Q}$ for some rotation R. Then the group $\mathcal{P}' = \mathcal{Q} + I \cdot R\mathcal{Q}$ is also a point group. (For details see [2])

Probably the most elegant way of deriving the 32 point groups is to start from the symmetry of the 7 holohedries [1]. These are simply the point symmetries of the lattices of the 7 crystal systems, and such a derivation highlights the central importance of the lattice itself. To do this, we just write down the holohedral point goups and list the subgroups that remain in the crystal system. The holohedral point groups are given as the last entry in the first column of Table 7 of the corresponding crystal system, see appendix C. We add the following remarks: the lattice has the highest symmetry, the basis can keep it, or may reduce it to a subgroup, being a member of the crystal system, but never raises the number of symmetry elements. The basis must have at

least the symmetry of the first entry for each crystal system in column 1 of Table 7, because these symmetry operations are used to derive the relations for the unit vectors (length and angles).

Thus, starting in the triclinic system, the holohedral group is $\bar{1}$ and its subgroups are 1 and $\bar{1}$ itself. These are the two point groups of the triclinic system. In the monoclinic system, the holohedral group is 2/m and its subgroups are 2, m and 2/m (we do not add 1 and $\bar{1}$, since they are in the triclinic system). In the orthorhombic system, the subgroups of mmm are 222, mm2, m2m, 2mm and mmm itself. In this case mm2, m2m and 2mm are equivalent since they only arise from an interchange of axes, and so in the orthorhombic system there are just three point groups. In the tetragonal system, we start from 4/mmm and obtain the subgroups 4, $\bar{4}$, 422, $\bar{4}$2m, 4m2, 4mm, 4/m and 4/mmm. Here again, $\bar{4}$2m and 4m2 are equivalent and so there are seven unique tetragonal point groups. For the remaining systems see Table 7 in appendix C, which contains in its second column the full notation of the International System. For example, n/mmm is the short form of $n/m2/m2/m$.

We finish this section with two questions. For example, can we put an object with just 1(C_1) point symmetry on a cubic Bravais lattice? Conversely, can we put an object with m$\bar{3}$m(O_h) point symmetry on a triclinic Bravais lattice? The answer to both these questions is no. The reason is that, physically, the potential energy of the crystal compatible with a cubic Bravais lattice can be expanded about a lattice point in combinations of spherical harmonics that have cubic symmetry. There are no combinations that have lower symmetry. Or putting it in an other way, since the symmetry operations must act through each lattice point, addition of a non-cubic object automatically forbids overall cubic symmetry. Thus, in a cubic Bravais lattice, the object must have one of the cubic point symmetries. Similarly, for a triclinic Bravais lattice the potentials expanded about a lattice point have triclinic symmetry and so these potentials would distort the object of higher symmetry and make it adopt triclinic point symmetry. However, remember that the distortion may be small and difficult to observe experimentally.

2.6 Space groups

Symmetry operations of space groups are combinations of point group operations and translations. For a description the *Seitz-Operator* $\{R|\mathbf{t}\}$ is used.

$$\mathbf{r}' = \mathbf{Rr} + \mathbf{t} \equiv \{\mathbf{R}|\mathbf{t}\}\mathbf{r} \tag{2.11}$$

We quickly show that Seitz-Operators form a group. With $\{R|\mathbf{t}\}$ and $\{S|\mathbf{u}\}$ the product is an element of the set,

$$\{R|\mathbf{t}\}\{\mathbf{S}|\mathbf{u}\}\mathbf{r} = \{\mathbf{R}|\mathbf{t}\}(\mathbf{Sr} + \mathbf{u}) = \mathbf{RSr} + \mathbf{Ru} + \mathbf{t} = \{\mathbf{RS}|\mathbf{Ru} + \mathbf{t}\}\mathbf{r} \tag{2.12}$$

because $R\mathbf{u}$ is again a translation. The identity is $\{E|0\} \equiv \{1|0\}$. The inverse element of $\{R|\mathbf{t}\}$ is denoted $\{R|\mathbf{t}\}^{-\mathbf{1}}$, with

$$\{R|\mathbf{t}\}^{-\mathbf{1}} = \{\mathbf{R}^{-\mathbf{1}}| - \mathbf{R}^{-\mathbf{1}}\mathbf{t}\}. \tag{2.13}$$

The pure translations form an invariant subgroup of the space group.

Later on we will see, that symmetry operations of the form $\{R|\tau\}$, with a translation τ being a fraction of a primitive translation, are possible. Operations like $\{R|\tau\}$ are not essential in all space groups. Therefore we distinguish

symmorphic Space groups: $\tau = \mathbf{0}$
nonsymmorphic Space groups: with at least one $\tau \neq \mathbf{0}$.

In symmorphic groups elements like $\{R|\tau\}$ may exist, but they are not essential, they are not needed as a generator, while in nonsymmorphic groups they are essential elements and qualify as generator.

The point group of a space group $\mathcal{G}$ is a set of all elements $\{R|0\}$. We denote it $\mathcal{P}_g$ and obtain all its elements from those of $\mathcal{G}$, by setting all $\mathbf{t_n}$ and $\boldsymbol{\tau}$ zero. This group is often called the isogonal point group.

There exist 230 space groups, 73 of them are symmorphic, the rest nonsymmorphic. This needs some explanation. Why not 14*32=448 space groups? Remember at the end of the last section we discussed that the basis cannot have an arbitrary symmetry. We add the following group theoretical arguments, by inspecting the hierarchy of the crystal systems: each system develops from on (two) by small distortions.

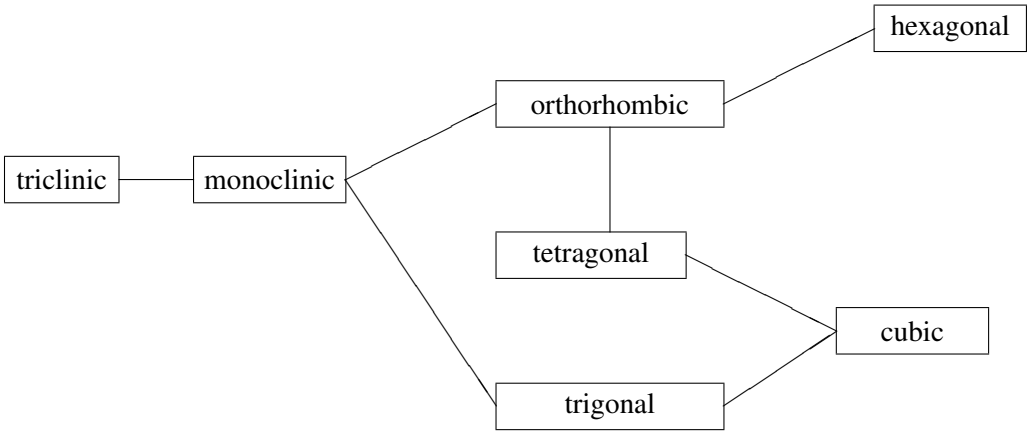

The symmetry of the unit cell of a crystal system is governed by the following rules:

a) all symmetry operations applied to the basis must produce a result which is compatible with occupied lattice points. The symmetry operations have to be elements of $\mathcal{P}_g$.

b) The set of symmetry elements of the basis must contain at least one element which does not belong to the system one level lower in the hierarchy.

2.6.1 Nonsymmorphic symmetry operations

We start with the screw operation, or more specific the screw rotation which is a combination of a proper rotation and a nonprimitive translation $\boldsymbol{\tau}$ parallel to the axis of rotation. This axis is called the screw axis. The order of performing the operations is unimportant. A n-fold rotation axis can be combined with nonprimitive translation of the form $\boldsymbol{\tau} = (m/n)\mathbf{t_n}$ with $m = 1, 2, 3, \ldots, n-1$. Figure 12 illustrates all possible screw operations in crystals including their names and symbols. The vector $\mathbf{t_n}$ is always parallel to the rotation axis.

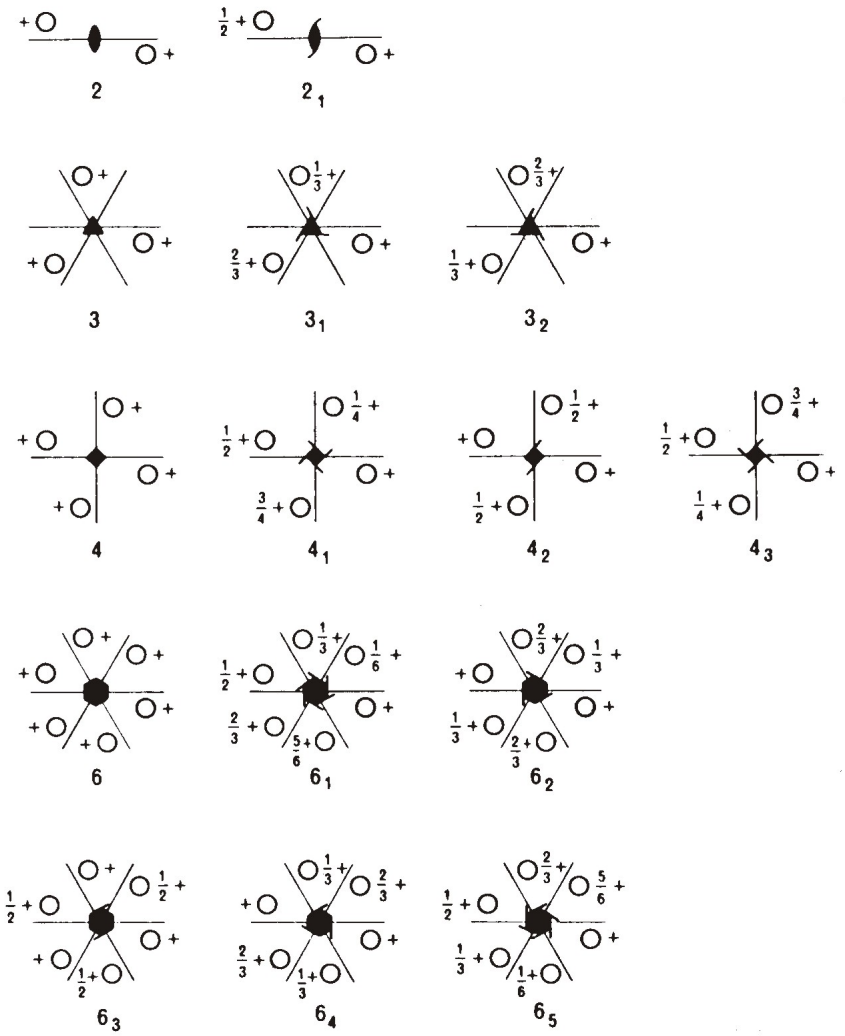

Figure 12: Allowed crystallographic screw operations, taken from [1].

The next operation to be discussed is the glide operation, which is a combination of a mirror operation and a nonprimitive translation. There are three types of glide planes known. In the axial glide the magnitude of the translation vector $\boldsymbol{\tau}$ is one half of a unit-cell translation parallel to the

reflection plane. We refer to the axial glide as an a-, b-, or c-glide according to the axis along which the translation is done. Figure 13 shows a b-glide.

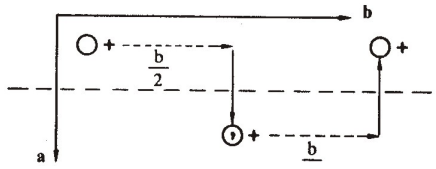

Figure 13: Two b-glide operations, taken from [1].

A diagonal glide, often called a n-glide, is a combination of a reflection and translations in two or three directions, e.g., $(\mathbf{a}+\mathbf{b})/\mathbf{2}$; $(\mathbf{b}+\mathbf{c})/\mathbf{2}$; $(\mathbf{a}+\mathbf{c})/\mathbf{2}$ or $(\mathbf{a}+\mathbf{b}+\mathbf{c})/\mathbf{2}$. The last operation works only in tetragonal and cubic crystals. In this case the direction of the translation has a component perpendicular to the mirror plane, while in all other cases the translation is parallel to the mirror plane. Figure 14 shows two n-glide operations, the mirror plane is perpendicular to $\mathbf{c}$.

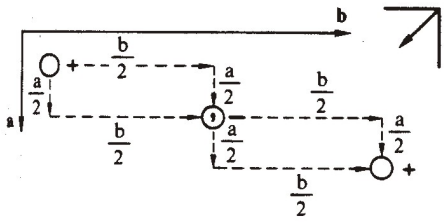

Figure 14: Two n-glide operations, taken from [1].

The diamond or d-glide has translations like $(\mathbf{a} \pm \mathbf{b})/\mathbf{4}$; $(\mathbf{b} \pm \mathbf{c})/$; $(\mathbf{a} \pm \mathbf{c})/\mathbf{4}$. For tetragonal and cubic systems the translations are $(\mathbf{a} \pm \mathbf{b} \pm \mathbf{c})/\mathbf{4}$.

2.6.2 Space group notations

Schönflies notation for space groups In this scheme the point groups of the space groups are used. Since a crystal system can have several space groups with the same point group $\mathcal{P}_g$, they are distinguished solely by a serial number. It is impossible to derive space group operations or lattices.

International notation for space groups, Herman-Mauguin This drawback is fixed in the International Notation. The general form is

$$\Gamma \ldots$$

Γ describes the type of lattice (P, A, B, C, I, F, R). The dots are place-markers for generators which correspond in monoclinic and orthorhombic systems to the three vectors $\mathbf{a}, \mathbf{b}, \mathbf{c}$. A C_2 rotation about $\mathbf{a}$ is denoted by a 2 at the position of the first point. An a-glide, having its mirror plane perpendicular to $\mathbf{c}$, is denoted by an *a* at the position of the third point. In tetragonal, trigonal, and

hexagonal systems the principal axis is along **c** and replaces the first dot. Table 8 in appendix D gives a summary of the conventions used for directions of symmetry elements and some space group examples.

Like for point groups there exist a short and a full version, for details consult the second edition of the International Tables [3].

2.6.3 Space group examples

In this section we continue to explain what kind of information can be taken from the knowledge of the space group of a crystal. Figure 15 shows the relevant parts of the pages of a tetragonal space group from the International tables. We start with an explanation of the first line.

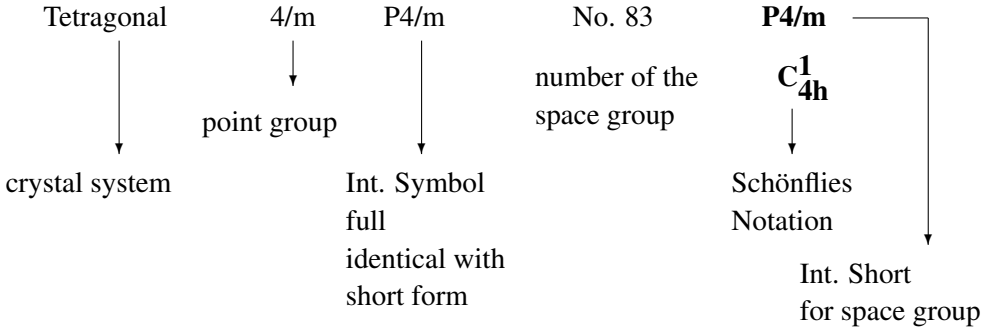

Figure 16 belongs to space group number 85. The symbol P4/n points directly to a nonsymmorphic space group, because it is a generator and 4/n means a n-glide perpendicular to the fourfold rotation axis. Below the first line some diagrams are drawn with axes following the conventions explained in Table 8 of appendix D. The left illustrates the action of symmetry operations on a general point, which is denoted by a small circle. The diagrams display the unit cell, which is identical with the primitive cell for P-lattices only. The diagram at the right demonstrates the symmetry elements within the cell. Please notice that the positions in the center of the cell for P4/n does not mean a centering of the lattice and thus a contradiction to the P-lattice. It is simply a consequence of the n-glide as a generator. Inside a unit cell the number of circles (bisected circles count twice) has to be equal to the order of the point group. In the conventional cells of the I-, F-, A-, B-, C- or R-lattices the number of circles is by a factor 2, 4, 2 or 3 larger according to the volume relations to the corresponding primitive cells. In the examples P4/m and P4/n we observe eight circles, since $\mathcal{P}_g = \{1, 4, 2, 4^3, \bar{1}, \bar{4}, m, \bar{4}^3\}$.

The meaning of the left diagram should be clear, otherwise have a look to Figure 3 and the corresponding discussion. For an understanding of the right diagram we need some explanation of the graphical symbols. In appendix D we give a selection from the International Tables [3], for details see pages 7 - 10 therein. We find inversion centers, fourfold-rotation axes and $\bar{4}$ operations, as well as a diagonal n-glide. Before discussing an additional tetragonal lattice (space group 100) with some more reflection planes we continue to discuss the information given in the pages of

$P\,4/m$ C_{4h}^1 $4/m$ **Tetragonal**

No. 83 $P\,4/m$ Patterson symmetry $P\,4/m$

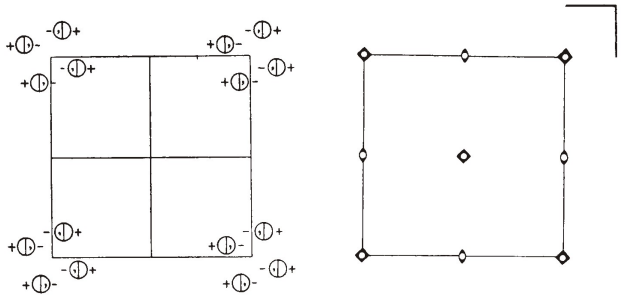

Origin at centre ($4/m$)

Asymmetric unit $0\le x\le\frac{1}{2};\ 0\le y\le\frac{1}{2};\ 0\le z\le\frac{1}{2}$

Symmetry operations

(1) 1 (2) 2 $0,0,z$ (3) 4^+ $0,0,z$ (4) 4^- $0,0,z$
(5) $\bar{1}$ $0,0,0$ (6) m $x,y,0$ (7) $\bar{4}^+$ $0,0,z;\ 0,0,0$ (8) $\bar{4}^-$ $0,0,z;\ 0,0,0$

Generators selected (1); $t(1,0,0)$; $t(0,1,0)$; $t(0,0,1)$; (2); (3); (5)

Positions

Multiplicity, Wyckoff letter, Site symmetry			Coordinates				Reflection conditions
							General:
8	l	1	(1) x,y,z	(2) $\bar{x},\bar{y},z$	(3) $\bar{y},x,z$	(4) $y,\bar{x},z$	no conditions
			(5) $\bar{x},\bar{y},\bar{z}$	(6) $x,y,\bar{z}$	(7) $y,\bar{x},\bar{z}$	(8) $\bar{y},x,\bar{z}$	
							Special:
4	k	m . .	$x,y,\frac{1}{2}$	$\bar{x},\bar{y},\frac{1}{2}$	$\bar{y},x,\frac{1}{2}$	$y,\bar{x},\frac{1}{2}$	no extra conditions
4	j	m . .	$x,y,0$	$\bar{x},\bar{y},0$	$\bar{y},x,0$	$y,\bar{x},0$	no extra conditions
4	i	2 . .	$0,\frac{1}{2},z$	$\frac{1}{2},0,z$	$0,\frac{1}{2},\bar{z}$	$\frac{1}{2},0,\bar{z}$	$hkl: h+k=2n$
2	h	4 . .	$\frac{1}{2},\frac{1}{2},z$	$\frac{1}{2},\frac{1}{2},\bar{z}$			no extra conditions
2	g	4 . .	$0,0,z$	$0,0,\bar{z}$			no extra conditions
2	f	$2/m$ . .	$0,\frac{1}{2},\frac{1}{2}$	$\frac{1}{2},0,\frac{1}{2}$			$hkl: h+k=2n$
2	e	$2/m$ . .	$0,\frac{1}{2},0$	$\frac{1}{2},0,0$			$hkl: h+k=2n$
1	d	$4/m$ . .	$\frac{1}{2},\frac{1}{2},\frac{1}{2}$				no extra conditions
1	c	$4/m$ . .	$\frac{1}{2},\frac{1}{2},0$				no extra conditions
1	b	$4/m$ . .	$0,0,\frac{1}{2}$				no extra conditions
1	a	$4/m$ . .	$0,0,0$				no extra conditions

Figure 15: The space group P4/m

the International Tables. Below the diagrams the origin is given. Often pages with information on positions corresponding to different origins are presented. This, for example, is true for space

$P\,4/n$ C_{4h}^3 $4/m$ Tetragonal

No. 85 $P\,4/n$ Patterson symmetry $P\,4/m$

ORIGIN CHOICE 1

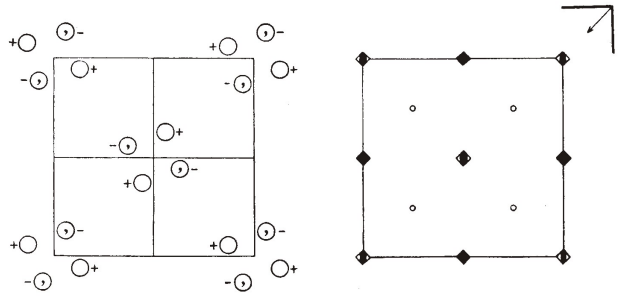

Origin at $\bar{4}$ on n, at $-\frac{1}{4},\frac{1}{4},0$ from $\bar{1}$

Asymmetric unit $0\le x\le\frac{1}{2}$; $0\le y\le\frac{1}{2}$; $0\le z\le\frac{1}{2}$

Symmetry operations

(1) 1	(2) 2 $0,0,z$	(3) 4^+ $0,\frac{1}{2},z$	(4) 4^- $\frac{1}{2},0,z$
(5) $\bar{1}$ $\frac{1}{4},\frac{1}{4},0$	(6) $n(\frac{1}{2},\frac{1}{2},0)$ $x,y,0$	(7) $\bar{4}^+$ $0,0,z;\ 0,0,0$	(8) $\bar{4}^-$ $0,0,z;\ 0,0,0$

Generators selected (1); $t(1,0,0)$; $t(0,1,0)$; $t(0,0,1)$; (2); (3); (5)

Positions

Multiplicity, Wyckoff letter, Site symmetry			Coordinates				Reflection conditions
							General:
8	g	1	(1) x,y,z	(2) $\bar{x},\bar{y},z$	(3) $\bar{y}+\frac{1}{2},x+\frac{1}{2},z$	(4) $y+\frac{1}{2},\bar{x}+\frac{1}{2},z$	$hk0$: $h+k=2n$
			(5) $\bar{x}+\frac{1}{2},\bar{y}+\frac{1}{2},\bar{z}$	(6) $x+\frac{1}{2},y+\frac{1}{2},\bar{z}$	(7) $y,\bar{x},\bar{z}$	(8) $\bar{y},x,\bar{z}$	$h00$: $h=2n$
							Special: as above, plus
4	f	2..	$0,0,z$	$\frac{1}{2},\frac{1}{2},z$	$\frac{1}{2},\frac{1}{2},\bar{z}$	$0,0,\bar{z}$	hkl : $h+k=2n$
4	e	$\bar{1}$	$\frac{1}{4},\frac{1}{4},\frac{1}{2}$	$\frac{3}{4},\frac{3}{4},\frac{1}{2}$	$\frac{1}{4},\frac{3}{4},\frac{1}{2}$	$\frac{3}{4},\frac{1}{4},\frac{1}{2}$	hkl : $h,k=2n$
4	d	$\bar{1}$	$\frac{1}{4},\frac{1}{4},0$	$\frac{3}{4},\frac{3}{4},0$	$\frac{1}{4},\frac{3}{4},0$	$\frac{3}{4},\frac{1}{4},0$	hkl : $h,k=2n$
2	c	4..	$0,\frac{1}{2},z$	$\frac{1}{2},0,\bar{z}$			no extra conditions
2	b	$\bar{4}$..	$0,0,\frac{1}{2}$	$\frac{1}{2},\frac{1}{2},\frac{1}{2}$			hkl : $h+k=2n$
2	a	$\bar{4}$..	$0,0,0$	$\frac{1}{2},\frac{1}{2},0$			hkl : $h+k=2n$

Figure 16: The space group P4/m

group 85. There are rules for the choice of the origin.

a) in symmorphic groups the origin has the symmetry of the point group

b) in nonsymmorphic groups the position with the highest site symmetry is chosen as origin.

Each possible site is denoted by a letter, starting with a for the site with the highest symmetry (however note, several sites can have equal site symmetry), and sequentially going through the alphabet until the lowest site symmetry 1 of a general point is reached. These letters are called Wyckoff notation. There is a number close to each Wyckoff letter which describes the number of symmetry-related positions that belong to this particular site. This number is often referred to as multiplicity and is placed to the left of the Wyckoff position. To its right information on the point group of this site is given. These point group labels are expanded by some dots, for details see the explanation in the International Tables [3]. In the next columns coordinates of positions follow. A site with multiplicity 1 can have only one position while a site with n-fold multiplicity has n different positions. If one applies space group operations to a certain position, it will permute with one of the other, never leaving this set. The last sentence sounds strange. We apply space group operations but characterize this Wyckoff position by a point group. The solution is simple. The point group of a Wyckoff position is obtained by taking this point as an origin and neglecting all fractional translations. Therefore the positions (0,0,0) and (0,0,$\frac{1}{2}$) in P4/m establish the site symmetry 4/m, while those in P4/n only the group $\bar{4}$. All equivalent positions can be occupied by atoms or even molecules. But please keep in mind

(a) there is no need to fill all possible Wyckoff positions with atoms

(b) it is allowed to fill one type of Wyckoff positions with different atoms, but they have to have different values for x, y, z

(c) all positions of a particular Wyckoff site have to be occupied by the same kind of atoms.

In groups with nonprimitive unit cells, e. g., $\Gamma \neq \mathrm{P}$ several positions are given under the line *Coordinates*. This means that all Wyckoff positions have to be combined with them.

As a last example we discuss the group P4bm (C_{4v}^2). This is a nonsymmorphic tetragonal space group with details in Figure 17. This group consists of the following 8 symmetry operations: the identity 1, the 2-fold rotation about **c**, a 4-fold rotation 4^+ and its reverse 4^-, both along **c**, axial glides $(a\ x, \frac{1}{4}, z)$ and $(b\ \frac{1}{4}, y, z)$, a mirror plane $(m\ x + \frac{1}{2}, \bar{x}, z)$ and a glide reflection (no standard type, thus no typical label). From this the symmetry operations can be derived and applied to a general point (x, y, z) to produce the coordinates listed for the Wyckoff position (d). The matrices for the operations (1) 1; (2) 2 $0, 0, z$; (3) 4^+ $0, 0, z$; (4) 4^- $0, 0, z$; can be taken directly from appendix A. The next is more complicate. Operation (5) $a\ x, \frac{1}{4}, z$ means an a-glide with a fractional translation $\boldsymbol{\tau} = (\frac{1}{2}, 0, 0)$ and a mirror plane through $(0, \frac{1}{4}, 0)$ perpendicular to **b** or parallel to (010) planes.

$$\{m[010]|\boldsymbol{\tau}(\frac{1}{2}, 0, 0)\}\mathbf{r} = \begin{pmatrix} 1 & 0 & 0 \\ 0 & -1 & 0 \\ 0 & 0 & 1 \end{pmatrix} \begin{pmatrix} x \\ y \\ z \end{pmatrix} + \begin{pmatrix} \frac{1}{2} \\ 0 \\ 0 \end{pmatrix} = \begin{pmatrix} x + \frac{1}{2} \\ -y \\ z \end{pmatrix}$$

with $m[010]$ from the appendix A. If we compare this with the entry (5) for the Wyckoff position d, a disagreement is observed. The problem is easily fixed, because in appendix A the matrices are given with respect to the origin $(0\,0\,0)$, but we have to operate at position $(0, \frac{1}{4}, 0)$. For a

P 4 b m C_{4v}^2 4 m m Tetragonal

No. 100 P 4 b m Patterson symmetry P 4/m m m

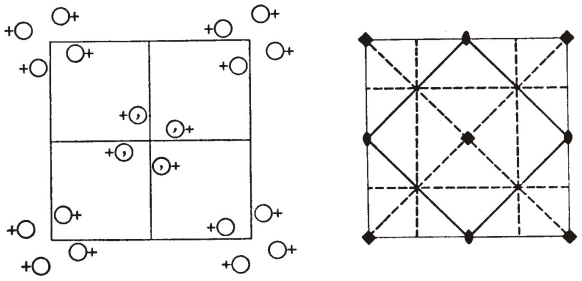

Origin on 4 1 *g*

Asymmetric unit $0 \le x \le \frac{1}{2}$; $0 \le y \le \frac{1}{2}$; $0 \le z \le 1$; $y \le \frac{1}{2} - x$

Symmetry operations

(1) 1	(2) 2 0,0,*z*	(3) 4^+ 0,0,*z*	(4) 4^- 0,0,*z*
(5) *a* $x,\frac{1}{4},z$	(6) *b* $\frac{1}{4},y,z$	(7) *m* $x+\frac{1}{2},\bar{x},z$	(8) *g*($\frac{1}{2},\frac{1}{4},0$) *x*,*x*,*z*

Generators selected (1); *t*(1,0,0); *t*(0,1,0); *t*(0,0,1); (2); (3); (5)

Positions

Multiplicity, Wyckoff letter, Site symmetry		Coordinates				Reflection conditions
						General:
8 *d* 1	(1) *x*,*y*,*z*	(2) $\bar{x},\bar{y},z$	(3) $\bar{y},x,z$	(4) $y,\bar{x},z$		*0kl* : *k* = 2*n*
	(5) $x+\frac{1}{2},\bar{y}+\frac{1}{2},z$	(6) $\bar{x}+\frac{1}{2},y+\frac{1}{2},z$	(7) $\bar{y}+\frac{1}{2},\bar{x}+\frac{1}{2},z$	(8) $y+\frac{1}{2},x+\frac{1}{2},z$		*h*00: *h* = 2*n*
						Special: as above, plus
4 *c* . . *m*	$x,x+\frac{1}{2},z$	$\bar{x},\bar{x}+\frac{1}{2},z$	$\bar{x}+\frac{1}{2},x,z$	$x+\frac{1}{2},\bar{x},z$		no extra conditions
2 *b* 2 . *m m*	$\frac{1}{2},0,z$	$0,\frac{1}{2},z$				*hkl* : *h*+*k* = 2*n*
2 *a* 4 . .	0,0,*z*	$\frac{1}{2},\frac{1}{2},z$				*hkl* : *h*+*k* = 2*n*

Figure 17: The space group P4bm

correction we have to add this shift twice, thus

$$\begin{pmatrix} x+\frac{1}{2} \\ -y \\ z \end{pmatrix} + 2\begin{pmatrix} 0 \\ \frac{1}{4} \\ 0 \end{pmatrix} = \begin{pmatrix} x+\frac{1}{2} \\ -y+\frac{1}{2} \\ z \end{pmatrix}.$$

The element (6) b $\frac{1}{4}, y, z$ denotes b-glide with a fractional translation $\boldsymbol{\tau} = (0, \frac{1}{2}, 0)$ and a mirror plane through $(\frac{1}{4}, 0, 0)$ perpendicular to $\mathbf{a}$ or parallel to (100) planes.

$$\{m[100]|\boldsymbol{\tau}(0,\frac{1}{2},0)\}\mathbf{r} = \begin{pmatrix} -1 & 0 & 0 \\ 0 & 1 & 0 \\ 0 & 0 & 1 \end{pmatrix}\begin{pmatrix} x \\ y \\ z \end{pmatrix} + \begin{pmatrix} 0 \\ \frac{1}{2} \\ 0 \end{pmatrix} + 2\begin{pmatrix} \frac{1}{4} \\ 0 \\ 0 \end{pmatrix} = \begin{pmatrix} -x+\frac{1}{2} \\ y+\frac{1}{2} \\ z \end{pmatrix}$$

Element (7) $m\ x+\frac{1}{2}, -x, z$ describes a mirror operation with a mirror plane bisecting the **a** and **-b** axes and intersecting **a** at $(\frac{1}{2}, 0, 0)$. Thus the mirror plane is perpendicular to $[1, 1, 0]$ (for the corresponding matrix see the appendix A) and with the help of Figure 17 we deduce its shortest distance from the origin to be in $(\frac{1}{4}, \frac{1}{4}, 0)$.

$$\begin{pmatrix} 0 & -1 & 0 \\ -1 & 0 & 0 \\ 0 & 0 & 1 \end{pmatrix} \begin{pmatrix} x \\ y \\ z \end{pmatrix} + 2 \begin{pmatrix} \frac{1}{4} \\ \frac{1}{4} \\ 0 \end{pmatrix} = \begin{pmatrix} -y+\frac{1}{2} \\ -x+\frac{1}{2} \\ z \end{pmatrix}$$

Finally we interpret the operation (8) $g(\frac{1}{2}, \frac{1}{2}, 0)\ x, x, z$. The first part means a fractional translation of $\boldsymbol{\tau}$ and the second a mirror plane bisecting **a** and **b** and going through the origin.

$$\{m[1\bar{1}0]|\boldsymbol{\tau}(\frac{1}{2}, \frac{1}{2}, 0)\}\mathbf{r} = \begin{pmatrix} 0 & 1 & 0 \\ 1 & 0 & 0 \\ 0 & 0 & 1 \end{pmatrix} \begin{pmatrix} x \\ y \\ z \end{pmatrix} + \begin{pmatrix} \frac{1}{2} \\ \frac{1}{2} \\ 0 \end{pmatrix} = \begin{pmatrix} y+\frac{1}{2} \\ x+\frac{1}{2} \\ z \end{pmatrix}$$

In section 11.2 and 11.3 of the International Tables procedures are discussed to calculate the matrices from the information given under the heading *Symmetry Operations*. Therefore the entries of the coordinates for each Wyckoff site are not superfluous but very helpful for a quick inspection and sufficient if no group theoretical representations but only structural knowledge is involved.

Realizations of this group look somewhat complicate. This is do to the tricky structure which asks for a large number of atoms in a formula unit. Typical building motifs are tetrahedra ($Ce_3Si_6N_{11}$, nitridosilicate) or octahedra (unfilled tungsten-bronze structure, like SBN) . In structure data bases information on SBN ($Sr_xBa_{1-x}Nb_2O_6$) is available, e. g., Table 4:

label	atom	multiplicity	Wyckhoff	x	y	z	occupancy
Nb1	Nb^{5+}	2	b	0.0	0.5	0.024	1.0
Nb2	Nb^{5+}	8	d	0.0745(1)	0.2114(1)	0.0080(3)	1.0
Sr1	Sr^{2+}	2	a	0.0	0.0	0.5000(4)	0.725(4)
Sr2	Sr^{2+}	8	d	0.1532(6)	0.6864(8)	0.5168(23)	0.202(8)
Ba1	Ba^{2+}	4	c	0.1729(1)	0.6729(1)	0.5002(9)	0.487(3)
O1	O^{2-}	8	d	0.3435(3)	0.0057(3)	-0.0224(27)	1.0
O2	O^{2-}	8	d	0.1393(3)	0.0687(3)	-0.0286(27)	1.0
O3	O^{2-}	4	c	0.2819(3)	0.7819(3)	-0.0192(23)	1.0
O4	O^{2-}	4	c	-0.0130(8)	0.4870(8)	0.4864(23)	0.5
O5	O^{2-}	8	d	0.3056(6)	0.4053(8)	0.4836(20)	0.5
O6	O^{2-}	8	d	0.2847(7)	0.4458(9)	0.4842(25)	0.5

Table 4: Selected structure data for SBN

A short inspection of Table 4 shows that there are general Wyckoff sites of type (d) which are occupied by all kind of elements except Ba. Only one Sr has site symmetry 4, the rest is placed in mirror planes. Taking this data the following Figure 18 can be prepared using commercial programmes or asking Mr. Betzler for help. The main motif is the Nb-O_6 octahedra. Two kind of such crystallographically independent octahedra exist and are linked via oxygen corners forming a

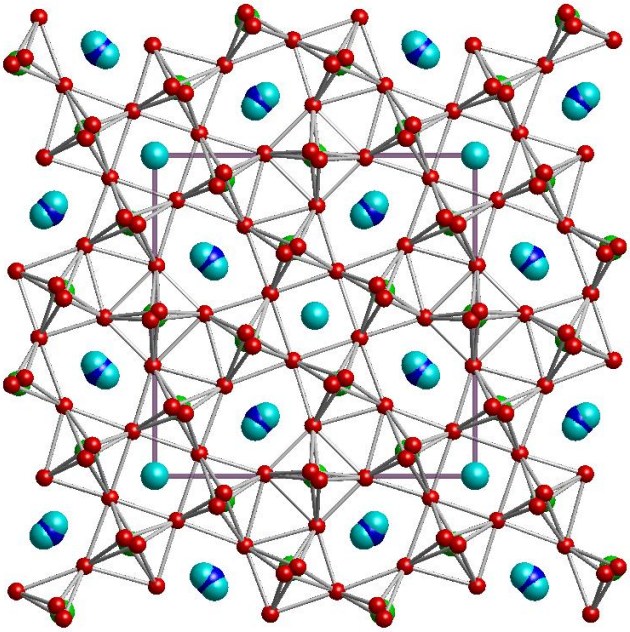

Figure 18: Illustration of the structure of SBN by a projection onto the c-plane using realistic fractions for the positions of the atoms.

three-dimensional network. As a result three kinds of empty channels (or cavities) along the polar axis c appear. The 12-coordinated cavity with 4-fold symmetry is either empty or occupied by Sr. The 15-fold-coordinated one has a pentagon shape and is again empty or occupied by Ba or Sr. The small 9-fold-coordinated cavity is always empty. Comparing Figure 17 and Figure 18 allows to become more familiar with the structure of SBN. For example, the mirror plane belonging to the symmetry operation (7), e. g., the solid line in the upper left of Figure 17 is easily recognized in the real crystal. Even the glide operation (8, dashed diagonal line in Figure 17) can be demonstrated by taking the projected Sr, Ba atoms at the lower left corner of the unit cell, reflect them at the diagonal mirror plane, applying a fractional translation $(\frac{1}{2}, \frac{1}{2}, 0)$ to come to the position at the upper right of the unit cell, with a change of the handedness. Further details should be explored by the reader.

References

[1] G. Burns, A. M. Glazer. *Space Groups for Solid State Scientists*. Academic Press, 2nd ed. edition, 1990.

[2] C. J. Bradley, A. P. Cracknell. *The Mathematical Theory of Symmetry in Solids*. Clarendon, Oxford, 1972.

[3] T. Hahn. *International Tables for Crystallography*. Kluwer Acad. Publishers, Dordrecht, 2. edition, 1989.

3 Symmetry induced tensor properties

A property tensor may exhibit intrinsic symmetry, often expressed by a permissible change of two or more indices. Such behavior follows from the physical property and very general relations introduced by Onsager or Kleinman, for the last see section 4.6.

3.1 Neumann's principle

In contrast to the intrinsic symmetry the crystal symmetry governs tensor properties, too. This is based on Neumann's well-known principle:

> If a system has a certain group of symmetry operations, $\mathcal{G}$, then any physical observable of that system must also possess these symmetry operations.

An alternative formulation is given in the book by Burns and Glazer [1] by emphasizing *that the macroscopic (tensor) properties of a crystal have* **at least** *the symmetry of the point group of the space group.* The physical reason for this is that in measuring a macroscopic property one would not expect to be able to detect the effect of a translation that is only a fraction of a primitive unit cell. On the other hand, the rotational part of the symmetry operation will relate points within the crystal that are separated by macroscopic distances and hence will have an effect on the macroscopic properties. Somewhat special is the optical activity, because such a property adds in phase from one unit cell to the next to result in an overall macroscopic effect.

Note the use of the words **at least** in the statement of Neumann's principle. It is important to understand that the point group of the space group is generally of lower symmetry than the symmetry of the physical properties. For example, if we consider properties specified by second-rank tensors, we find that cubic crystals (those having cubic point groups) are isotropic, i.e., the diagonal elements of the tensor are equal and nonzero, while the nondiagonal elements are zero. This means that such properties are the same in all directions and therefore have spherical symmetry. Clearly, all of the symmetry operations of the cubic point groups are contained by such spherical symmetry, so that we can say that the cubic point groups are subgroups of a spherically symmetric group. With properties that are described by tensors of higher rank, the situation is more involved [1].

According to Neumann's principle the tensor representing any physical property has to be invariant with regard to all symmetry operations of the crystal. This condition reduces the number of the independent tensor components because of relationships between the tensor components. There are different ways known to extract the information from such relations, one deals with solving a set of equations with the tensor components as unknowns, the second uses a reducible representation of the group, its reduction into irreducible representations and projection operator techniques.

3.2 Relationships for tensor components

A tensor of rank m is transformed according to

$$t'_{ijk...m} = a_{ip}a_{jq}\ldots a_{mu}t_{pqr...u}. \tag{3.1}$$

where the a_{ij} direction cosines are the elements of the (a_{ij}) matrix. The (a_{ij}) matrix connects the original and the *new* co-ordinates, and are identical in our case with the r_{ij}. The invariance changes this general equation 3.1 to

$$t_{ijk...m} = r_{ip}r_{jq}\ldots r_{mu}t_{pqr...u}. \tag{3.2}$$

where r is the matrix corresponding to a particular symmetry operation of the point group. The last equation holds for a polar tensor, but has to be modified to

$$t_{ijk...m} = |r_{ij}|r_{ip}r_{jq}\ldots r_{mu}t_{pqr...u}. \tag{3.3}$$

with $|r_{ij}|$ denoting the determinant, whose value is (+1) if the transforming operation consists of a pure rotation and (-1) if an inversion (as part of a mirror operation) is involved changing the handedness. Note that $|r_{ij}|$ is a number and not a transformation matrix.

It is not difficult to find out whether the tensor representing any physical property is polar or axial, since this can be easily decided by the eq. (2.1) defining the physical property in question. If only one of the physical quantities in (3.1) is axial (for example the magnetic field) then the property tensor will be axial, in every other case the tensor is polar.

An immediate consequence of equations (3.3) and (3.2) is that axial tensors of even rank (optical activity) and polar tensors of odd rank (pyroelectricity, second harmonic generation) must vanish identically in centrosymmetrical crystals with the inversion as a single symmetry operation. This forces $|r_{ij}|$ to be (-1) and thus $t_{ijk...m} = -t_{ijk...m}$ for axial tensors. If the rank p is odd, then polar tensors behave like $(-1)^p = -1$, while axial ones like $(-1)^p * |r_{ij}| = 1$. For an even rank we find for polar tensors $(-1)^p = 1$, but $(-1)^p * |r_{ij}| = 1 * (1-) = -1$ for axial tensors.

Application of all symmetry operations to both (3.2) and (3.3) produce a set of $|g|$ equations, with $|g|$ being the order of the group. Of course not all of these equations are independent, because we know that a group is described by a set of few generators. These are sufficient to deduce relationships, but sometimes equations obtained from additional operations may make the derivation easier. Such approaches have been used to calculate the properties for all tensors up to rank four for nonmagnetic and magnetic groups (not covered here), for details see the books by [2, 3, 4] and have a look to section 4.7.

3.3 Direct group theoretical approach

A much more direct approach uses group theoretical methods, but one has to apply all symmetry operations (not only the generators) to form a representation of the tensor. We rewrite Eq. (3.2)

$$U_g T_{i_1 i_2 \ldots i_m} = \sum_{j_1}\sum_{j_2}\ldots\sum_{j_m} D_{j_1 i_1}(g)\, D_{j_2 i_2}(g)\ldots D_{j_m i_m}(g) T_{j_1 j_2 \ldots j_m} = T_{i_1 i_2 \ldots i_m} \quad \forall\ g \in \mathcal{G} \tag{3.4}$$

U_g is the operator which transforms the tensor $T_{i_1 i_2 \ldots i_m}$ according to the point group symmetry element g. The direct product of the m three-dimensional representations $D_{j_k i_k}(g)$ forms the 3^m-dimensional tensor representation $D^T(g)$. Like in section 3.2 we can distinguish between polar representations $D^{(p)} = D_-$ and axial $D^{(a)} = D_+$ ones. An example for a polar vector, a polar tensor of rank 1 is $\mathbf{r}$, thus D_- is a representation of the coordinates, while D_+ is that of the angular momentum.

The invariance condition (3.4) means that the independent tensor components transform according to the totally symmetric (trivial) irreducible representation. To calculate the number of such independent components one has to reduce the reducible representation $D^T(g)$ into its irreducible ones and and count how often the trivial irreducible representation shows up. This number is given by

$$Z = m_{\alpha=1} = \frac{1}{|g|} \sum_{g \in \mathcal{G}} 1 \cdot \chi^T(g) \tag{3.5}$$

where $\chi^T(g)$ denotes the character of the reducible representation of the symmetry element g and the factor 1 represents the character of the trivial repesentation. Then with the help of the projection operator

$$P^{(\alpha=1)} T_{i_1 i_2 \ldots i_m} = \frac{1}{|g|} \sum_{g \in \mathcal{G}} U_g \, T_{i_1 i_2 \ldots i_m} = T_{i_1 i_2 \ldots i_m} \tag{3.6}$$

the independent tensor components can be calculated. The action of U_g on $T_{i_1 i_2 \ldots i_m}$ is described by the corresponding transformation of the coordinates, the r_{ij}.

For an example we consider the point group 4mm (C_{4v}), which has the following symmetry elements, if we take the principal axis along z: 1, 4, 4^3, $4^2 \equiv 2$, $\sigma_v \equiv \bar{2}[100]$, $\sigma_v' \equiv \bar{2}[010]$, $\sigma_d \equiv \bar{2}[110]$, $\sigma_d' \equiv \bar{2}[1\bar{1}0]$. From the corresponding matrices in appendix A and in Table 5 we immediately construct the representation for a polar vector, because this is identical with the set of matrices. To calculate Z for a polar vector (see Eq. 3.5) we need the characters of this representation, they are given in Table 5, too. We obtain

$$Z = \frac{1}{8}(1 \cdot 3 + 1 \cdot 1 + 1 \cdot 1 + 1 \cdot (-1) + 1 \cdot 1 + 1 \cdot 1 + 1 \cdot 1 + 1 \cdot 1) = \frac{8}{8} = 1$$

which means that a polar tensor of rank 1 exists in the point group C_{4v}. But this is not new for us, because we know that SBN is a ferroelectric. Using the projection operator P^{A_1} we can calculate which component transforms like the trivial representation A_1. Eq. 3.6 reduces to

$$P^{A_1} T_i = \frac{1}{8} \sum_{g \in \mathcal{G}} U_g T_i$$

with $i = x, y, z$. The action of U_g on T_i can be taken from the corresponding matrices in Table 5. For $g = C_4$ we read $x \to -y$, $y \to x$, $z \to z$ and for $g = \sigma_d$ we read $x \to -y$, $y \to -x$, $z \to z$, respectively. Applying P^{A_1} to all three components results in

$$P^{A_1} x \;\; = \;\; \frac{1}{8}(x + (-y) + y + (-x) + (-x) + x + (-y) + y) = 0$$

C_{4v}	E 1	C_4 4	C_4^3 4^3	C_2 2
(x,y,z) or (R_x,R_y,R_z)	$\begin{pmatrix} 1 & 0 & 0 \\ 0 & 1 & 0 \\ 0 & 0 & 1 \end{pmatrix}$	$\begin{pmatrix} 0 & -1 & 0 \\ 1 & 0 & 0 \\ 0 & 0 & 1 \end{pmatrix}$	$\begin{pmatrix} 0 & 1 & 0 \\ -1 & 0 & 0 \\ 0 & 0 & 1 \end{pmatrix}$	$\begin{pmatrix} -1 & 0 & 0 \\ 0 & -1 & 0 \\ 0 & 0 & 1 \end{pmatrix}$
$\chi^{(p)}(g)$	3	1	1	-1
$\chi^{(a)}(g)$	3	1	1	-1
$\chi^{(p)}(g^2)$	3	-1	-1	3
$\chi^{(a)}(g^2)$	3	-1	-1	3

C_{4v}	σ_v $\bar{2}[100]$	σ_v' $\bar{2}[010]$	σ_d $\bar{2}[110]$	σ_d' $\bar{2}[1\bar{1}0]$
(x,y,z) or $(-R_x,-R_y,-R_z)$	$\begin{pmatrix} -1 & 0 & 0 \\ 0 & 1 & 0 \\ 0 & 0 & 1 \end{pmatrix}$	$\begin{pmatrix} 1 & 0 & 0 \\ 0 & -1 & 0 \\ 0 & 0 & 1 \end{pmatrix}$	$\begin{pmatrix} 0 & -1 & 0 \\ -1 & 0 & 0 \\ 0 & 0 & 1 \end{pmatrix}$	$\begin{pmatrix} 0 & 1 & 0 \\ 1 & 0 & 0 \\ 0 & 0 & 1 \end{pmatrix}$
$\chi^{(p)}(g)$	1	1	1	1
$\chi^{(a)}(g)$	-1	-1	-1	-1
$\chi^{(p)}(g^2)$	3	3	3	3
$\chi^{(a)}(g^2)$	3	3	3	3

Table 5: Group theoretical information for the point group C_{4v}. The first column denotes the transformation properties of the components of polar (x,y,z) and axial (R_x,R_y,R_z) vectors or the characters of the corresponding representation.

$$\begin{aligned} P^{A_1}y &= \frac{1}{8}(y+x+(-x)+(-y)+y+(-y)+(-x)+x) = 0 \\ P^{A_1}z &= \frac{1}{8}(z+z+z+z+z+z+z+z) = z, \end{aligned}$$

which means that the spontaneous polarization will be aligned along the c-axis. If we calculate Z for an axial vector, using χ^a, we obtain

$$Z = \frac{1}{8}(1\cdot 3+1\cdot 1+1\cdot 1+1\cdot(-1)+1\cdot(-1)+1\cdot(-1)+1\cdot(-1)+1\cdot(-1)) = 0,$$

thus no spontaneous magnetization can be expected in crystals with point group C_{4v}. At a first glance this looks surprising, but if we remember that the magnetization originates from ring currents, then we immediately understand this results, because mirror planes like σ reverse the current and thus no magnetization can occur.

As a next example we discuss a symmetric tensor of rank 2 with both components transforming according to polar vectors. (electrical and thermal conductivity, dielectric constant). Here the

tensor representation to be reduced is not $D^{(p)}(g) \otimes D^{(p)}(g) = D^T(g)$ with $g \in \mathcal{G}$, but

$$D^T_+(g) = \left[D^{(p)}(g) \otimes D^{(p)}(g)\right]_+ \qquad g \in \mathcal{G} \tag{3.7}$$

where the index $+$ denotes the symmetric product representation, because the components i, j are interchangeable. The number Z for such a symmetric representation follows from

$$Z^{2.\,rank}_{sym} = \frac{1}{|g|} \sum_{g \in \mathcal{G}} \frac{1}{2} \left[(\chi^{(p)}(g))^2 + \chi^{(p)}(g^2)\right]. \tag{3.8}$$

For our favorite point group C_{4v} we obtain with the help of Table 5

$$\begin{aligned} Z^{2.\,rank}_{sym} &= \frac{1}{8}\frac{1}{2}[(3^2+3) + (1^2+(-1)) + (1^2+(-1)) + ((-1)^2+3) + \\ &+ ((-1)^2+3) + (1^2+3) + (1^2+3) + (1^2+3)] = 2, \end{aligned}$$

we expect two independent tensor components. Does this mean that two components are nonzero and the others are zero? The answer is no! There are two independent components, but the number of nonzero components can be calculated only with the projection operator!

With

$$P^{A_1}\, xx = \frac{1}{8}(x^2+y^2+y^2+x^2+x^2+x^2+y^2+y^2) = \frac{1}{2}(x^2+y^2)$$

and

$$P^{A_1}\, yy = P^{A_1}\, xx \qquad \text{but} \qquad P^{A_1}\, zz = z^2$$

we find $T_{11} = T_{22} \neq T_{33}$ and $P^{A_1}\, , ij = 0$ with $i, j = x, y, z;\ i \neq j$, a result well-known to most of us.

The extension to a third rank tensor is straight forward. The piezoelectric tensor $d_{k,ij}$ has three components each one transforming as a polar vector, but the last two are interchangeable. Thus Eq. 3.7 reads now

$$D^T(g) = D^{(p)}(g) \otimes \left[D^{(p)}(g) \otimes D^{(p)}(g)\right]_+ \qquad g \in \mathcal{G} \tag{3.9}$$

Notice that the representations of those components which are commutable have been written after the non-commutable ones. This will help us later when we project the nonzero components from introducing a commutability which is not valid in general. The number of independent components follows from

$$Z^{3.\,rank} = \frac{1}{|g|} \sum_{g \in \mathcal{G}} \chi^{(p)}(g) \frac{1}{2} \left[(\chi^{(p)}(g))^2 + \chi^{(p)}(g^2)\right]_+ \quad . \tag{3.10}$$

and for C_{4v} symmetry we calculate

$$\begin{aligned} Z^{3.\,rank} &= \frac{1}{8}\frac{1}{2}[3(9+3) + 1(1-1) + 1(1-1) + (-1)(1+3) + \\ &+ 1(1+3) + 1(1+3) + 1(1+3) + 1(1+3)] = 3 \end{aligned}$$

Now we start a tiresomely lengthy work, because up to $3^3 = 27$ times we have to apply the projection operator to a component, with 8 terms in each sum, so a Mathematica notebook would be a nice tool, but unfortunately no student has presented such one to the author. Lets hope for the future! As pointed out above, we have to obey the order of the components which do not commute, therefore we write the first with capital letters and the second and third, which commute with small letters. For the notation we use both the tensor notation and the reduced matrix notation, for details see section 4.8.

$$
\begin{aligned}
d_{Xxx} &= d_{11} = P^{A_1} Xxx = \frac{1}{8}(Xx^2 - Yy^2 + Yy^2 - Xx^2 - Xx^2 + Xx^2 - Yy^2 + Yy^2) = 0 \\
d_{Xyy} &= d_{12} = P^{A_1} Xyy = \frac{1}{8}(Xy^2 - Yx^2 + Yx^2 - Xy^2 - Xy^2 + Xy^2 - Yx^2 + Yx^2) = 0 \\
d_{Xzz} &= d_{13} = P^{A_1} Xzz = \frac{1}{8}(Xz^2 - Yz^2 + Yz^2 - Xz^2 - Xz^2 + Xz^2 - Yz^2 + Yz^2) = 0 \\
d_{Xyz} &= d_{14} = P^{A_1} Xyz = \frac{1}{8}(Xyz - Yxz - Yxz + Xyz - Xyz - Xyz + Yxz + Yxz) = 0 \\
d_{Xzy} &= d_{14} = 0 \\
d_{Xxz} &= d_{15} = P^{A_1} Xxz = \frac{1}{8}(Xxz + Yyz + Yyz + Xxz + Xxz + Xxz + Yyz + Yyz) \\
&= \frac{1}{2}(Xxz + Yyz) \\
d_{Xzx} &= d_{15} = \frac{1}{2}(Xzx + Yzy) \quad \text{because i, j commute} \\
d_{Xxy} &= d_{16} = P^{A_1} Xxy = \frac{1}{8}(Xxy + Yyx - Yyx - Xxy + Xxy - Xxy - Yyx + Yyx) = 0 \\
d_{Xyx} &= d_{16} = 0 \\
d_{Yxx} &= d_{21} = P^{A_1} Yxx = \frac{1}{8}(Yx^2 + Xy^2 - Xy^2 - Yx^2 + Yx^2 - Yx^2 - Xy^2 + Xy^2) = 0 \\
d_{Yyy} &= d_{22} = P^{A_1} Yyy = \frac{1}{8}(Yy^2 + Xx^2 - Xx^2 - Yy^2 + Yy^2 - Yy^2 - Xx^2 + Xx^2) = 0 \\
d_{Yzz} &= d_{23} = P^{A_1} Yzz = \frac{1}{8}(Yz^2 - Xz^2 + Xz^2 - Yz^2 + Yz^2 - Yz^2 - Xz^2 + Xz^2) = 0 \\
d_{Yyz} &= d_{24} = P^{A_1} Yyz = \frac{1}{8}(Yyz + Xxz + Xxz + Yyz + Yyz + Yyz + Xxz + Xxz) \\
&= \frac{1}{2}(Yyz + Xxz) = d_{15} \\
d_{Yzy} &= d_{Yyz} = d_{24} \\
d_{Yxz} &= d_{25} = P^{A_1} Yxz = \frac{1}{8}(Yxz - Xyz - Xyz + Yxz - Yxz - Yxz + Xyz + Xyz) = 0 \\
d_{Yzx} &= d_{Yxz} = d_{25} = 0 \\
d_{Yxy} &= d_{26} = P^{A_1} Yxy = \frac{1}{8}(Yxy - Xyx + Xyx - Yxy - Yxy + Yxy - Xyx + Xyx) = 0 \\
d_{Yyx} &= d_{Yxy} = d_{26} = 0 \\
d_{Zxx} &= d_{31} = P^{A_1} Zxx = \frac{1}{8}(Zx^2 + Zy^2 + Zy^2 + Zx^2 + Zx^2 + Zy^2 + Zy^2) \\
&= \frac{1}{2} Z(x^2 + y^2)
\end{aligned}
$$

$$
\begin{aligned}
d_{Zyy} &= d_{32} = P^{A_1} Zyy = \frac{1}{8}(Zy^2 + Zx^2 + Zx^2 + Zy^2 + Zy^2 Zx^2 + Zx^2 + Zx^2) \\
&= \frac{1}{2} Z(x^2 + y^2) = d_{31} \\
d_{Zzz} &= d_{33} = P^{A_1} Zzz = \frac{1}{8}(Zz^2 + Zz^2 + Zz^2 + Zz^2 + Zz^2 + Zz^2 + Zz^2 + Zz^2) = Zz^2 \\
d_{Zyz} &= d_{34} = P^{A_1} Zyz = \frac{1}{8}(Zyz + Zxz - Zxz - Zyz + Zyz - Zyz - Zxz + Zxz) = 0 \\
d_{Zzy} &= d_{Zyz} = d_{34} = 0 \\
d_{Zxz} &= d_{35} = P^{A_1} Zxz = \frac{1}{8}(Zxz - Zyz + Zyz - Zxz - Zxz + Zxz - Zyz + Zyz) = 0 \\
d_{Zzx} &= d_{Zxz} = d_{35} = 0 \\
d_{Zxy} &= d_{36} = P^{A_1} Zxy = \frac{1}{8}(Zxy - Zyx - Zyx + Zxy - Zxy - Zxy + Zyx + Zyx) = 0 \\
d_{Zyx} &= d_{Zxy} = d_{36} = 0
\end{aligned}
$$

In matrix notation our calculations result in

$$
\begin{pmatrix}
0 & 0 & 0 & 0 & d_{15} & 0 \\
0 & 0 & 0 & d_{15} & 0 & 0 \\
d_{31} & d_{31} & d_{33} & 0 & 0 & 0
\end{pmatrix}
\quad \text{with} \quad
\begin{aligned}
d_{15} &= \tfrac{1}{2}(Xxz + Yyz) \\
d_{31} &= \tfrac{1}{2} Z(x^2 + y^2) \\
d_{33} &= Zz^2 \,.
\end{aligned}
\tag{3.11}
$$

As predicted by Eqn. 3.10 we obtained three independent components but five nonzero components. If we consider instead of the piezoelectric tensor that of the second harmonic, then due to Kleinman symmetry the elements $d_{15} = d_{31}$ are equal, because we do not distinguish between capital and small letters, in agreement with the results in section 4.7.

Finally we comment shortly on polar 4. rank tensors (electrostriction, piezooptic effect, quadratic electrooptic effect). Commutability like $ij, kl = ji, kl = ij, lk = ji, lk$ yields

$$
D^T(g) = \left[D^{(p)}(g) \otimes D^{(p)}(g) \right]_+ \otimes \left[D^{(p)}(g) \otimes D^{(p)}(g) \right]_+ \quad g \in \mathcal{G} \tag{3.12}
$$

with

$$
\begin{aligned}
Z &= \frac{1}{|g|} \sum_{g \in \mathcal{G}} \left\{ \frac{1}{2} \left[(\chi^{(p)}(g))^2 + \chi^{(p)}(g^2) \right] \right\}^2 && (3.13) \\
&= \frac{1}{|g|} \sum_{g \in \mathcal{G}} \frac{1}{4} \left[(\chi^{(p)}(g))^4 + 2(\chi^{(p)}(g))^2 \, \chi^{(p)}(g^2) + \chi^{(p)}(g^2) \right] . && (3.14)
\end{aligned}
$$

If we assume permutation with respect to index pairs $([ij], [kl] = [kl], [ij])$ the representation reads

$$
D^T(g) = \left[\left(D^{(p)}(g) \otimes D^{(p)}(g) \right)_+ \otimes \left(D^{(p)}(g) \otimes D^{(p)}(g) \right)_+ \right]_+ \quad g \in \mathcal{G} \tag{3.15}
$$

and

$$Z = \frac{1}{|g|}\sum_{g\in\mathcal{G}}\frac{1}{2}\left[\left(\chi^{(p\otimes p)}(g)\right)^2+\chi^{(p\otimes p)}(g^2)\right] \tag{3.16}$$

$$= \frac{1}{|g|}\sum_{g\in\mathcal{G}}\frac{1}{2}\left\{\left[\frac{1}{2}\left(\chi^{(p)}(g)\right)^2+\frac{1}{2}\chi^{(p)}(g^2)\right]^2+\frac{1}{2}\left[\left(\chi^{(p)}(g^2)\right)^2+\chi^{(p)}(g^4)\right]\right\} \tag{3.17}$$

$$= \frac{1}{|g|}\sum_{g\in\mathcal{G}}\frac{1}{8}\left[\left(\chi^{(p)}(g)\right)^4+2\left(\chi^{(p)}(g)\right)^2\chi^{(p)}(g^2)+3\left(\chi^{(p)}(g^2)\right)^2+2\chi^{(p)}(g^4)\right] \tag{3.18}$$

So far we have not discussed axial tensors of higher rank. There is nothing special with them, examples are given in [5] (in German), together with Tables of independent polar tensor components for all point groups. Even more extended Tables are presented in the famous book by Birss [3], where magnetic groups with i-tensors (invariant with respect to time reversal, electric polarization) and c-tensors (change sign tensors with respect to time reversal, magnetization) are discussed.

References

[1] G. Burns, A. M. Glazer. *Space Groups for Solid State Scientists*. Academic Press, 2nd ed. edition, 1990.

[2] J. F. Nye. *Physical Properties of Crystals*. Oxford UP, 1956.

[3] R. Birss. *Symmetry and Magnetism*. North-Holland, Amsterdam, second edition, 1966.

[4] W. A. Wooster. *Tensors and group theory for the physical properties of crystals*. Clarendon Pr., Oxford, 1973.

[5] M. Böhm. *Symmetrien in Festkörpern*. Wiley-VCH, Berlin, 2002.

4 Nonlinear Optical Susceptibilities

All electromagnetic phenomena are governed by the Maxwell equations for the electric and magnetic fields E, D, B, and H:

$$\nabla D = \rho \tag{4.1}$$

$$\nabla B = 0 \tag{4.2}$$

$$\nabla \times E = -\frac{\partial B}{\partial t} \tag{4.3}$$

$$\nabla \times H = j + \frac{\partial D}{\partial t} \tag{4.4}$$

where ρ and j are electric charge and current.

The fields are related by

$$D = \epsilon\epsilon_0 E \quad \text{and} \quad B = \mu\mu_0 H \tag{4.5}$$

where ϵ and μ, the dielectric constant and the relative permittivity, describe material properties. In general, both are second rank tensors. ϵ_0 and μ_0 are the permittivity and the permeability of the vacuum, fundamental physical constants.

Approximations often introduced to simplify calculations include

- $\diamond$ $\mu = 1$ for non-magnetic materials,
- $\diamond$ $\epsilon = 1,\ \mu = 1$ for vacuum,
- $\diamond$ $j = 0$ for isolators,
- $\diamond$ $\rho = 0$ for vanishing charges,
- $\diamond$ $\frac{\partial}{\partial t} = 0$ for the static case.

A more detailed overview is given in the lecture notes on *Linear Response Theory* by P. Hertel [1] and in numerous textbooks in the field.

In the linear case, the polarization **P** may be written in a simple form

$$\mathbf{P}(\mathbf{r}, t) = \epsilon_0 \int_{-\infty}^{\infty} \chi^{(1)}(\mathbf{r} - \mathbf{r}', t - t') \cdot \mathbf{E}(\mathbf{r}', t') d\mathbf{r}' dt' \tag{4.6}$$

where $\chi^{(1)}$ is the linear susceptibility of the medium. Usually monochromatic plane waves are assumed, $\mathbf{E}(\mathbf{k}, \omega) = E(\mathbf{k}, \omega) \exp(i\mathbf{k} \cdot \mathbf{r} - i\omega t)$, then a Fourier transformation applied to Eq. 4.6 yields

$$\mathbf{P}(\mathbf{k}, \omega) = \epsilon_0 \chi^{(1)}(\mathbf{k}, \omega) \mathbf{E}(\mathbf{k}, \omega) \tag{4.7}$$

with

$$\chi^{(1)}(\mathbf{k}, \omega) = \int_{-\infty}^{\infty} \chi^{(1)}(\mathbf{r}, t) \exp(-i\mathbf{k}\mathbf{r} + i\omega t) d\mathbf{r} dt \ . \tag{4.8}$$

The dependence of χ on **k** is only weak, in nearly all practical cases it can be neglected.

4.1 Nonlinear Polarization

In the nonlinear case, **P** can be expanded into a power series of **E** – at least as long as **E** is sufficiently weak

$$\begin{aligned}\mathbf{P}(\mathbf{r},t) = \epsilon_0 &\int_{-\infty}^{\infty} \chi^{(1)}(\mathbf{r}-\mathbf{r}',t-t')\cdot\mathbf{E}(\mathbf{r}',t')d\mathbf{r}'dt' \\ +\epsilon_0 &\int_{-\infty}^{\infty} \chi^{(2)}(\mathbf{r}-\mathbf{r}_1,t-t_1;\mathbf{r}-\mathbf{r}_2,t-t_2)\mathbf{E}(\mathbf{r}_1,t_1)\mathbf{E}(\mathbf{r}_2,t_2)d\mathbf{r}_1dt_1d\mathbf{r}_2dt_2 \\ +\epsilon_0 &\int_{-\infty}^{\infty} \chi^{(3)}(\mathbf{r}-\mathbf{r}_1,t-t_1;\mathbf{r}-\mathbf{r}_2,t-t_2;\mathbf{r}-\mathbf{r}_3,t-t_3)\mathbf{E}(\mathbf{r}_1,t_1) \\ &\times\mathbf{E}(\mathbf{r}_2,t_2)\mathbf{E}(\mathbf{r}_3,t_3)d\mathbf{r}_1dt_1d\mathbf{r}_2dt_2d\mathbf{r}_3dt_3 \\ +&\ldots\end{aligned} \tag{4.9}$$

where $\chi^{(n)}$ is the nth-order nonlinear susceptibility. As in the linear case, the problem can be Fourier transformed. Yet, for **E** now a sum of monochromatic plane waves should be assumed

$$\mathbf{E}(\mathbf{r},t) = \sum_i \mathbf{E}(\mathbf{k}_i,\omega_i)\ , \tag{4.10}$$

yielding for the polarization

$$\mathbf{P}(\mathbf{k},\omega) = \mathbf{P}^{(1)}(\mathbf{k},\omega) + \mathbf{P}^{(2)}(\mathbf{k},\omega) + \mathbf{P}^{(3)}(\mathbf{k},\omega) + \ \ldots \tag{4.11}$$

with

$$\begin{aligned}\mathbf{P}^{(1)}(\mathbf{k},\omega) &= \epsilon_0\chi^{(1)}(\mathbf{k},\omega)\cdot\mathbf{E}(\mathbf{k},\omega)\ , \\ \mathbf{P}^{(2)}(\mathbf{k},\omega) &= \epsilon_0\chi^{(2)}(\mathbf{k}=\mathbf{k}_i+\mathbf{k}_j,\omega=\omega_i+\omega_j)\mathbf{E}(\mathbf{k}_i,\omega_i)\mathbf{E}(\mathbf{k}_j,\omega_j)\ , \\ \mathbf{P}^{(3)}(\mathbf{k},\omega) &= \epsilon_0\chi^{(3)}(\mathbf{k}=\mathbf{k}_i+\mathbf{k}_j+\mathbf{k}_l,\omega=\omega_i+\omega_j+\omega_l) \\ &\qquad \mathbf{E}(\mathbf{k}_i,\omega_i)\mathbf{E}(\mathbf{k}_j,\omega_j)\mathbf{E}(\mathbf{k}_l,\omega_l)\ .\end{aligned} \tag{4.12}$$

The $\chi^{(n)}(\mathbf{k},\omega)$ can be expressed in a similar way as in the linear case as integrals over the respective $\chi^{(n)}(\mathbf{r},t)$. Again, the dependence on **k** can be neglected.

$\chi^{(n)}$ is an $(n+1)$st-rank tensor representing material properties. Using Einstein's summation convention, the above equations may be rewritten in component form, e. g.

$$P_k^{(2)}(\omega) = \epsilon_0\chi_{kmn}^{(2)}(\omega=\omega_i+\omega_j)E_m(\omega_i)E_n(\omega_j)\ . \tag{4.13}$$

4.2 The *Phase-Matching* Problem

We have arrived now at the nonlinear *polarization* of a medium. The fundamental waves generate an oscillating polarization through the medium which oscillates with ω. The phases at different locations are defined and connected by the fundamental waves travelling through the medium. That means that the polarization wave travels through the medium at a velocity $v(\omega_i, \omega_j)$ for the fundamental frequencies ω_i, ω_j.

The local polarization at every location acts as a source of electromagnetic dipole radiation. The generated free waves, yet, travel through the medium at a velocity $v(\omega)$ characteristic for their own frequency ω.

The velocities are defined by the respective refractive indices and – due to the dispersion present in all materials – generally are different. In an extended medium the two relevant waves – polarization wave and generated free wave – thus come out of phase after a typical distance commonly referred to as *coherence length*. The sum free wave is amplified due to constructive interference up to this coherence length, then attenuated due to destructive interference. No efficient generation of nonlinear radiation seems to be possible. Yet, there are some solutions to the problem.

4.3 Mechanisms for the Nonlinear Polarization

As for the linear polarization in matter, various mechanisms are responsible for the nonlinear polarization, too. Depending on the frequencies of the applied fields and of the resulting nonlinear polarizations the possible mechanisms may contribute more or less. At comparably low electromagnetic fields all of these mechanisms (excepts for the last one) can be regarded as being strictly linear, nonlinearities show up when the fields are increased.

Electronic polarization: The distortion of the outer-shell electronic cloud of atoms, ions, and molecules, respectively, in gases, liquids, or solids, compared to the undisturbed state. This mechanism has very fast response time ($< 10^{-15}$ s). Most optical frequency mixing effects such as second harmonic and third harmonic generation, sum-frequency mixing, optical parametric oscillation, four-photon parametric interaction use this mechanism.

Ionic polarization: The contribution from an optical-field induced relative motion (vibration, rotation in molecules, optical phonons in solids) between nuclei or ions. The response time of this mechanism is around 10^{-12} seconds. Examples: Raman resonance-enhanced four-wave-mixing effects, Raman enhanced refractive index change.

Molecular reorientation: It denotes the additional electric polarization contribution from an optical-field induced reorientation of anisotropic molecules in a liquid. The response time of this process is dependent on the rotational viscosity of molecules in the liquid and is approximately 10^{-12}–10^{-13} seconds. Examples: Stimulated Kerr scattering, Kerr-effect related refractive index change.

Induced acoustic motion: It is the polarization contribution from an optical induced acoustic motion related to the so-called electrostriction interaction. The response time of this mechanism is around 10^{-9}–10^{-10} seconds depending on the medium. Examples: Brillouin scattering, self focusing, optical breakdown.

Induced population change: The contribution of electrons to the polarization depends on their eigenstates. Their populations are changed by one-photon or two-photon absorption and by other resonant interactions (e. g. in Raman processes). The response time strongly depends on the respective electronic transition, but is in general slower than in the above discussed mechanisms. Examples are all resonance-enhanced nonlinear processes.

Spatial redistribution of electrons: Excited charge carriers in solids – electrons or holes – can be spatially redistributed due to a spatially modulated light pattern. This is a major effect in all so-called photorefractive materials. The response time depends on the mobility of the carriers and on the internal electric field, in general it is slow compared to the response times discussed up to here. Examples are all processes which can be summarized under the term *Photorefractive Nonlinearity*.

Spatial redistribution of ions: There are some materials where not electrons but – also or instead – ions are redistributed by a spatially modulated light pattern. Of course this effect again is considerably slower. It is only of minor importance within the photorefractive materials.

4.4 The Anharmonic Oscillator as a Qualitative Model

As a crudely qualitative but nevertheless vivid model for the nonlinear polarization one can use the classical anharmonic oscillator. Physically, the oscillator describes an electron bound to a core or an infrared-active molecular vibration. The potential may exhibit anharmonicities of odd or even symmetry as sketched in Fig. 19.

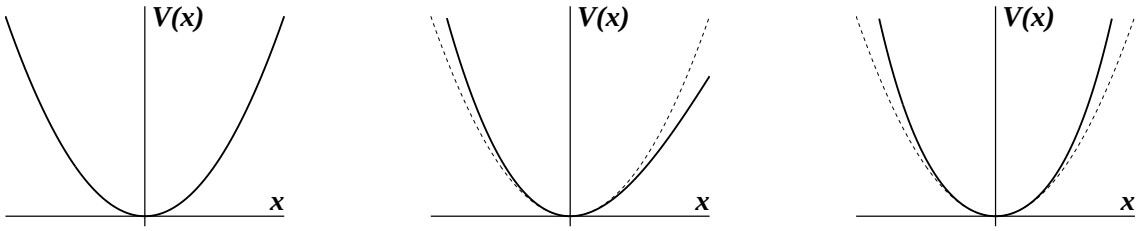

Figure 19: Potential forms for the anharmonic oscillator. Left: harmonic potential $V_h(x) = \frac{a}{2}x^2$, middle: odd-symmetric anharmonicity $V_o(x) = V_h(x) + \frac{b}{3}x^3$, right: even-symmetric anharmonicity $V_e(x) = V_h(x) + \frac{c}{4}x^4$. The dashed curve denotes the respective harmonic part.

The equation of motion for the oscillator in the presence of a driving force F can be written as

$$\frac{d^2x}{dt^2} + \gamma\frac{dx}{dt} + ax + bx^2 + cx^3 = F\ . \tag{4.14}$$

For the harmonic case $b = c = 0$, for an odd-symmetric anharmonicity $b \neq 0$, for an even-symmetric $c \neq 0$. Both b and c are assumed to be small so that they can be treated as perturbations.

As driving force we consider an applied electric field with Fourier components at the frequencies $\pm\omega_1$ and $\pm\omega_2$

$$F = \frac{q}{m}\left[E_1\left(e^{-i\omega_1 t} + e^{i\omega_1 t}\right) + E_2\left(e^{-i\omega_2 t} + e^{i\omega_2 t}\right)\right] . \tag{4.15}$$

q and m are charge and mass of the oscillating particle (electron, ion, etc.).

When we neglect the anharmonic perturbations b and c, we get the first order solution $x^{(1)}$ for x

$$x^{(1)} = \sum_i x^{(1)}(\omega_i) , \qquad x^{(1)}(\omega_i) = \frac{(q/m)E_i}{\omega_0^2 - \omega_i^2 - i\omega_i\gamma} e^{-i\omega_i t} \tag{4.16}$$

where $\omega_0^2 = a$.

For a density of N such classical anharmonic oscillators per unit volume the induced electric polarization is simply

$$\mathbf{P} = Nqx . \tag{4.17}$$

Higher order solutions are obtained by substituting lower order solutions for the nonlinear terms in Eq. 4.14, e. g. $bx^{(1)\,2}$ for bx^2.

First we look at the second order solution in the presence of an odd-symmetric anharmonicity only ($b \neq 0$, $c = 0$). Omitting the first order solution, we use $-bx^{(1)\,2}$ as driving force

$$\frac{d^2x}{dt^2} + \gamma\frac{dx}{dt} + ax = -bx^{(1)\,2} . \tag{4.18}$$

$-bx^{(1)\,2}$ introduces terms with frequencies $2\omega_i$, $\omega_i + \omega_j$, $\omega_i - \omega_j$, $\omega_i - \omega_i = 0$. Thus we have included second-harmonic generation, sum-frequency and difference-frequency generation, and optical rectification. A typical solution (here for second harmonic generation) is of the form

$$x^{(2)}(2\omega_i) = \frac{-b(q/m)^2E_i^2}{(\omega_0^2 - \omega_i^2 - i\omega_i\gamma)^2(\omega_0^2 - 4\omega_i^2 - i2\omega_i\gamma)} e^{-i2\omega_i t} . \tag{4.19}$$

Second we assume that only an even-symmetric anharmonicity is present which means that $b = 0$, $c \neq 0$. We now have to use $-cx^{(1)\,3}$ as driving force

$$\frac{d^2x}{dt^2} + \gamma\frac{dx}{dt} + ax = -cx^{(1)\,3} . \tag{4.20}$$

Obviously the driving force now introduces only terms with an odd number of ωs, e. g. $3\omega_i$, $2\omega_i - \omega_i = \omega_i$, $\omega_i + \omega_j + \omega_k$, $\omega_i + \omega_j - \omega_k$. Thus third-harmonic generation, nonlinear refraction and similar effects are described. Even-symmetric anharmonicities are present in all types of materials, even in isotropic ones like liquids and gases. From the above we can conclude that such materials are only suited for odd-harmonic generation and other odd-order effects.

From Eqs. 4.16, 4.19, and 4.17 we can roughly estimate the ratio between linear and second order nonlinear polarization. If we assume that we are far from any resonance, i. e. $\omega_0 \gg \omega_i$, we find for this ratio

$$\left|\frac{P^{(2)}}{P^{(1)}}\right| \approx \left|\frac{qbE}{m\omega_0^4}\right| . \tag{4.21}$$

For the limit that for a bound electron harmonic and anharmonic force, $m\omega_0^2 x$ and mbx^2, are of the same order of magnitude, one can assume that both are of the order of magnitude of the total binding force of the electron $|qE_{at}|$ (one can show that this is only valid for large anharmonicities b)

$$|qE_{at}| \approx m\omega_0^2 x \approx mbx^2 \tag{4.22}$$

or, eliminating x,

$$|qE_{at}| \approx \frac{m\omega_0^4}{b} . \tag{4.23}$$

Eq. 4.21 then becomes

$$P^{(2)}/P^{(1)} \approx E/E_{at} \tag{4.24}$$

and for the susceptibilities

$$\chi^{(2)}/\chi^{(1)} \approx 1/E_{at} . \tag{4.25}$$

This can be generalized to

$$P^{(n+1)}/P^{(n)} \approx E/E_{at} \quad \text{and} \quad \chi^{(n+1)}/\chi^{(n)} \approx 1/E_{at} . \tag{4.26}$$

The inner-atomic fields E_{at} are in the order of 3×10^{10} V/m [2], thus with $\chi^{(1)} \approx 3$ we arrive at 10^{-10} m/V for the second order nonlinear susceptibility. Some typical measured values are listed in Table 7.1 of Ref. [2]. They range from approximately 10^{-12} m/V for materials with low anharmonicities (Quartz: $\chi^{(2)}_{xxx} = 0.8 \times 10^{-12}$ m/V) up to 10^{-10} m/V for typical nonlinear optical materials ($LiNbO_3$: $\chi^{(2)}_{zzz} = 0.8 \times 10^{-10}$ m/V).

4.5 Structural Symmetry of Nonlinear Susceptibilities

The susceptibility tensors must remain unchanged upon symmetry operations allowed for the medium. This reduces the number of independent and nonzero elements. The most important conclusion from this property is that for all centrosymmetric crystals and for all isotropic media (gases, liquids, amorphous solids) all tensor elements of the even-order susceptibility tensors ($\chi^{(2)}$, $\chi^{(4)}$, ...) must be zero. This has been already shown qualitatively for the model of the anharmonic oscillator in section 4.4. Thus, e. g., no second harmonic generation can be observed in such media. Odd-order susceptibility tensors, yet, will be non-zero and will provide nonlinear effects. Using gases or metal vapors, e. g., only odd-order harmonics can be produced.

4.6 Permutation Symmetry of Nonlinear Susceptibilities

When tensors are multiplied with vectors, usually the order of the vector multiplication can be changed. In nonlinear optics it should not matter which of the fundamental fields is the first to be multiplied. From this, permutation symmetry for the nonlinear susceptibilities follows, for the second order

$$\chi^{(2)}_{ijk}(\omega_1, \omega_2) = \chi^{(2)}_{ikj}(\omega_2, \omega_1) \; , \tag{4.27}$$

or for the third order susceptibility

$$\chi^{(3)}_{ijkl}(\omega_1, \omega_2, \omega_3) = \chi^{(3)}_{iklj}(\omega_2, \omega_3, \omega_1) = \chi^{(3)}_{iljk}(\omega_3, \omega_1, \omega_2) = \chi^{(3)}_{ijlk}(\omega_1, \omega_3, \omega_2) = \ldots \tag{4.28}$$

Besides this trivial one, a more general permutation symmetry can be defined due to time reversal symmetry resulting in relations like

$$\chi^{(2)*}_{ijk}(\omega = \omega_1 + \omega_2) = \chi^{(2)}_{jki}(\omega_1 = -\omega_2 + \omega) = \chi^{(2)}_{kij}(\omega_2 = \omega - \omega_1) \; . \tag{4.29}$$

Time reversal symmetry can be applied as long as absorption can be neglected.

If the dispersion of χ can also be neglected, then the permutation symmetry becomes independent of the frequencies. Consequently, then a very general permutation symmetry exists between different elements of χ: elements remain unchanged under *all* permutations of the Cartesian indices. This so-called *Kleinman's conjecture* or *Kleinman symmetry* [3] reduces the number of independent elements further. Yet, it should be noted that it's a good approximation only at frequencies far from resonances such that dispersion really can be neglected.

4.7 Example: Strontium Barium Niobate

Strontium Barium Niobate is a crystal which is in a ferroelectric phase at room temperature, its point symmetry group is 4mm. The symmetry operations present in the point group include

$$\begin{aligned}
4: \quad & \begin{pmatrix} x & \to & y \\ y & \to & -x \\ z & \to & z \end{pmatrix} \quad \begin{pmatrix} x & \to & -x \\ y & \to & -y \\ z & \to & z \end{pmatrix} \quad \begin{pmatrix} x & \to & -y \\ y & \to & x \\ z & \to & z \end{pmatrix} \\
m_1: \quad & \begin{pmatrix} x & \to & -x \\ y & \to & y \\ z & \to & z \end{pmatrix} \quad \begin{pmatrix} x & \to & x \\ y & \to & -y \\ z & \to & z \end{pmatrix} \\
m_2: \quad & \begin{pmatrix} x & \to & y \\ y & \to & x \\ z & \to & z \end{pmatrix} \quad \begin{pmatrix} x & \to & -y \\ y & \to & -x \\ z & \to & z \end{pmatrix} \; .
\end{aligned} \tag{4.30}$$

The tensor elements transform like products of the respective coordinates, they must remain unchanged under all the transformations listed. The mirror plane m_1 changes x into $-x$ or y into $-y$, thus all elements with an odd number of indices 1 or an odd number of indices 2 have to be zero. The mirror plane m_2 transform x to y and y to x, thus elements where 1s are replaced by 2s have to be equal.

For the second order susceptibility tensor for second harmonic generation, e. g., we arrive at the nonzero elements

$$\chi_{311} = \chi_{322} \,, \quad \chi_{333} \,, \quad \chi_{131} = \chi_{113} = \chi_{232} = \chi_{223} \,. \tag{4.31}$$

All other elements must be zero. Kleinman symmetry further reduces the number of independent elements to two (χ_{311} and equivalent, and χ_{333}).

4.8 Contraction of Indices

Especially for the susceptibility tensor for second harmonic generation it is common to write it in a different form. As the last two indices can be exchanged, there are 18 different elements left from the full set of 27. These 18 are written as a 2-dimensional matrix d_{ij}, the last two indices kl of the elements χ_{ikl} are contracted to one index j such that

$$11 \to 1 \,, \qquad 22 \to 2 \,, \qquad 33 \to 3 \,, \qquad 23, 32 \to 4 \,, \qquad 31, 13 \to 5 \,, \qquad 12, 21 \to 6 \,. \tag{4.32}$$

Using this matrix form of the susceptibility tensor, the second harmonic polarization is written as

$$\begin{pmatrix} P_x \\ P_y \\ P_z \end{pmatrix} = \epsilon_0 \begin{pmatrix} d_{11} & d_{12} & d_{13} & d_{14} & d_{15} & d_{16} \\ d_{21} & d_{22} & d_{23} & d_{24} & d_{25} & d_{26} \\ d_{31} & d_{32} & d_{33} & d_{34} & d_{35} & d_{36} \end{pmatrix} \times \begin{pmatrix} E_x^2 \\ E_y^2 \\ E_z^2 \\ 2E_yE_z \\ 2E_zE_x \\ 2E_xE_y \end{pmatrix} . \tag{4.33}$$

References

[1] P. Hertel. *Linear Response Theory*. University of Osnabrück, 2001. http://www.physik.uni-osnabrueck.de/virtual-campus.html.

[2] Y. R. Shen. *The Principles of Nonlinear Optics*. John Wiley & Sons, Inc., 1984.

[3] D. A. Kleinman. *Nonlinear Dielectric Polarization in Optical Media*. Phys. Rev. **126**, 1977 (1962).

5 Harmonic Generation

One of the most important nonlinear optical processes for technical applications is the generation of harmonics from laser light. We will discuss here second-harmonic generation, widely used for producing visible and near ultraviolet coherent light, and the generation of higher harmonics in gases, used for EUV (extreme ultraviolet) light sources.

5.1 Second-Harmonic Generation

Second-harmonic generation (SHG) was the first experiment in the history of nonlinear optics carried out by Franken et al. [1] soon after the invention of the Ruby laser [2]. Presently it is one of the main applications of nonlinear optics, maybe the only really important one. In the preceding chapter we already discussed some important points concerning the nonlinear susceptibility. The general symmetry arguments have to be adopted in a suitable way for SHG. The responsible tensor is of third rank, materials for SHG thus must be non-centrosymmetric. For practical reasons, usually the d-tensor described is used instead of the more general χ-tensor. Because of a different definition, most authors use the convention $d = \chi/2$ for the tensor elements.

The *local* second harmonic polarization can be calculated according to Eq. 4.12. For the generated second-harmonic intensity, yet, we face the phase-matching problem shortly discussed. Fig. 20 visualizes the principle.

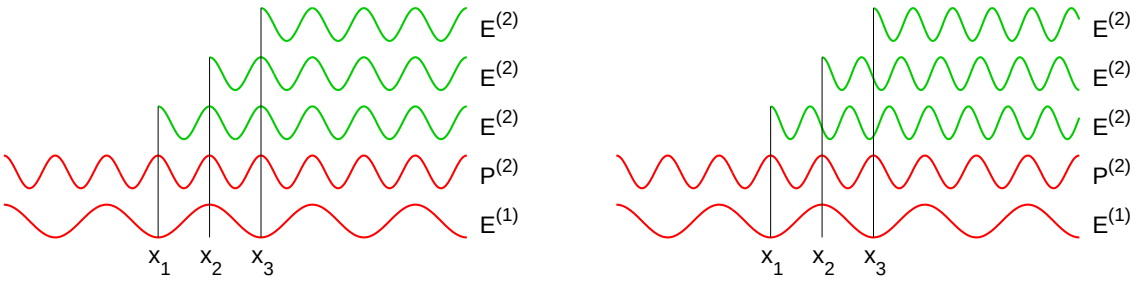

Figure 20: Fundamental wave $E^{(1)}$, induced second-harmonic polarization $P^{(2)}$, and second-harmonic waves $E^{(2)}$, generated at the positions x_1, x_2, and x_3 in a nonlinear material for two different cases. Left: second-harmonic waves travel at the same velocity as the fundamental wave, all are in-phase throughout. Right: different velocities, the usual case, mismatch between the phases of the second-harmonic waves $E^{(2)}$.

Due to dispersion present in all materials, waves of different frequencies travel at different velocities, yielding a phase-mismatch between second-harmonic waves generated at different positions in a nonlinear material. To get the total second-harmonic intensity produced, we have to integrate over the generated waves taking into account the different velocities. For simplicity we omit all pre-factors and all rapidly oscillating factors and calculate only the phase-factors with respect to

$x = 0$. For $E^{(1)}(x)$ and $P^{(2)}(x)$ we can write

$$E^{(1)}(x) = E^{(1)}(0) \cdot e^{-ik_1 x} , \tag{5.1}$$
$$P^{(2)}(x) = \chi E^{(1)}(x) E^{(1)}(x) = \chi E^{(1)}(0) E^{(1)}(0) \cdot e^{-i2k_1 x} . \tag{5.2}$$

Taking $P^{(2)}$ as driving force in a wave equation for $E^{(2)}$ yields

$$E^{(2)}(x) = K' \cdot P^{(2)}(x) = K \cdot E^{(1)}(0) E^{(1)}(0) \cdot e^{-i2k_1 x} \tag{5.3}$$

where the K contains all necessary constants like nonlinear susceptibility or refractive indices.

$E^{(2)}$ now travels through the material with a velocity characteristic for the frequency $\omega_2 = 2\omega_1$ and wave vector k_2. Thus at an arbitrary position x' where we could measure the second-harmonic

$$E^{(2)}(x') = E^{(2)}(x) \cdot e^{-ik_2(x'-x)} = K \cdot E^{(1)}(0) E^{(1)}(0) \cdot e^{-ik_2 x'} e^{-i(2k_1 - k_2)x} . \tag{5.4}$$

Assuming homogeneous material for $0 < x < L$, we have to integrate

$$\begin{aligned} E^{(2)}_{\text{total}}(x') &= K \cdot E^{(1)}(0) E^{(1)}(0) \cdot e^{-ik_2 x'} \int_0^L e^{-i(2k_1 - k_2)x} dx \\ &= K \cdot E^{(1)}(0) E^{(1)}(0) \cdot e^{-ik_2 x'} \frac{1}{i\Delta k} \left[e^{i\Delta k L} - 1 \right] \\ &= K \cdot E^{(1)}(0) E^{(1)}(0) \cdot e^{-ik_2 x'} e^{i\frac{\Delta k}{2} L} \frac{1}{i\Delta k} \left[e^{i\frac{\Delta k}{2} L} - e^{-i\frac{\Delta k}{2} L} \right] \\ &= K \cdot E^{(1)}(0) E^{(1)}(0) \cdot e^{-ik_2 x'} e^{i\frac{\Delta k}{2} L} \cdot \frac{\sin(\Delta k\, L/2)}{\Delta k/2} \end{aligned} \tag{5.5}$$

with

$$\Delta k = k_2 - 2k_1 = \frac{2\pi}{\lambda_2} n(\omega_2) - 2\frac{2\pi}{\lambda_1} n(\omega_1) = \frac{4\pi}{\lambda_1} (n(\omega_2) - n(\omega_1)) . \tag{5.6}$$

λ_1 and $\lambda_2 = \lambda_1/2$ are the wavelengths of the fundamental and second harmonic waves, respectively, in vacuum.

Often a characteristic length, the so-called *coherence length* L_c, is defined. Yet one has to be careful as two different definitions are used – the length after which the sine reaches its maximum or the length after which the sine changes sign. Thus it may be defined as

$$\text{either} \qquad L_c = \frac{\pi}{\Delta k} \qquad \text{or} \qquad L_c = \frac{2\pi}{\Delta k} . \tag{5.7}$$

The generated second-harmonic intensity depends mainly on the phase mismatch Δk, and of course on the square of the input intensity and the tensor elements involved. For the latter often a so-called *effective* tensor element is used which is a suitable combination for the geometry considered

$$I^{(2)} = C \cdot d_{\text{eff}}^2 \cdot I^{(1)\,2} \cdot \frac{\sin^2(\Delta k\, L/2)}{(\Delta k/2)^2} . \tag{5.8}$$

If one is interested in calculating numerical results for $I^{(2)}$, an appropriate constant C may be adopted from textbooks on nonlinear optics.

As already discussed, due to dispersion, Δk in Eq. 5.8 generally is non-zero, the intensity oscillates in a sine-square way. If, however, Δk approaches zero, we have to calculate the limit

$$\lim_{\Delta k \to 0} \frac{\sin(\Delta k\, L/2)}{\Delta k/2} = L\,. \tag{5.9}$$

In this case, the second-harmonic intensity increases quadratically with L – at least as long as we are in the limit of low second-harmonic intensities where $I^{(1)}$ is unchanged (undepleted fundamental wave approximation). The spatial variation of second-harmonic intensities for some characteristic values Δk are sketched in Fig: 21.

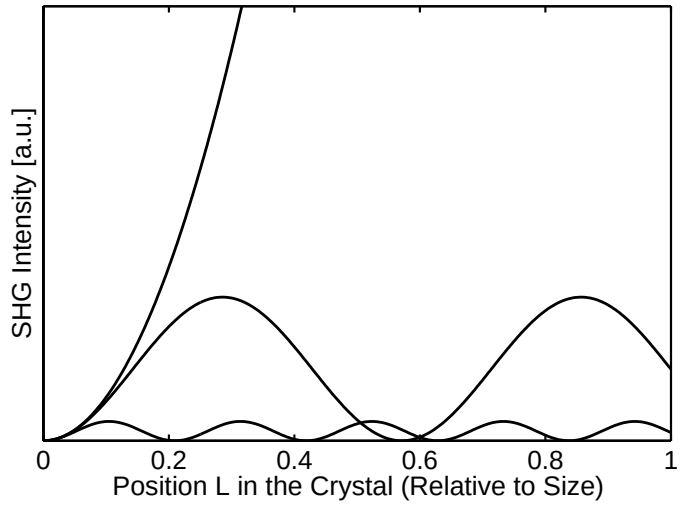

Figure 21: Second-harmonic intensities as a function of the position in the nonlinear material for different Δk.

5.2 Phase Matching

For an efficient generation of second-harmonic light it is highly desirable to achieve phase matching, $\Delta k = 0$. Usually the refractive indices are governed by *normal dispersion* which means that in Eq. 5.6 the difference $n(\omega_2) - n(\omega_1)$ is larger than zero, revealing $\Delta k > 0$. One way out is to utilize the birefringence which is present in crystals of all symmetry classes except the cubic one. *Uniaxial* classes with two different principal refractive indices include the tetragonal, hexagonal and trigonal ones; *biaxial* classes, where all three principal indices are different, include the orthorhombic, monoclinic and triclinic ones.

The refractive index of a material is derived from the linear susceptibility, a second rank tensor. This tensor can be visualized by a general ellipsoid – general means that all three axes of the ellipsoid are of different lengths and that the orientation is arbitrary. However, this ellipsoid has to be

compatible with the point symmetry of the material regarded. That means that certain symmetry elements may fix the orientation of the ellipsoid and may force two or all three axes to be equal. This reveals the above classification. In all uniaxial classes, the orientation of the ellipsoid is fixed, and the ellipsoid is rotationally symmetric. In the biaxial classes where all three axes are different in length, the orientation is fixed for orthorhombic crystals, one axis is fixed for monoclinic crystals, and the orientation is completely free for triclinic ones. For the latter two cases, moreover, the orientation is wavelength dependent.

The **k**-vector of light propagating in the material defines a plane perpendicular to it through the center of the ellipsoid. This plane intersects the ellipsoid yielding an ellipse as intersection curve. The directions of the major and minor axes of this ellipse define the two polarization directions allowed, the length of these axes determine the respective refractive indices. These two different indices for every crystallographic direction can be plotted as index surfaces which reveal the two refractive indices as intersections with the respective **k**-vector direction.

This directional dependence of the refractive indices for the two cases – uniaxial and biaxial – is schematically shown in Fig. 22. For every direction of the wave vector in an uniaxial or biaxial crystal two different refractive indices are found which are valid for the two light polarizations possible. The two refractive indices define the two possible velocities of light – a maximal and a

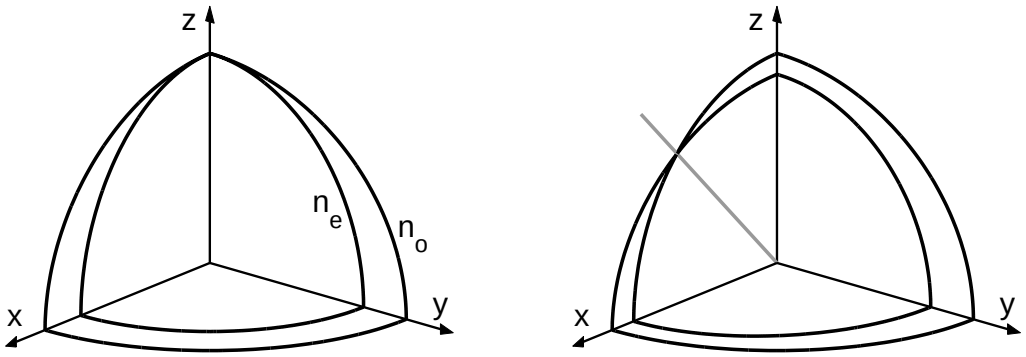

Figure 22: Refractive index surfaces in an uniaxial crystal (left) and in a biaxial one (right). The two surfaces indicate the refractive indices for the respective crystallographic directions.

minimal one – for every propagation direction. Two fixed polarization directions inside the crystal, perpendicular to each other, are connected with the two refractive indices. There are obvious distinct exceptions to this general rule of two different refractive indices. For the uniaxial case in the left drawing light propagating along the crystallographic z-axis finds only one refractive index. The same is valid in the biaxial case for light travelling along the direction denoted by the gray line in the right drawing. For these special propagation directions arbitrary light polarizations are possible. These crystallographic directions are called the *optic axes*. There is one in uniaxial crystals – the z-axis – and there are two in biaxial crystals – the gray line and its symmetry equivalent.

Utilizing the birefringence of a material, it may be possible to find propagation directions where the velocities of fundamental and harmonic waves are identical. Drawing the index surfaces for fundamental and harmonic frequencies, these directions are found as the intersection curves be-

tween the index surfaces. Fig. 23 shows this for an uniaxial material, one of the simplest cases. The index surfaces for the ordinary index at the fundamental frequency, $n_o^{(1)}$, and for the extraordinary index at the harmonic frequency, $n_e^{(2)}$, are sketched, the intersection curve is a circle, all propagation directions with a fixed angle Θ versus the z-axis are phase-matched.

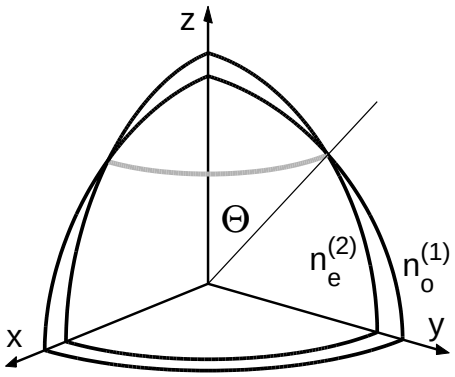

Figure 23: Refractive index surfaces for the ordinary index at the fundamental frequency, $n_o^{(1)}$, and for the extraordinary index at the harmonic frequency, $n_e^{(2)}$ in a uniaxial material with so-called negative birefringence ($n_e < n_o$). The gray intersection curve (circular in the uniaxial case) determines the phase-match angle Θ.

The idealized conditions sketched in Fig. 23, which enable phase matching, *may* be reality for certain materials, yet they *need* not. To check whether phase matching is really possible, one has to consider the dispersion behavior of the material. Typical dispersion curves for uniaxial crystals are sketched in Fig. 24. A fundamental wavelength of 1000 nm, consequently a harmonic at 500 nm are assumed. Low birefringence (left) inhibits phase matching, higher birefringence (right) allows it. Or – to put it in other terms – every birefringent material has a certain restricted wavelength range with a characteristic short-wavelength limit, in which phase-matching is possible.

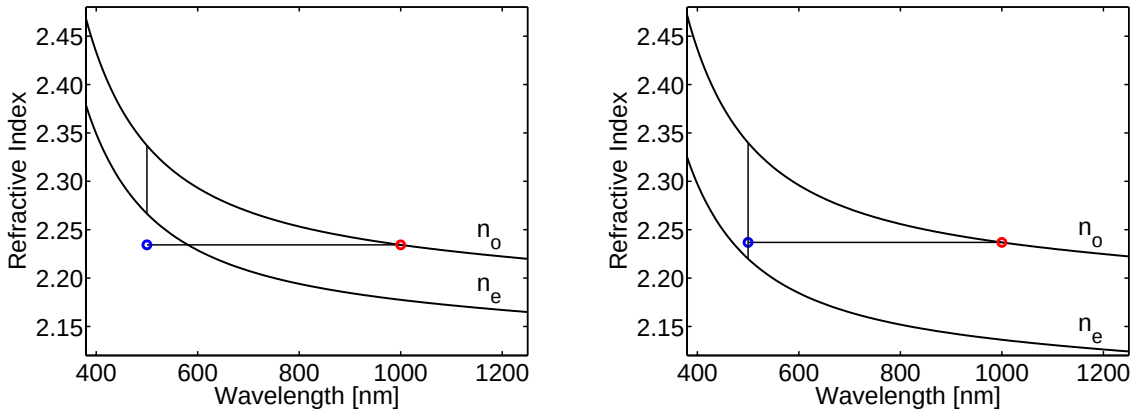

Figure 24: Dispersion of the refractive indices in uniaxial crystals. Left: low birefringence, right: higher birefringence. The refractive index for the ordinary fundamental wave is fixed, the index for the extraordinary harmonic wave can be angle-tuned along the vertical lines drawn.

The refractive index of the harmonic beam is defined as a function of the angle Θ as

$$\frac{1}{n_e^2(\Theta)} = \frac{\cos^2\Theta}{n_0^2} + \frac{\sin^2\Theta}{n_e^2} \,. \tag{5.10}$$

From Eq. 5.10, in turn the phase-matching angle Θ can be deduced demanding a value $n_e(\Theta)$ at the harmonic wavelength to be equal to n_o at the fundamental wavelength. A *real* solution for Θ then indicates that we are inside the wavelength range where phase matching is possible.

The above considerations assume that the two relevant fundamental waves are identical. This is referred to as *Type I* phase matching. Instead, two different fundamentals can be combined which usually are split from one incident wave. We then speak of *Type II* phase matching.

The angle Θ also determines the effective tensor element d_{eff} used in Eq. 5.8. A suitable combination defined by the polarization directions involved has to be used.

Besides the phase-matching issues discussed, some more conditions have to be fulfilled to make a material suitable for efficient second-harmonic generation:

Absorption: The material considered must not absorb both at the fundamental and the harmonic wavelength. This is usually automatically fulfilled as near the absorption edge of a material the refractive indices rise considerably and thus prevent phase matching.

Susceptibility Tensor: Trivially, the point symmetry of the crystal must allow for at least one nonzero tensor element contributing to the geometry necessary for phase matching.

5.3 Quasi Phase Matching

Already in one of the first theoretical publications on nonlinear optics [3], Bloembergen and coworkers discussed a different method to achieve phase matching for nonlinear optical processes, especially for second-harmonic generation. They proposed to reverse the sign of the respective tensor element periodically after an appropriate crystal thickness. In ferroelectric materials this can be done by an antiparallel poling of crystal regions, ferroelectric domains. The geometry for a typical example (lithium niobate or lithium tantalate) is sketched in Fig. 25.

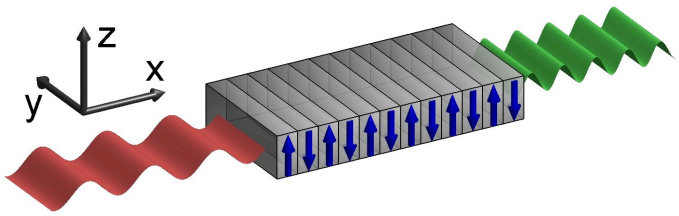

Figure 25: Periodically poled domain structure for second-harmonic generation in materials like lithium niobate or lithium tantalate.

The usage of such *periodically poled* structures is commonly referred to as *quasi phase matching*. The momentum conservation law is fulfilled with the help of the additional vector $\mathbf{K}$ which describes the periodicity of the antiparallel domains:

$$\mathbf{k}_2 = \mathbf{k}_1 + \mathbf{k}_1' + \mathbf{K} \,. \tag{5.11}$$

The second-harmonic intensity achieved through the periodically poled geometry is depicted in Fig. 26. The intensity dependencies are calculated for phase-matched, quasi-phase-matched, and

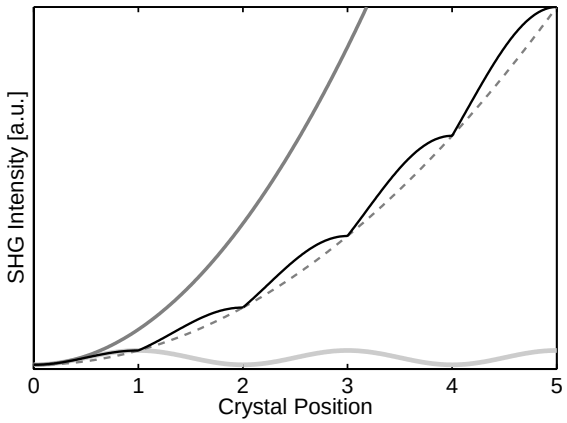

Figure 26: Intensities of phase-matched (dark gray parabola), quasi-phase-matched (black curve), and non-phase-matched SHG (light gray), assuming identical tensor elements and identical beam geometries.

non-phase-matched conditions under the assumption of identical tensor elements d involved.

For *real* SHG materials, however, the situation often can be dramatically improved when large tensor elements can be used which do not suit conventional phase matching. Let us look at lithium niobate as an example. For phase-matched SHG from 1000-nm light the tensor element d_{31} is used with an absolute value of about 4.3 pm/V [4]. The effective d has approximately the same value, as the phase matching angle is nearly 90°. In a suitable periodically poled domain pattern, yet, quasi phase matching can be attained using the tensor element d_{33} with an absolute value of approximately 27 pm/V [4]. For quasi phase matching an effective d may also be defined using the approximation drawn as dashed parabola in Fig. 26, it is the original d multiplied by $2/\pi$. Thus we arrive at d_{eff} of approximately 17 pm/V, four times the value of d_{33}, yielding a sixteen fold second harmonic intensity. Fig. 27 shows the two dependencies.

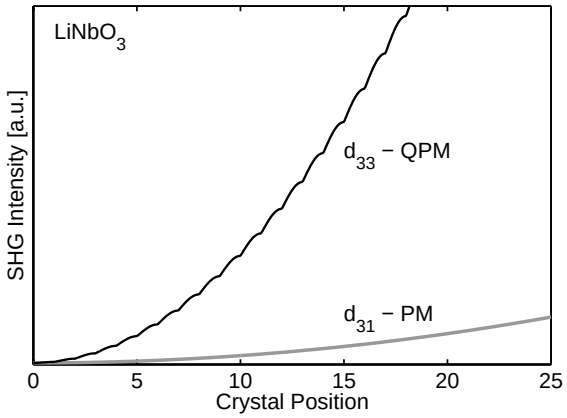

Figure 27: Case study lithium niobate: Comparison of the intensities of phase-matched and quasi-phase-matched SHG, using d_{31} and d_{33}, respectively. For the calculations ideal conditions are assumed: a phase-matching angle of 90° for the PM, and an exact periodically poled domain pattern without any deterioration due to domain walls for the QPM second-harmonic intensity.

Fig. 27 clearly demonstrates the attractiveness of quasi-phase-matching geometries. They gained increasing interest in the recent years because of several reasons:

- Successful techniques for the fabrication of periodically poled structures have been devel-

oped [5].

- Nonlinear optical materials – especially lithium niobate and lithium tantalate – have been improved to facilitate poling.
- The demand for doubling of low light intensities has increased due to the rapid development of semiconductor lasers.
- Quasi phase matching extends the wavelength range for nonlinear optical processes up to the full transparency range of the material.

It should be emphasized that the technique is only applicable to ferroelectric nonlinear optical materials, thus is not suitable for a number of classical materials.

A periodically poled structure is mathematically described by a square function, and in the fourier transform of such a square function all odd harmonics of the base periodicity are present. Thus a periodically poled structure is also usable in higher order [6]. Besides odd harmonics of the square function, even harmonics can be reached by changing the 'duty cycle' appropriately. For higher orders, $\mathbf{K}$ in Eq. 5.11 has to be replaces by $m\mathbf{K}$ where m is the order. Compared to first order, the effective d is reduced by this factor m. Therefore higher orders are only used when it is not possible to fabricate structures for first order.

5.4 Walk-Off

A well-known effect in birefringent materials is visualized in Fig. 28: Unpolarized light propagating in an arbitrary direction is refracted in two different ways (*double refraction*).

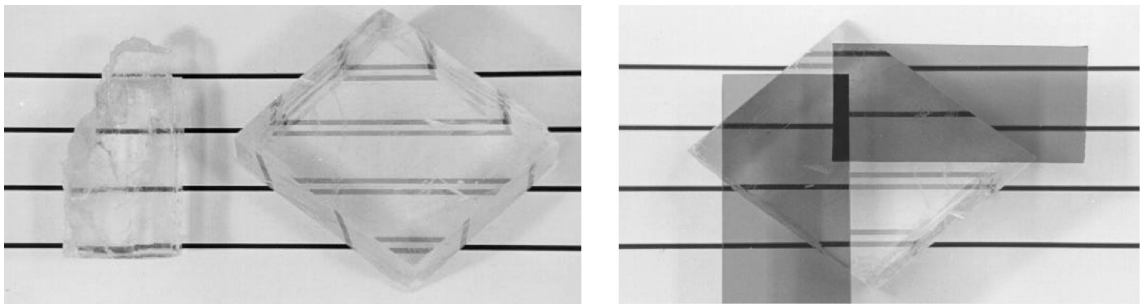

Figure 28: Double refraction: The left picture shows the propagation of unpolarized light through an optically isotropic (left) and an anisotropic crystal (right) – calcite. In the right picture two polarizers are used to select ordinary and extraordinary light polarization. Picture taken from Ref. [7].

Fig. 28 shows this *double refraction* for calcite, a crystal with point group 32/m – thus optically uniaxial. Inside the crystal, the light is split into two parts for the two possible polarizations. The ordinary light passes straightly, the extraordinary one is distinctly displaced.

As discussed in the subsection about phase matching, for second-harmonic generation birefringent crystals are used. Ordinary and extraordinary polarizations have to be applied for the two waves, fundamental and harmonic, to match the relevant refractive indices. Thus we do suffer the described problem of *double refraction* which is called *walk-off* in the field of nonlinear optics as it causes a geometric walk-off of one beam from the other one. Fig. 29 shows such a walk-off geometry for an ordinary fundamental and an extraordinary harmonic beam in an arbitrary crystal direction of a uniaxial crystal. The effect of the walk-off is a reduction of that interaction volume

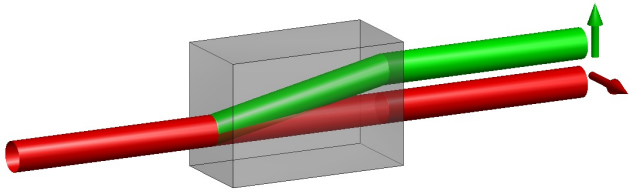

Figure 29: Walk-Off: Ordinarily polarized fundamental and extraordinarily polarized harmonic beam. The regime of quadratic intensity increase is restricted to the overlapping volume between the two beams. It decreases when the fundamental beam is strongly focussed. As simplification only the part of the harmonic beam generated in the entrance region of the crystal is drawn, the contribution of the successive regions is omitted.

where the second-harmonic intensity increases quadratically as a function of crystal length. The regime of quadratic increase is restricted to the overlapping volume between fundamental and harmonic beam, i. e. to an effective length L_e. For a crystal of length L the total intensity then scales with $L \cdot L_e$ instead of L^2 (see Eqs. 5.8 and 5.9).

For a qualitative description of the walk-off, the Maxwell equations have to be concerned:

$$\nabla \times \mathbf{E} = -\dot{\mathbf{B}} \,, \quad \nabla \times \mathbf{H} = \dot{\mathbf{D}} + \mathbf{J} \,, \quad \nabla \mathbf{D} = \rho \,, \quad \nabla \mathbf{B} = 0 \,. \tag{5.12}$$

Assuming monochromatic plane waves

$$\mathbf{E}(\mathbf{r}, t) = \mathbf{E}_0 e^{i(\omega t - \mathbf{kr})} \,, \quad \mathbf{H}(\mathbf{r}, t) = \dots \,, \quad \mathbf{D}(\mathbf{r}, t) = \dots \,, \quad \mathbf{B}(\mathbf{r}, t) = \dots \tag{5.13}$$

and no charges and currents, we arrive at

$$\nabla \mathbf{D} = \mathbf{k} \cdot \mathbf{D} = 0, \quad \nabla \mathbf{B} = \mathbf{k} \cdot \mathbf{B} = 0 \tag{5.14}$$

and

$$\nabla \times \mathbf{E} = \mathbf{k} \times \mathbf{E} = -\dot{\mathbf{B}} = -i\omega \mathbf{B} \,, \quad \nabla \times \mathbf{H} = \mathbf{k} \times \mathbf{H} = \dot{\mathbf{D}} = i\omega \mathbf{D} \,. \tag{5.15}$$

Assuming further that we are not disturbed by magnetics, i. e. that the relative permeability is $\mu = 1$, thus $\mathbf{B} = \mu_0 \mathbf{H}$, from Eqs. 5.14 and 5.15 follows that **k**, **D** and **B** are perpendicular to each other. Due to Eq. 5.15 (left) **B** is perpendicular to **E**, thus **k**, **E** and **D** are lying in the same plane perpendicular to **B**. **D** and **E** are connected by the permittivity ϵ

$$\mathbf{D} = \epsilon_0 \epsilon \mathbf{E} \tag{5.16}$$

where ϵ is a second rank tensor of the form

$$\epsilon = \begin{pmatrix} \epsilon_{11} & 0 & 0 \\ 0 & \epsilon_{22} & 0 \\ 0 & 0 & \epsilon_{33} \end{pmatrix} . \tag{5.17}$$

For optically isotropic materials, $\epsilon_{11} = \epsilon_{22} = \epsilon_{33}$, thus always $\mathbf{E} \parallel \mathbf{D}$. For uniaxial materials, $\epsilon_{11} = \epsilon_{22}$, thus $\mathbf{E} \parallel \mathbf{D}$ for ordinary polarization and $\mathbf{E} \nparallel \mathbf{D}$ for extraordinary polarization.

The direction of energy flow is defined by the Poynting vector

$$\mathbf{S} = \mathbf{E} \times \mathbf{H} \tag{5.18}$$

which for extraordinary polarization thus is not parallel to the **k**-vector – we have walk-off. This uniaxial situation is sketched in Fig. 30.

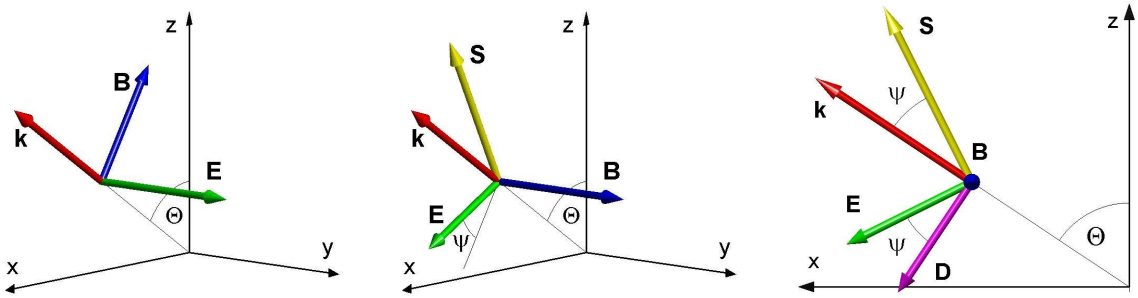

Figure 30: Light propagation in a uniaxial material, the optical axis is in z-direction. Left: Ordinary polarization, **E** *and* **D** *(not shown) are parallel to each other and perpendicular to* **k**. *Middle: Extraordinary polarization,* **E** *not perpendicular to* **k**, *thus* **S** *not parallel to* **k** *– walk-off. Right: only xz-plane shown. ψ is the walk-off angle.*

The walk-off angle usually is in the order of some degrees. Quantitative formulas are given in many articles and textbooks for the various doubling geometries. For the case of negative birefringent materials (ordinary fundamental, extraordinary harmonic wave) and the usual case of Type I phase matching,e. g., Boyd et al. [8] give the formula

$$\tan\psi = \frac{1}{2}(n_\omega^o)^2 \left\{ \frac{1}{(n_{2\omega}^e)^2} - \frac{1}{(n_{2\omega}^0)^2} \right\} \sin 2\Theta \, . \tag{5.19}$$

Eq. 5.19 shows that there is no walk-off, i. e. the walk-off angle ψ will be zero, for $\Theta = 0$ and for $\Theta = 90°$. In uniaxial crystals that means propagation along and perpendicular to the optical axis, respectively. With **k** along the optical axis of course no phase matching is possible. However, it might be possible for **k** perpendicular to it if the magnitude of the birefringence suits. Often this can be tuned within certain limits by varying the temperature. This sort of phase matching is known as 90° phase matching or temperature phase matching. As the two relevant refractive index surfaces in this case do not intersect, instead are tangent to each other, thus allowing for a larger angle uncertainty, it is also referred to as *Non Critical Phase Matching*.

There is a second type of geometries where walk-off is completely absent – that's in all quasi-phase-matching schemes. The periodically poled structures there are always made for a wave propagation along a highly symmetric crystal direction. To make use d_{33} in lithium niobate, e. g., the beams propagate perpendicular to the c-direction of the crystal, allowing the polarization of both, fundamental and harmonic wave, respectively, to be in c-direction. This complete absence of walk-off problems is an important additional advantage of quasi-phase-matching configurations.

5.5 High-Order Harmonic Generation

For an efficient generation of harmonic light commonly crystals are used which show large nonlinear susceptibilities. For the generation of even harmonics, e. g. the second harmonic, these crystals, in addition, have to be acentric. A very crucial condition, however, is good transparency, the absence of absorption, at both the fundamental and harmonic wavelengths. In solids, this can be accomplished down to approximately 150 nm. For shorter wavelengths, therefore, one has to use other arrangements.

Besides the scientific interest, shorter wavelengths are important at least in two fields of current optical applications:

- Lithographical techniques for the fabrication of integrated circuits are limited by the wavelength of light employed. Presently excimer laser light of 192 nm is used in combination with silica optics, the next step will be 157 nm in combination with calcium fluoride optics. This will be the limit of excimer lasers and conventional optics. Beyond this limit, new light sources (and new optical concepts) are in demand.

- For many studies – especially in biological systems – one would like to have single short pulses of X-rays. A very interesting X-ray wavelength region is the so called 'water window' (3–4 nm) where water and carbon have a reduced absorption. This allows diffraction and absorption imaging of biological systems on a molecular scale, and – if pulses can be used – with an extremely good time resolution.

To accomplish the generation of harmonic light well below 150 nm, media transparent in this region – gases or clusters – have to be used. Atoms, molecules, clusters in general are centrosymmetric or even isotropic, thus only odd harmonics are generated. For a good conversion efficiency, the light of a pulsed high-power laser is focused onto the gaseous medium. Doing this, the electromagnetic field becomes of the same magnitude as the Coulomb field, which binds a 1s electron in a Hydrogen atom (5.1×10^9 Vm^{-1}). At such high fields various nonlinear phenomena can happen [9], three typical processes are sketched in Fig. 31:

- Electrons initially in the ground state absorb a large number of photons, many more than the minimum number required for ionization, thus being ionized with a high kinetic energy. This process, shown for the first time in 1979 [10], is called Above Threshold Ionisation (ATI).

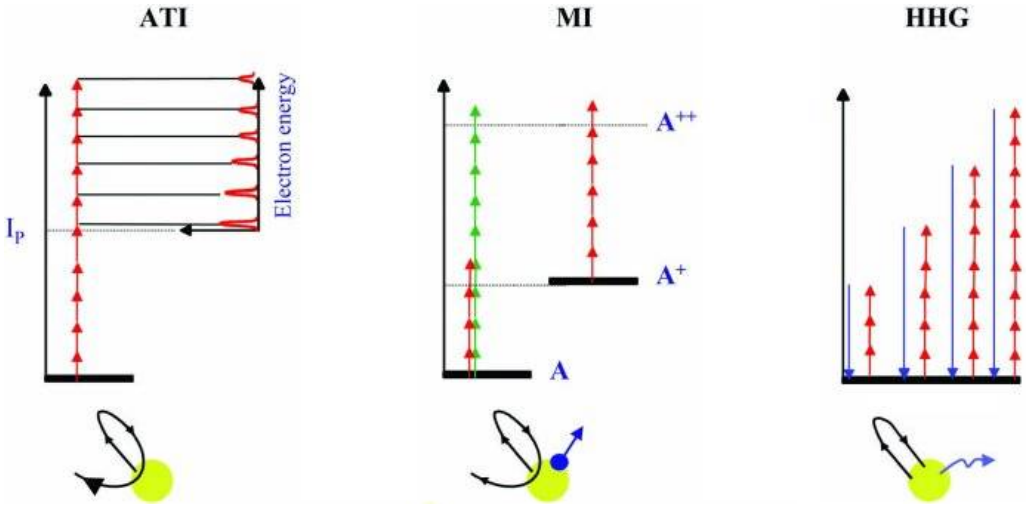

Figure 31: Excitation processes in atoms in strong laser fields [9]. ATI: above threshold ionization, MI: multiple ionization, HHG: high-order harmonic generation.

- Not only one, but many electrons can be emitted from atoms subject to strong laser fields. They can be emitted one at a time, in a sequential process, or simultaneously, a mechanism called direct, or non-sequential. Double ionization of alkaline earth atoms was observed as early as in 1975 [11] and the first evidence for non-sequential ionization of rare gas atoms was first demonstrated in 1983 [12].

- Finally, efficient photon emission in the extreme ultraviolet (EUV) range, in the form of high-order harmonics of the fundamental laser field (HHG), shown for the first time in 1987 [13, 14], can occur.

The described processes are mutually competing, all are scaling with a high power of the incident light intensity. Only the third one (HHG) leads to the generation of coherent EUV light.

About the spectrum generated, Anne L'Huillier, one of the pioneers in this field, writes [9]: *A high-order harmonic spectrum consists of a sequence of peaks centered at frequency $q\omega$, where q is an odd integer. Only odd orders can be observed, owing to inversion symmetry in an atomic gas. A HHG spectrum has a characteristic behavior: A fast decrease for the first few harmonics, followed by a long plateau of harmonics with approximately constant intensity. The plateau ends up by a sharp cut-off. Most of the early work on harmonic generation concentrated on the extension of the plateau, i. e. the generation of harmonics of shorter wavelength. Today, harmonic spectra produced with short and intense laser pulses extend to more than 500 eV, down to the water window below the carbon K-edge at 4.4 nm. A large effort has been devoted to optimize and characterize the properties of this new source of EUV radiation. A milestone in the understanding of HHG processes was the finding by Kulander and coworkers in 1992 [15] that the cut-off position in the harmonic spectrum follows the universal law $E_{\max} \approx I_p + 3U_p$. This result was immediately interpreted in terms of the simple man's theory, and led to the formulation of the strong field*

approximation (SFA). A realistic description of HHG involves, however, not only the calculation of the single atom response, but also the solution of propagation (Maxwell) equations for the emitted radiation.

Simplified, the above expression for $E_{\max}$ means that the maximum energy in the generated harmonic spectrum corresponds to the maximum energy imposed on a quasi-free electron by the electromagnetic field of the incident laser pulse. A schematic sketch of this *strong field approximation* is given in Fig. 32. In the strong electromagnetic field of the focused laser beam the atomic

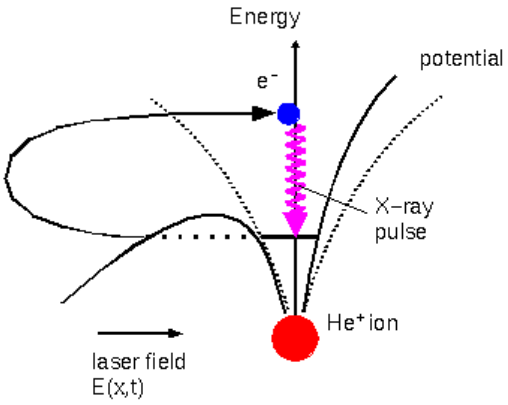

Figure 32: Potential distortion in an extremely strong light field. An electron is accelerated in the strong field and produces X-rays when falling back to the ionic core (picture taken from Ref. [16]).

potential is highly distorted, an electron is accelerated. When the field reverses, the electron can fall back to the ionic core and emit photons during the collision process. The result is a burst of X-rays. This process repeats itself many times over the duration of the laser pulse each time the electromagnetic field reverses sign. As shown in Fig. 33, the X-ray pulses itself are significantly shorter (sub-femtosecond) than the period of the original electromagnetic wave. Using

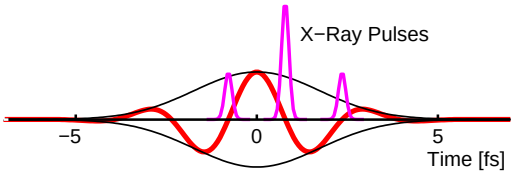

Figure 33: Electromagnetic field oscillation in an ultrashort light pulse. Near the zero crossings bunches of X-rays are generated.

extremely short light pulses will produce a single X-ray pulse in the attosecond regime for each of the incident light pulse.

The wavelength of the emitted light depends on the amount of energy acquired by the electrons over a half-cycle. Yet, despite the similarity to bremsstrahlung no continuous X-ray spectrum is generated. Due to the short overall interaction time the excitation and the X-ray generation are not independent from each other. Thus conservation laws and symmetry relations have to be obeyed, yielding peaks at odd harmonics of the fundamental frequency.

Several techniques can be used to enhance special regions in the generated X-ray spectrum. For lower energies, e. g., enhancement due to resonances in the electronic potential scheme is possible. Of course this doesn't work at higher energies where the electrons are regarded as quasi-free. And, albeit not so expressed as in the case of nonlinear crystals, phase matched [17] and quasi phase

matched arrangements [18] are important enhancement schemes also in the case of harmonic generation in gases.

References

[1] P. A. Franken, A. E. Hill, C. W. Peters, G. Weinreich. *Generation of Optical Harmonics*. Phys. Rev. Lett. **7**, 118 (1961).

[2] T. H. Maiman. *Stimulated Optical Radiation in Ruby*. Nature **187**, 493–494 (1960).

[3] J. A. Armstrong, N. Bloembergen, J. Ducuing, P. S. Pershan. *Interactions between Light Waves in a Nonlinear Dielectric*. Phys. Rev. **127**, 1918–1939 (1962).

[4] David A. Roberts. *Simplified Characterization of Uniaxial and Biaxial Nonlinear Optical Crystals: A Plea for Standardization of Nomenclature and Conventions*. IEEE J. Quantum Electron. **QE-28**, 2057 (1992).

[5] V. Ya. Shur, E. L. Rumyantsev, E. V. Nikolaeva, E. I. Shishkin, R. G. Batchko, M. M. Fejer, R.L. Byer. *Recent Achievements in Domain Engineering in Lithium Niobate and Lithium Tantalate*. Ferroelectrics **257**(191–202) (2001).

[6] M. M. Fejer, G. A. Magel, D. H. Jundt, R. L. Byer. *Quasi-Phase-Matched Second Harmonic Generation Tuning and Tolerances*. IEEE J. Quantum Electron. **QE-28**, 2631 (1992).

[7] Jörg Schmiedmayer. *Laser Physics and Photonics*. University of Heidelberg, 2002. http://www.physi.uni-heidelberg.de/ schmiedm/Vorlesung/LasPhys02.

[8] G. D. Boyd, A. Ashkin, J. M. Dziedzic, D. A. Kleinman. *Second-Harmonic Generation of Light with Double Refraction*. Phys. Rev. **137**, 1305 – 1320 (1965).

[9] Anne L'Huillier. *Atoms in Strong Laser Fields*. Europhysics News **33**, No. 6 (2002).

[10] P. Agostini, F. Fabre, G. Mainfray, G. Petite, N. K. Rahman. *Free-Free Transitions Following Six-Photon Ionization of Xenon Atoms*. Phys. Rev. Lett. **42**, 1127 (1979).

[11] V. V. Suran, I. P. Zapesochnyi. Sov. Tch. Phys. Lett. **1**, 420 (1975).

[12] A. L'Huillier, A. Lompre, G. Mainfray, C. Manus. *Multiply charged ions induced by multi-photon absorption in rare gases at 0.53 μm*. Phys. Rev. A **27**, 2503 (1983).

[13] A. McPherson, G. Gibson, H. Jara, U. Johann, T. S. Luk, I. A. McIntyre, K. Boyer, C. K. Rhodes. J. Opt. Soc. Am. B **4**, 595 (1987).

[14] M. Ferray, A. L'Huillier, X. F. Li, L. A. Lompré, G. Mainfray, C. Manus. J. Phys. B: At. Mol. Opt. Phys. **21**, L31 (1988).

[15] J. K. Krause, K. J. Schafer, K. C. Kulander. *High-order harmonic generation processes from atoms and ions in the high intensity regime*. Phys. Rev. Lett. **68**, 3535 (1992).

[16] *Ultrafast X-ray Generation via Harmonic Generation*. Vrije Universiteit Amsterdam. http://www.nat.vu.nl/atom/x-ray.html.

[17] Katsumi Midorikawa, Yusuke Tamaki, Jiro Itatani. *Phase-matched high-order harmonic generation with self-guided intense femtosecond laser pulses*. RIKEN Review **31**, 38 (2000).

[18] A. Paul, R. A. Bartels, R. Tobey, H. Green, S. Weiman, I. P. Christov, M. M. Murmane, H. C. Kapteyn, S. Backus. *Quasi-phase-matched generation of coherent extreme-ultraviolet light*. Nature **421**, 51 – 54 (2003).

6 Measurement of Nonlinear Optical Properties

Nonlinear optical materials are important for many applications in optics. Therefore an intensive search for new, better materials is still in progress in many research institutes. To characterize these new materials, several techniques have been developed which are widely applied [1]. Various properties are of importance. If a material should be usable, e. g., for second-harmonic generation, it should belong to a non-centrosymmetric point group. Thus a test for this should be possible at a very early state, the powder technique may be used for this purpose. All other investigation methods need larger crystals which are more difficult and time-consumptive to fabricate. Larger crystals in general are also necessary for the investigation of the *linear* optical properties important for nonlinear optical applications like transmission range and refractive index.

6.1 Powder Technique

This technique is described in the comprehensive article *A Powder Technique for the Evaluation of Nonlinear Optical Materials* by S. K. Kurtz and T. T. Perry in 1968 [2]. Since that time it is widely used as one of the simplest methods for a rapid classification of new materials. For the application of the technique the material is only required in powder form (which is easily available in most cases). Thus it can be applied at a very early state after the first fabrication of a new material, for instance in a chemists lab. The basic configuration for powder SHG is shown in Fig. 34 (the figure is taken from the original article, in a present-day setup several parts would be replaced by up-to-date ones).

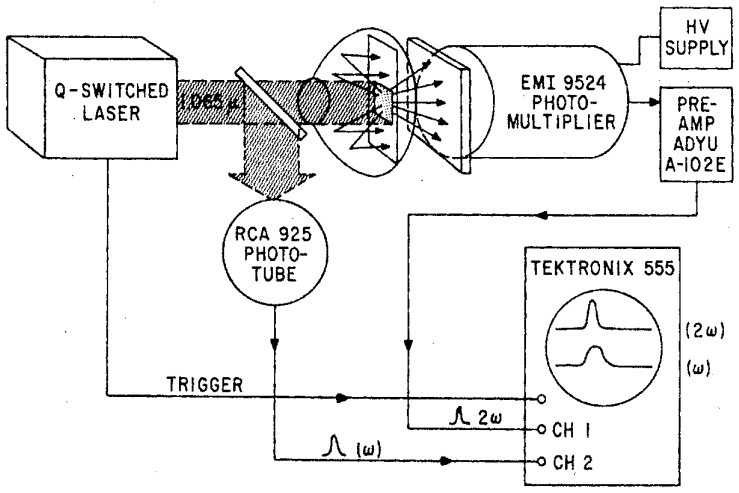

Figure 34: Setup for studying the second-harmonic generation in powder samples.

Light from a Q-switched Nd:YAG laser is directed onto the powder sample, the second-harmonic light is collected by appropriate optics and – after filtering out the fundamental light – detected by a photomultiplier. In this original setup the photomultiplier signal and a monitor signal from the fundamental beam are displayed on an oscilloscope.

In the powder sample the light, fundamental and harmonic, is randomly scattered. This scattering can be greatly reduced when the powder is immersed in a liquid of similar refractive index. Usually, however, immersion is regarded as an additional complication, and, what is more important, it is difficult to find liquids with matching refractive index – especially when working with materials of high refractive index and/or large birefringence. Thus the usual way is to work without immersion. The scattering leads to an angular distribution, which is similar to that of a planar radiator obeying Lambert's cosine law, with an appreciable amount in backward direction. This angular dependence is sketched in Fig. 35.

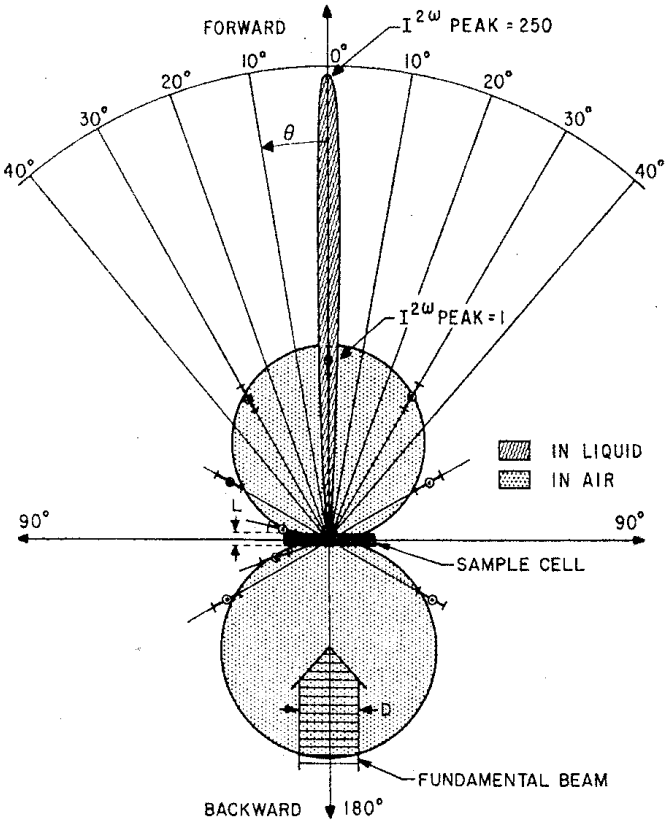

Figure 35: Angular distribution of second harmonic generated in a powder sample (picture taken from [2]). When the powder is immersed in an index-matching liquid, a narrow angular distribution in forward direction shows up, otherwise a broad angular distribution in forward and in backward direction is found.

In a practical application it is thus advisable to collect the generated light from all spatial directions. This can be done by placing the sample within an integrating Ulbricht sphere [3, 4] which collects a certain amount of light from all directions.

The generated harmonic intensity depends in a characteristic way on the average particle size in the powder. This size dependence is different for materials which are phase matchable and those which are not. The two dependences are schematically sketched in Fig. 36.

A detailed theory for these dependences can be found in [2], to understand it in principle, we can find simpler arguments. Let us assume that we have a powder volume V completely filled with randomly oriented particles of size r. The number of particles will be in the order of $N = V/r^3$. All particles are illuminated by the fundamental laser light, every particle contributing an area

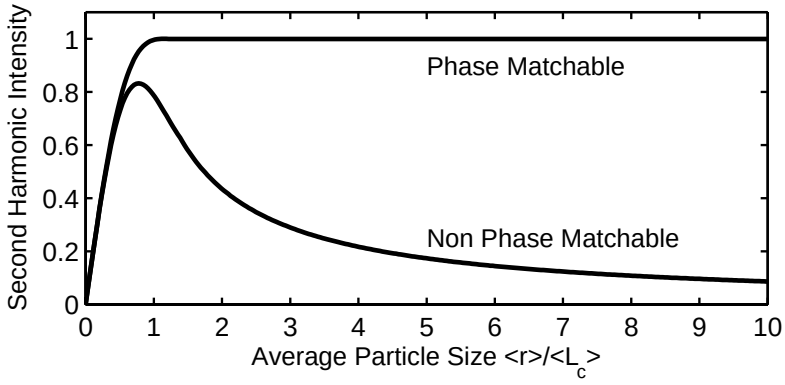

Figure 36: Schematic representation of different particle-size dependences for phase-matchable and non-phase-matchable materials.

$A = r^2$. Due to the random orientation, the second harmonic intensities of different particles add up incoherently. According to Fig. 21, for a non-phase-matchable material the SHG intensity I_s for a single particle of size r will increase quadratically for small sizes $I_s(r < L_c) \propto r^2$, then approaching a constant average value $I_s(r > L_c) \propto L_c^2$. The total SHG intensity $I = N \cdot A \cdot I_s$ then is proportional to r for $r < L_c$ and proportional to L_c^2/r for $r > L_c$.

For a phase-matchable material we get the same result for small particle sizes. For large particles the single-particle intensity still would further increase quadratically with the particle size – but only for particles properly oriented. The 'sharpness' of this condition scales with particle size, thus the share of properly oriented particles scales with r^{-1}. Putting all together, we get constant intensity for large particle sizes in a phase-matchable material.

Using the powder technique, materials can be classified into different categories at a very early state of the investigations. Thus an early decision about new materials is possible. These categories include:

Centrosymmetric: No second-harmonic intensity found by the powder technique.

Phase Matchable: Constant second-harmonic intensity at increasing particle sizes.

Non Phase Matchable: Second-harmonic intensity decreasing as a function of the particle size.

The decision about centric symmetry can be found in one measurement without the necessity of using particle size fractions. A test for phase matching can be made using several particle sizes which have to be larger than the average coherence length. Comparing different materials – known and unknown ones – it is also possible to get a rough estimate about the magnitude of the effective tensor elements of the SHG tensor.

6.2 Maker Fringe Method

The observation of periodic maxima and minima in the second-harmonic intensity as a plane parallel slab is rotated about an axes perpendicular to the laser beam was first reported by Maker et al. [5] for SiO_2 in 1962. The geometry for such a measurement is sketched in Fig. 37. A thin

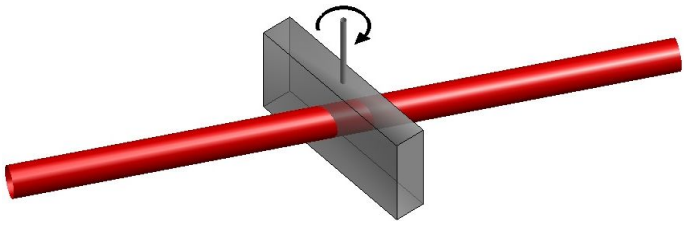

Figure 37: Rotating slab geometry for the measurement of Maker fringes. The plane parallel slab is rotated around the indicated axis which is perpendicular to the beam direction. The generated second-harmonic intensity is measured as a function of the rotation angle.

crystal platelet is rotated, thus a variation in the wave vector mismatch $\Delta\mathbf{k}$ between the harmonic polarization (forced wave) and free harmonic waves is caused

$$|\Delta\mathbf{k}| = |\mathbf{k}_{2\omega} - 2\mathbf{k}_{\omega}| = (4\pi/\lambda)|n_{2\omega}\cos\beta_2 - n_{\omega}\cos\beta_1| \tag{6.1}$$

where β_1 and β_2 are the angles of refraction for the fundamental and harmonic waves, respectively. As shown in Fig: 38, the wave vector mismatch $\Delta\mathbf{k}$ remains perpendicular to the crystal faces even for arbitrary nonnormal incidence of the fundamental beam. This can be derived from simple

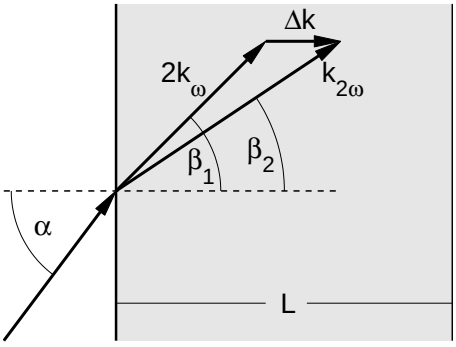

Figure 38: Wave vectors of the second-harmonic polarization (forced wave) and of the free harmonic wave and the corresponding mismatch $\Delta\mathbf{k}$ for a fundamental wave incident at an arbitrary angle α onto a slab.

geometric considerations. From Snellius law we get

$$\sin\beta_1 = \sin\alpha/n_{\omega} \quad \text{and} \quad \sin\beta_2 = \sin\alpha/n_{2\omega}\,. \tag{6.2}$$

The lengths of the wave vectors are

$$|2\mathbf{k}_{\omega}| = (4\pi/\lambda)n_{\omega} \quad \text{and} \quad |\mathbf{k}_{2\omega}| = (4\pi/\lambda)n_{2\omega} \tag{6.3}$$

where λ is the fundamental wavelength. Their components parallel to the crystal faces are equal

$$|2\mathbf{k}_{\omega,||}| = |2\mathbf{k}_{\omega}|\sin\beta_1 = (4\pi/\lambda)\sin\alpha \quad \text{and} \quad |\mathbf{k}_{2\omega,||}| = |\mathbf{k}_{2\omega}|\sin\beta_2 = (4\pi/\lambda)\sin\alpha\,. \tag{6.4}$$

Therefore the difference vector $\Delta\mathbf{k}$ is perpendicular to the crystal faces and can be expressed according to Eq. 6.1.

The total second-harmonic intensity is found by integration over the slab thickness L (similar as in section 5.1, Eqs. 5.5–5.8)

$$I^{(2)}(\alpha) = C \cdot d_{\text{eff}}^2(\alpha) \cdot I^{(1)\,2} \cdot \frac{\sin^2(\Delta k(\alpha)\, L/2)}{(\Delta k(\alpha)/2)^2} \,. \tag{6.5}$$

This angular dependence of the second-harmonic intensity calculated for a slab of 1 mm thickness with the refractive indices 2.00 and 2.04 and for a fundamental wavelength of 1 µm is shown in Fig. 39.

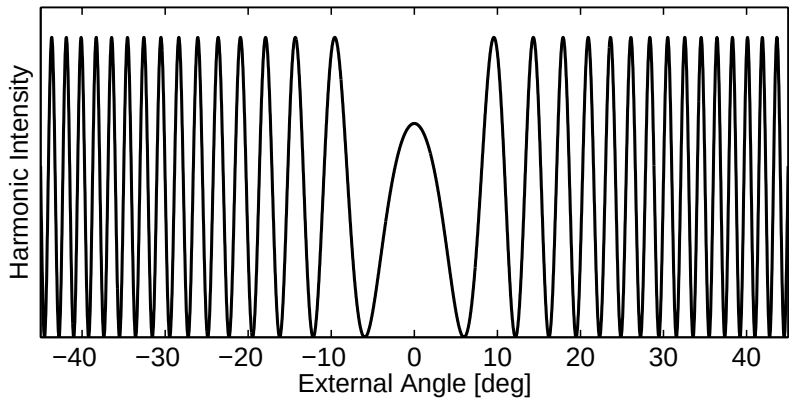

Figure 39: Calculated Maker fringes for a slab geometry: angular dependence of the second-harmonic intensity for a plane parallel slab rotated about an axes perpendicular to the laser beam.

Fitting the angular dependence given in Eq. 6.5 to a measured fringe pattern yields $\Delta k(\alpha)$. Relative measurements of the various tensor elements of one material d_{eff} and extrapolations to the respective d_{ik} are possible by using plates of different orientations and different light polarizations.

The values of one material can be referred to a 'standard' by comparing to slabs of this standard material using the identical geometry. The magnitude of the effective second-harmonic tensor element relative to that of the standard material can be obtained from the relation [1]

$$\frac{d_{\text{eff}}}{d_{\text{eff}}^{\text{std}}} = \left[\frac{I_M(0)}{I_M^{\text{std}}(0)} \frac{\eta}{\eta^{\text{std}}}\right]^{1/2} \frac{L_c^{\text{std}}(0)}{L_c(0)} \tag{6.6}$$

where I_M is the intensity envelope, η the reflection correction, and L_c the coherence length, all taken at normal incidence ($\alpha = 0$).

Instead of rotating a plane parallel slab, one can use a wedge shaped crystal to produce Maker fringes. The geometry is shown in Fig. 40. In such a geometry the orientation of the crystal is fixed, the wave vector mismatch $\Delta\mathbf{k}$ thus is kept constant, only the effective length L is varied according to the lateral shift. The second-harmonic intensity is given in a similar way as in Eq. 6.5

$$I^{(2)}(L) = \int C \cdot d_{\text{eff}}^2 \cdot I^{(1)\,2}(r) \cdot \frac{\sin^2(\Delta k\, L(r)/2)}{(\Delta k/2)^2} dr \,, \tag{6.7}$$

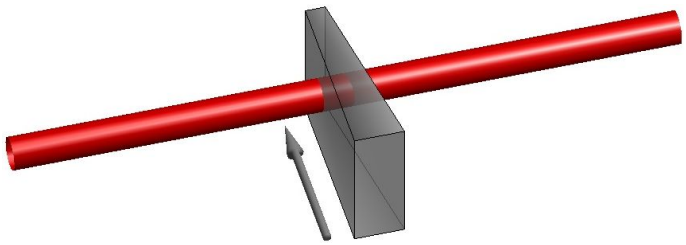

Figure 40: Wedge geometry for the measurement of Maker fringes. A crystal wedge is moved perpendicular to the laser beam, the second-harmonic intensity is measured as a function of the lateral shift.

the integration has to be performed over the laser beam area. Depending on crystal orientation and light polarizations, d_{eff} in general can be expressed by a single element d_{ik}. Again, accurate relative measurements are possible using different orientations and polarizations and comparisons to standard crystals.

Typical (calculated) intensity dependences as a function of the lateral shift of the wedge are shown in Fig. 41. Due to the constant wave vector mismatch $\Delta\mathbf{k}$ the measured dependences in a wedge measurement are much simpler – strongly sinusoidal with constant amplitude if absorption can be neglected – and thus easier to evaluate than in a slab measurement.

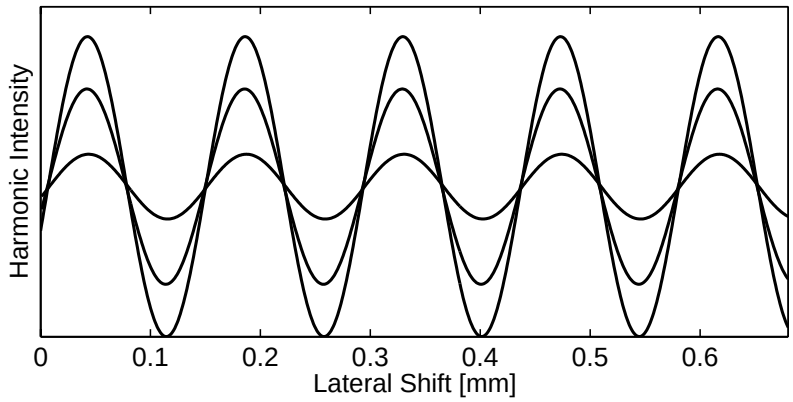

Figure 41: Calculated Maker fringes for a wedge geometry: second-harmonic intensity as a function of the lateral shift for three different laser beam sizes (0, 70, 200 µm). For the calculation refractive indices of 2.00 and 2.04 were assumed, a fundamental wavelength of 1 µm and a wedge angle of 5°.

6.3 Absolute Measurements by Phase-Matched SHG

The methods discussed in the preceding two sections both are not well suited for absolute measurements of d, although Maker fringe measurements in principle could be evaluated in that way.

Properties of Gaussian beams

For most theoretical considerations in optics, plane waves are assumed as a solution of the wave equation. Things are kept simple in that way. In all practical systems, however, wave fronts can not extend to infinity, we never have exact plane waves.
To describe, what we colloquially characterize as a 'light beam', the so-called *paraxial* approximation can be used. It's useful for the description of laser beams as well as e. g. for wave transformation calculations in conventional optical systems like combinations of lenses.
Restricting it to a single frequency and separating off the time dependence, from the wave equation the Helmholtz equation is derived

$$(\Delta + k^2)\mathbf{E}(\mathbf{r}) = 0\,. \tag{6.8}$$

In the paraxial approximation, it is assumed, that the wave propagates only in z direction, not in the x and y direction

$$\mathbf{E}(\mathbf{r}) = \Psi(x,y,z)e^{-ikz}\,. \tag{6.9}$$

Neglecting $\partial^2\Psi/\partial z^2$, as Ψ varies only slowly with z, we arrive at the *paraxial wave equation*

$$\frac{\partial^2\Psi}{\partial x^2} + \frac{\partial^2\Psi}{\partial y^2} - 2ik\frac{\partial\Psi}{\partial z} = 0\,. \tag{6.10}$$

The further treatment of this equation can be found in textbooks about optics, e. g. in [6]. The simplest solution is a circular symmetric Gaussian amplitude distribution. Such a *Gaussian beam* then can be characterized by parameters which all can be referred to the minimum beam waist w_0 and the wavelength λ

$$\Psi(x,y,z) = A_0\frac{w_0}{w(z)}\exp\left(-\frac{x^2+y^2}{w^2(z)}\right) \cdot \exp\left(-ik\frac{x^2+y^2}{2R(z)} + i\arctan\frac{z}{z_0}\right)\,, \tag{6.11}$$

A_0 is an amplitude factor. The geometry near the minimum beam waist is sketched in Fig. 42.

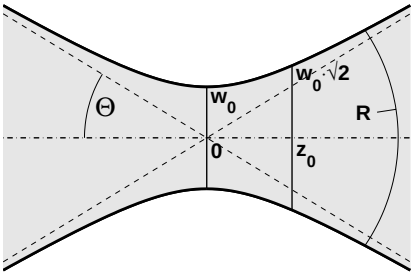

Figure 42: Profile of a Gaussian beam near the focus.

The beam waist w is defined as the distance from the beam axis where the amplitude has decreased to $1/e$. In terms of the minimum beam waist it is given by

$$w(z) = w_0\sqrt{1+(z/z_0)^2}\,. \tag{6.12}$$

The distance z_0 from the minimum beam waist, where the beam area is twice the minimum area, is called the *confocal parameter* or *Rayleigh length*

$$z_0 = \frac{\pi}{\lambda}w_o^2\,. \tag{6.13}$$

The curvature radius R of the phasefront of the wave is

$$R(z) = z\left[1+(z_0/z)^2\right]\,, \tag{6.14}$$

the beam divergence

$$\Theta = w_0/z_0 = \frac{\lambda}{\pi w_0}\,. \tag{6.15}$$

From Eq. 6.14 follows that the phasefronts have their maximum curvature at z_0. The region $|z| < z_0$ is often called *near field*, that outside ($|z| > z_0$) *far field*.
The minimum achievable beam waist for a Gaussian beam can be derived from Eq. 6.15 (it is limited by *Fresnel* diffraction)

$$w_{0,\min} = \frac{\lambda}{\pi\Theta_{\max}} = \frac{F_\#\lambda}{2\pi} \tag{6.16}$$

where $F_\#$ is the F number (aperture) of the optical system used.

To get accurate absolute values, one can apply phase-matched harmonic generation carried out under a well-defined geometry.

One scenario of a 'well-defined geometry' is the application of Gaussian beams as delivered e. g. by an ideal laser working in TEM_{00} mode. Some basics of Gaussian beams are summarized in the box on page 66. As shown there, the spatial behavior of the light amplitude in a Gaussian beam can be exactly described. In a nonlinear crystal this spatial behavior is modified by the refractive index, in addition, walk-off effects (see section 5.4) may hamper the generation of harmonic light.

Considering all these geometry influences, Boyd and Kleinman obtained an exact integral expression for the second harmonic power generated by a focused Gaussian beam. The mathematical description is found in their rather comprehensive publication [7] or – summarized – in [1]. The application of their mathematical formalism allows for the absolute determination of effective SHG tensor elements d_{eff} from the measurements of fundamental and second harmonic powers and the evaluation of the beam and crystal geometries. Many authors have shown in numerous measurements that an accuracy of approximately 10 % for d_{eff} may be achieved. A drawback of the method is that it delivers the effective d for the special phase-matching configuration which for many symmetries is an angle-dependent combination of several d_{ik}s. To get the individual elements, the method thus has to be combined with a relative one (Maker fringes).

6.4 Z-Scan Technique

Some nonlinear properties of materials can be measured using an experimental setup where the material under consideration is moved along the beam axis (z axis) through the focus region of a focused beam. The properties which can be measured in such a geometry include nonlinear absorption, also referred to as two-photon absorption, and nonlinear refraction. Measuring these two quantities, the complex third order susceptibility can be derived.

According to Eq. 4.12 the third order nonlinear polarization for $\omega = \omega + \omega - \omega$ can be written as

$$\mathbf{P}^{(3)}(\mathbf{k},\omega) = \epsilon_0 \chi^{(3)}(\mathbf{k} = \mathbf{k} + \mathbf{k} - \mathbf{k}, \omega = \omega + \omega - \omega)\mathbf{E}(\mathbf{k},\omega)\mathbf{E}(\mathbf{k},\omega)\mathbf{E}(\mathbf{k},\omega)\,. \tag{6.17}$$

This is a contribution to the (linear) polarization at ω which acts like an intensity-proportional contribution to the linear susceptibility. Writing absorption and refractive index with constant and intensity-dependent terms

$$\alpha = \alpha_0 + \beta I \quad \text{and} \quad \mathrm{n} = \mathrm{n}_0 + \mathrm{n}_2\mathrm{I}\,, \tag{6.18}$$

the real and imaginary part of $\chi^{(3)}$ can be derived from the intensity-dependent terms

$$\mathrm{Re}\,\chi^{(3)} \propto n_2 \quad \text{and} \quad \mathrm{Im}\,\chi^{(3)} \propto \beta\,. \tag{6.19}$$

In Z-scan measurements the light intensity on the sample varies when moving through the focus of a Gaussian beam (for the properties of Gaussian beams see the box on page 66). Thus the intensity-dependent parts of absorption and refraction are influenced.

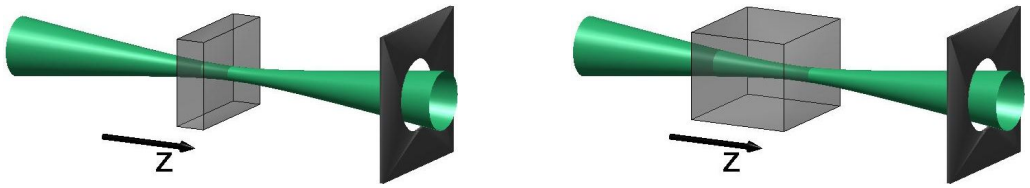

Figure 43: Z-scan: open aperture geometry, the integrated light intensity is measured as a function of crystal position. Left: thin sample ($< z_0$ of the Gaussian beam), right: thick sample ($> z_0$).

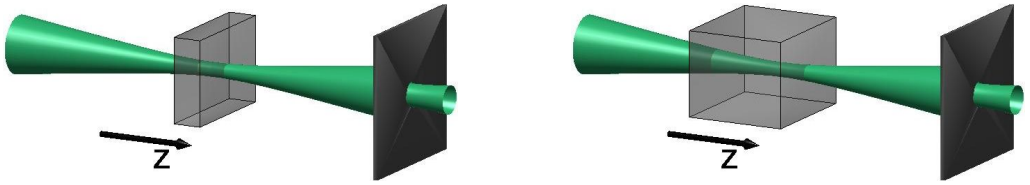

Figure 44: Z-scan: closed aperture geometry, the light intensity in the center of the beam is measured as a function of crystal position.

The typical geometries for Z-scan measurements are sketched in Fig. 43 and 44. The focused Gaussian beam is propagating in z direction, the crystal is moved through the focus. The integrated intensity will be influenced mainly by the nonlinear absorption, the angular distribution of the intensity, however, will be affected by both nonlinear absorption and refraction. Thus in an *open aperture* geometry the nonlinear absorption can be measured, in a *closed aperture* geometry the nonlinear refraction. One has to discriminate whether the sample is thin or thick (compared to z_0 of the Gaussian beams). For both cases comprehensive mathematical descriptions have been developed [8, 9] which can be used for the evaluation of Z-scan measurements.

The experimental results of typical Z-scan measurements (here on lithium niobate crystals) are shown in Fig. 45 together with fit curves [10]. From the fit, the authors derive the values for the real and imaginary parts of $\chi^{(3)}$ to be 1.02×10^{-20} m^{2}V^{-2} and 2.03×10^{-21} m^{2}V^{-2}, respectively.

It should be emphasized that for Z-scan measurements lasers with extremely short high-power pulses should be used due to two main reasons:

- Values of $\chi^{(3)}$ in general are small and the (relative) effects scale with the laser power. High laser power thus facilitates the measurement distinctly.
- Thermal effects and other slow effects like the photorefractive effect may lead to similar results as the third order susceptibility. They can be efficiently suppressed when extremely short pulses are applied.

References

[1] Herbert Rabin, C. L. Tang, editors. *Quantum Electronics, Volume I: Nonlinear Optics, Part A*, Chapter 3. Stewart K. Kurtz: *Measurement of Nonlinear Optical Susceptibilities*, page

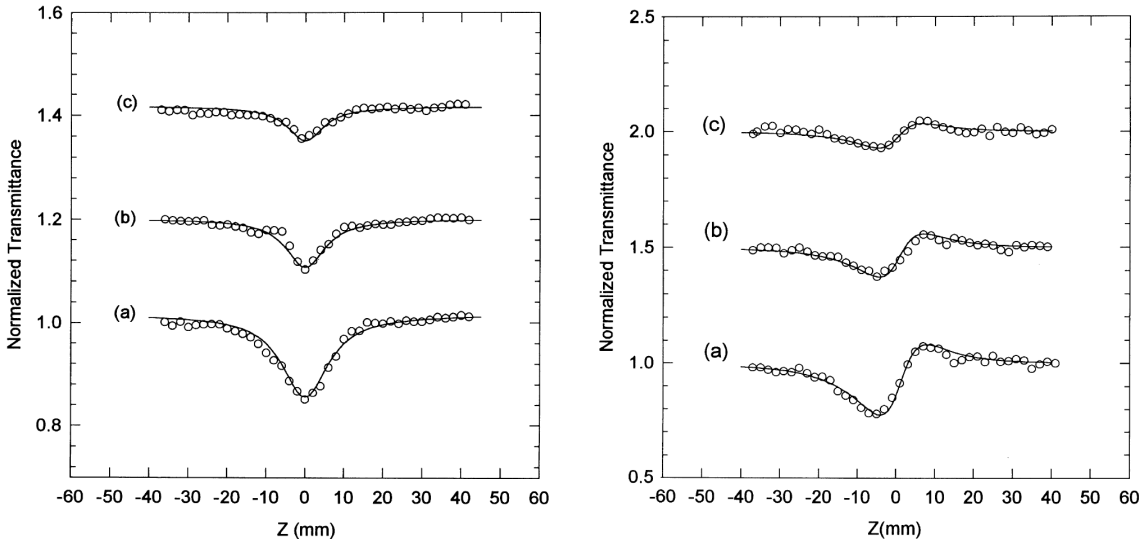

Figure 45: Z-scan measurements on lithium niobate for various laser intensities [10]: (a) 22, (b) 12, (c) 6 GW/cm^2. Experimental data (circles) and theoretical fits (solid lines). Left: open aperture geometry – nonlinear absorption, right: closed aperture geometry – nonlinear refraction. The curves for (b) and (c) are vertically shifted for presentation.

209. Academic Press, Inc., 1975.

[2] S. K. Kurtz, T. T. Perry. *A Powder Technique for the Evaluation of Nonlinear Optical Materials*. J. Appl. Phys. **39**, 3798 (1968).

[3] R. Ulbricht. *Das Kugelphotometer*. R. Oldenburg, München und Berlin, 1920.

[4] D. G. Goebel. *Generalized Integrating-Sphere Theory*. Appl. Opt. **6**, 125–128 (1967).

[5] P. D.Maker, R. W. Terhune, M. Nisenoff, C. M. Savage. *Effect of Dispersion and Focusing on the Production of Optical Harmonics*. Phys. Rev. Lett. **8**, 21 (1962).

[6] Robert D. Guenther. *Modern Optics*. John Wiley & Sons, 1990.

[7] G. D. Boyd, D. A. Kleinman. *Parametric interaction of focused gaussian light beams*. J. Appl. Phys. **39**, 3597–3639 (1968).

[8] P. P. Banerjee, R. M. Misra, M. Maghraoui. *Theoretical and experimental studies of porpagation of beams through a finite sample of a cubically nonlinear material*. J. Opt. Soc. Am. B **8**, 1072–1080 (1991).

[9] J. A. Hermann, R. G. McDuff. *Analysis of spatial scanning with thick optically nonlinear media*. J. Opt. Soc. Am. B **10**, 2056–2064 (1993).

[10] Heping Li, Feng Zhou, Xuejun Zhang, Wei Ji. *Picosecond Z-scan study of bound electronic Kerr effect in $LiNbO_3$ crystal associated with two-photon absorption*. Appl. Phys. B **64**, 659–662 (1997).

7 Non-Collinear Harmonic Generation

Usually nonlinear optical processes are regarded to be *collinear* which means that all participating light beams are pointing approximately into the same direction. Such collinear geometries have the advantage of large interaction lengths, thus optimize the efficiency of the nonlinear interaction – provided that phase matching or quasi phase matching is obeyed. In collinear geometries the momentum conservation law is fulfilled in a scalar sense, the lengths k_i of all vectors $\mathbf{k}_i$ add up to zero.

However, it's not a must to work with collinear beams, non-collinear interactions are possible as well. The momentum conservation law then is only fulfilled in a vectorial sense

$$\sum \mathbf{k}_i = 0 \quad \text{yet} \quad \sum k_i \neq 0 \,. \tag{7.1}$$

As the interacting beams are inclined to each other, the intersection volume will be small, the resulting short interaction length will hamper efficiency. Non-collinear geometries are therefore not suitable for efficient frequency conversion, they are 'only' interesting for their physics and – as we will see – they can be useful for material characterization. Some examples for non-collinear interactions shall illustrate this.

7.1 Induced Non-Collinear Frequency Doubling

This technique utilizes two fundamental light beams inclined to each other to fulfill the vectorial phase matching condition

$$\mathbf{k}_2 = \mathbf{k}_1 + \mathbf{k}_1' \,. \tag{7.2}$$

The corresponding geometry is sketched in Fig. 46.

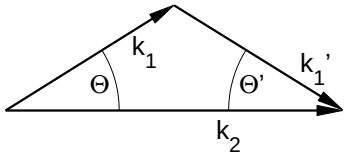

Figure 46: Momentum diagram for induced non-collinear frequency doubling.

The vectorial phase matching condition of Eq. 7.2 can be referred to a condition for the respective refractive indices $n(\omega, \mathbf{k})$. Using

$$|\mathbf{k}_2| = |\mathbf{k}_1| \cos\Theta + |\mathbf{k}_1'| \cos\Theta' \quad \text{and} \quad |\mathbf{k}| = \frac{\omega}{c} n_p(\omega, \mathbf{k}) \tag{7.3}$$

(p indicates the light polarization) yields

$$(\omega_1 + \omega_1')n_p(\omega_1 + \omega_1', \mathbf{k}_1 + \mathbf{k}_1') = \omega_1 n_q(\omega_1, \mathbf{k}_1)\cos\Theta + \omega_1' n_r(\omega_1', \mathbf{k}_1')\cos\Theta' \,. \tag{7.4}$$

The two fundamental beams usually are derived from the same laser as schematically sketched in Fig. 47 which means $\omega_1 = \omega_1' = \omega$. Furthermore, a geometry can be chosen where the

two fundamental beams are arranged symmetrically with respect to the index ellipsoid and have symmetric polarization, which further simplifies Eq. 7.4 to

$$n_p(2\omega, \mathbf{k}_2) = n_q(\omega, \mathbf{k}_1) \cos\Theta \; . \tag{7.5}$$

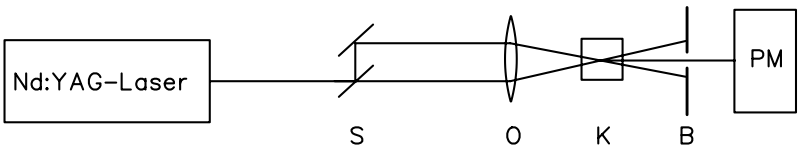

Figure 47: Experimental arrangement for measuring induced non-collinear frequency doubling. S: beam splitter, O: focussing lens, K: temperature controlled sample holder, moveable in all three spatial directions, B: aperture for blocking the fundamental beams, PM: photomultiplier.

The angle Θ and the polarizations of the incident beams have to be chosen in an appropriate way to fulfill Eq. 7.5. Obviously this condition is very sensitive to variations in the refractive indices. As in more detail shown in Fig. 48, the interaction volume, i. e. the region from which second harmonic light originates, is limited in all three spatial dimensions. Thus such an experiment can

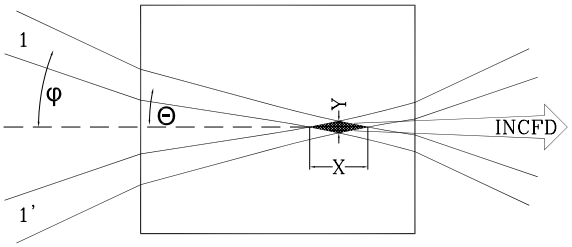

Figure 48: Induced non-collinear frequency doubling: detailed beam geometry inside the sample.

be used to get information just about the volume element under illumination. Moving the sample in all spatial directions yields a fully three-dimensional topography. The resolution depends on the beam geometries and on the angle Θ.

The technique may be illustrated by two typical applications concerning the characterization of optical crystals – composition measurements in lithium niobate and detection of domain borders in potassium niobate [1].

Composition Measurements in Lithium Niobate Lithium niobate is one of the most important crystals for many electro-optic and acousto-optic devices. Its chemical formula is $LiNbO_3$ but the real composition usually deviates from the stoichiometry described by the formula. Crystals of lithium niobate are commonly grown at the congruently melting composition, i. e. at the composition where liquid and solid states of equal compositions are in an equilibrium. This composition is at approximately 48.5 mole% of lithium oxide. Crystals grown at this congruently melting composition are of excellent optical quality and of good homogeneity. Some of the properties, however, could be improved in crystals of stoichiometric composition. So for instance the electric field necessary for periodic poling would be considerably lowered. Various efforts therefore have been made to achieve material of stoichiometric composition.

One technique now used by several groups is the so-called *vapor transport equilibration* (VTE) where thin plates of lithium niobate are heated up in a stoichiometric mixture of lithium oxide and niobium oxide. Diffusion then leads to the composition equilibration between crystal and surrounding oxide powder. To improve and optimize the technique, the success of these treatments has to be carefully checked. Induced non-collinear frequency doubling is one possibility to monitor the composition inside the crystal after the treatment with a good spatial resolution.

Many of the material properties of lithium niobate depend on the composition, these include the refractive indices. The ordinary index is practically independent from composition, the extraordinary index shows an expressed dependence which is approximately linear. The two dependences for various wavelengths are shown in the left part of Fig. 49.

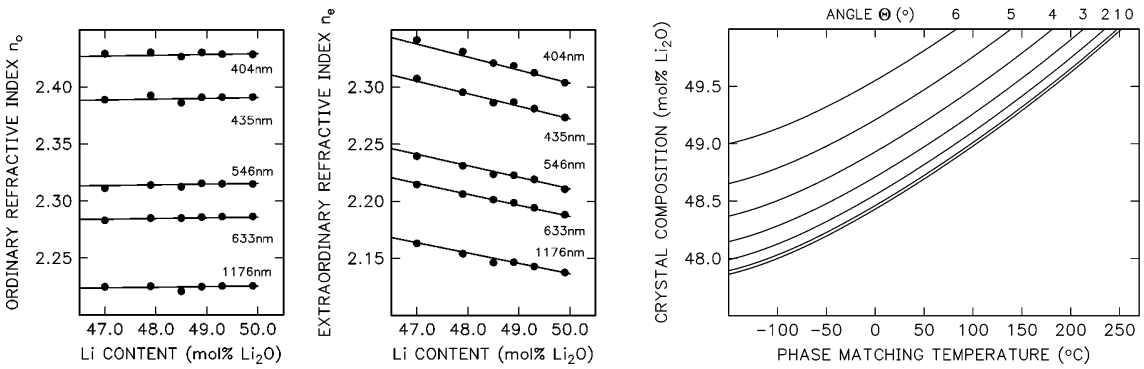

Figure 49: Composition dependence of the refractive indices of lithium niobate for various wavelengths (left) [2] and therefrom calculated functional dependence between phase matching temperature for induced non-collinear frequency doubling and composition for several angles Θ *(right) [3]. The calculation is made for a fundamental wavelength of 1064 nm (Nd:YAG laser).*

As – like in every material – the refractive indices are temperature dependent, phase matching conditions can be adjusted using the temperature as a parameter. The two dependences can be combined, the measured phase matching temperature for a fixed angle Θ can be utilized as a very sensitive indicator for the crystal composition. This functional dependence, composition versus phase matching temperature, is shown in the right part of Fig. 49 for several angles Θ. The curves are calculated using a generalized fit for the refractive indices of lithium niobate as a function of wavelength, composition, temperature, and doping [3, 4].

From the dependences in Fig. 49 an excellent sensitivity of the method is apparent, at least for relative measurements. One degree variation in the phase matching temperature corresponds to a variation of 0.005 mole% in the lithium oxide concentration in the crystal.

A typical measurement on a VTE-treated sample is shown in Fig. 50. The sample had been treated for a comparably short time, thus the crystal had not reached the final homogeneity. Instead, the diffusion profiles in two different directions, z and x, with their characteristic form of a complementary error function (erfc) are observed.

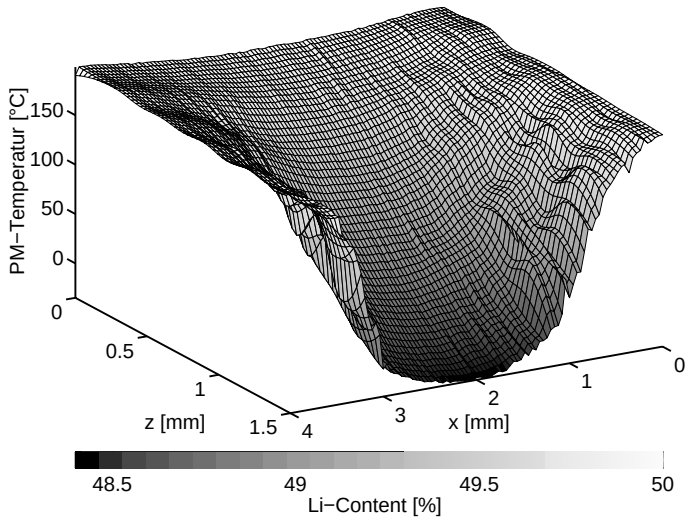

Figure 50: Composition profile in a VTE-treated lithium niobate sample. At the borders ($z = 0$, $x = 0$, $x = 4$) a stoichiometric composition of 50 mole% lithium oxide is reached whereas near the center of the sample the composition is still the congruently melting one of the untreated material.

Domain Borders in Potassium Niobate Ferroelectric materials commonly undergo a phase transition from a high temperature paraelectric to a low temperature ferroelectric phase. Depending on the symmetries of the high- and the low-temperature phases ferroelectric materials may contain ferroelectric domains in different geometric configurations. Thus materials with a tetragonal or trigonal symmetry both in the high- and in the low-temperature phase can form domains only in two polarization directions – parallel or antiparallel to the crystallographic c-axis. The refractive indices are identical for both domain directions. In contrast to this, materials with a high-temperature cubic and a low-temperature tetragonal phase can form domains with their polar axis pointing into any of the six directions of the former cubic axes. There are thus three possible orientations of the index ellipsoid. Materials belonging to the first group include lithium niobate, lithium tantalate and strontium barium niobate. To the second group belong all perovskites including barium titanate and potassium niobate.

To detect such misoriented domains one can utilize the different phase-matching directions for the different orientations. Adjusting the two crossed laser beams such that phase matching for one orientation is achieved, large second-harmonic intensities are measured when inside a properly oriented domain and practically no intensity outside. The spatial derivative of the intensity field then yields the borders between adjacent domains of different orientation. Fig. 51 gives an example for such a measurement.

7.2 Spontaneous Non-Collinear Frequency Doubling

In contrast to *induced* non-collinear frequency doubling, *spontaneous* non-collinear frequency doubling is a type of optical second harmonic generation that uses randomly scattered light to provide additional fundamental beams in order to accomplish non-collinear phase matching [5]. This scattered light may arise from the crystal itself due to inhomogeneities or impurities or may be forced by suitable optics (ground glass plate in front of the sample).

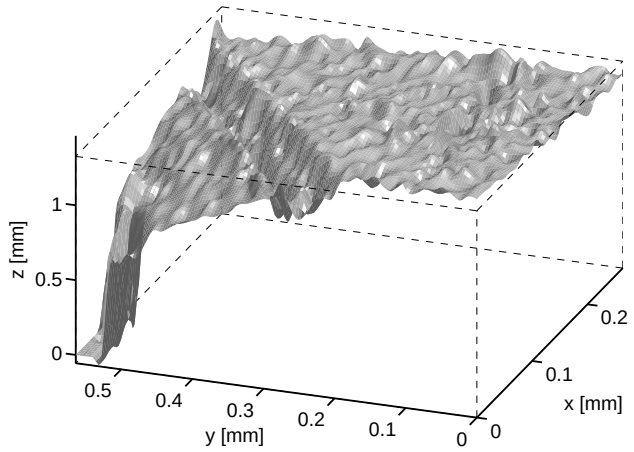

Figure 51: Border plane between two domains in potassium niobate which have different orientation.

The corresponding momentum diagram is shown in Fig. 52. Again the vectorial phase matching condition described by Eqs. 7.2 – 7.4 has to be fulfilled.

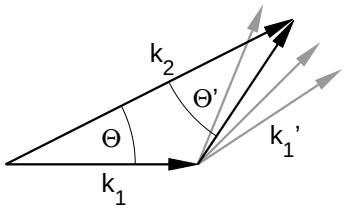

Figure 52: Momentum diagram for spontaneous non-collinear frequency doubling. Out of the infinite number of scattering angles (indicated by the gray vectors) only $\Theta + \Theta'$ matches.

As light is scattered in all three-dimensional directions, phase matching now can be achieved for a multitude of angles $\Theta + \Theta'$ around the direction of the fundamental beam. This leads to a cone of second harmonic light. The cone angle Θ depends on the crystallographic direction and the respective effective refractive indices. To keep it simple, the fundamental beam is directed along one of the axes of the index ellipsoid yielding a cone of approximately elliptic shape. A typical experimental arrangement for the measurement is shown in Fig. 53

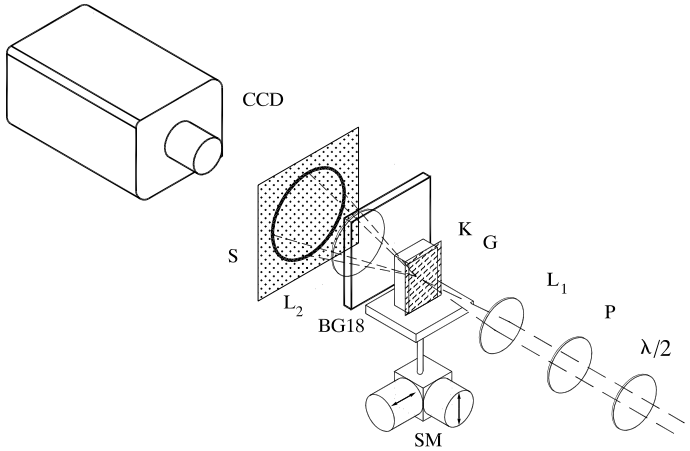

Figure 53: Setup for measuring spontaneous non-collinear frequency doubling. The input polarization can be varied by half-wave plate $\lambda/2$ and polarizer P. The beam is slightly focused by lens L_1 onto the crystal K which can be scanned in two directions by means of stepping motors SM. The generated light cone is projected onto the ground glass plate S yielding an elliptic ring which is viewed by a CCD camera.

The cone of second-harmonic light is projected onto a ground glass plate yielding a nearly elliptic ring which is captured by a video system. The fundamental light is removed by an appropriate optical filter of type BG18. The ring parameters depend very sensitively on the refractive indices for the fundamental and the second harmonic light at the position of the focused fundamental light beam. Thus a two-dimensional topographical characterization of crystals is possible when the sample is moved perpendicular to the fundamental beam direction. The spatial resolution depends on the fundamental beam geometry, i. e. the focusing of the Gaussian beam (see box on page 66).

The result of such a measurement, where a sample is two-dimensionally scanned, is usually a large set of ring images. One can show that it is sufficient to measure the length of one of the principal axes of the ellipses, thus the amount of data can be drastically reduced. An automatic scheme had to be developed to do this in a reliable way [6]. Fig. 54 shows some typical ring pictures (left) and the ellipses calculated by the evaluation program (right).

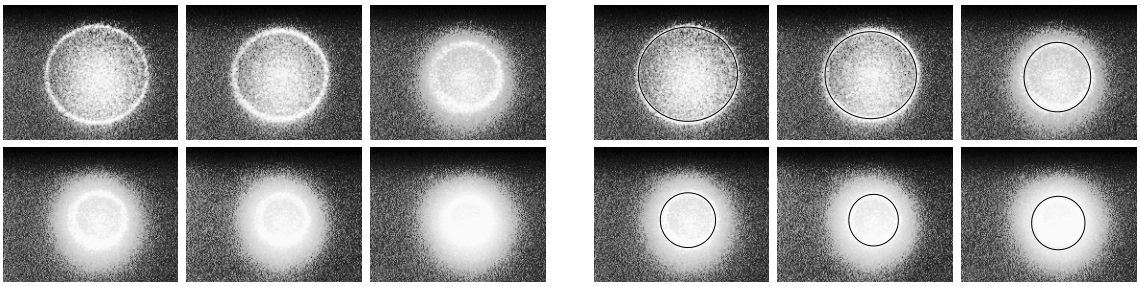

Figure 54: Spontaneous non-collinear frequency doubling: ring pictures from different positions of a lithium niobate sample. Left: original video images, right: overlaid with the calculated ellipses.

Again, two examples may illustrate the application of the technique for materials characterization, the homogeneity and composition measurement of a pure lithium niobate crystal and the characterization of so-called growth striations in Mg-doped lithium niobate.

Homogeneity and composition of lithium niobate A lithium niobate crystal grown near the stoichiometric composition had to be characterized. The crystal had been grown along the z-direction. For the measurements a small sample was cut out of the grown crystal and was two-dimensionally scanned with the technique along the z- and the x-axis. From the detected ellipses the refractive indices and therefrom the crystal composition can be derived. The result is plotted in Fig. 55, a two-dimensional topography of the crystal composition.

A nearly linear variation of the composition in the growth direction of the crystal is clearly detectable. The figure also gives an impression of the sensitivity of the technique, composition variations down to approximately 0.01 mole% in the lithium oxide content can be detected.

Growth striations in Mg-doped lithium niobate In crystals sometimes narrow stripes are visible which indicate some sort of inhomogeneity. Crystal growers call these *striations*. Several ex-

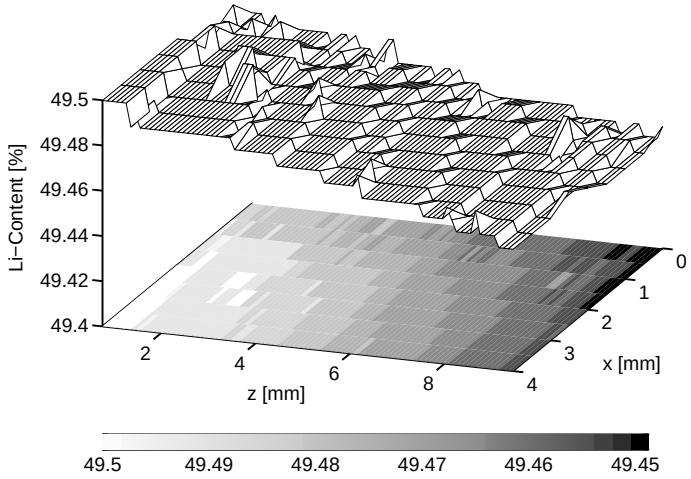

Figure 55: Homogeneity and composition of a lithium niobate crystal grown with a lithium oxide content of approximately 49.5 mole%.

planations are possible: conglomeration of impurities, internal stress, composition variations etc. Fig. 56 shows the topography of such striations in Mg-doped lithium niobate measured with the spontaneous non-collinear frequency doubling technique. At the striations small deviations in the refractive indices are detectable which indicate a corresponding slight variation in the composition of the crystal.

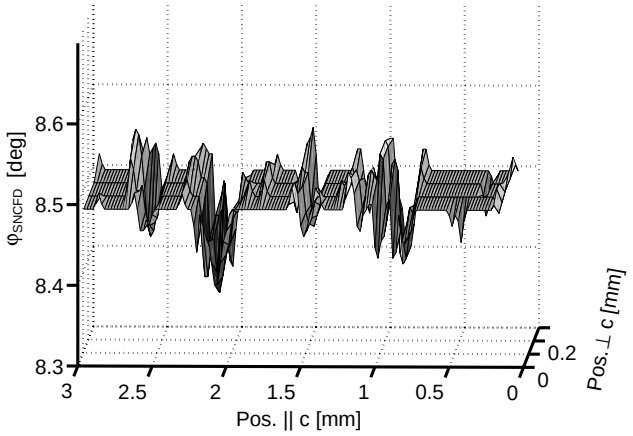

Figure 56: Growth striations in Mg-doped lithium niobate. The striations are found to be perpendicular to the growth direction (z). The slight variations in the cone angle indicate corresponding variations in the refractive indices and in the crystal composition.

7.3 Non-Collinear Scattering

In a strict definition, non-collinear scattering is not a real non-collinear harmonic generation process. However, the experimental results are quite similar. It was described by Kawai et al. [7] who detected it in strontium barium niobate. If a strong infrared laser is directed onto a crystal of strontium barium niobate perpendicular to the polar axis (c-axis) non-collinear second-harmonic light propagating in a plane perpendicular to the c-axis is visible. Fig. 57 gives an illustration.

The effect is only detected in unpoled crystals where needle-like microdomains exist. In the domains second-harmonic light is generated via the tensor elements d_{31}, d_{32}, and d_{33}. No collinear

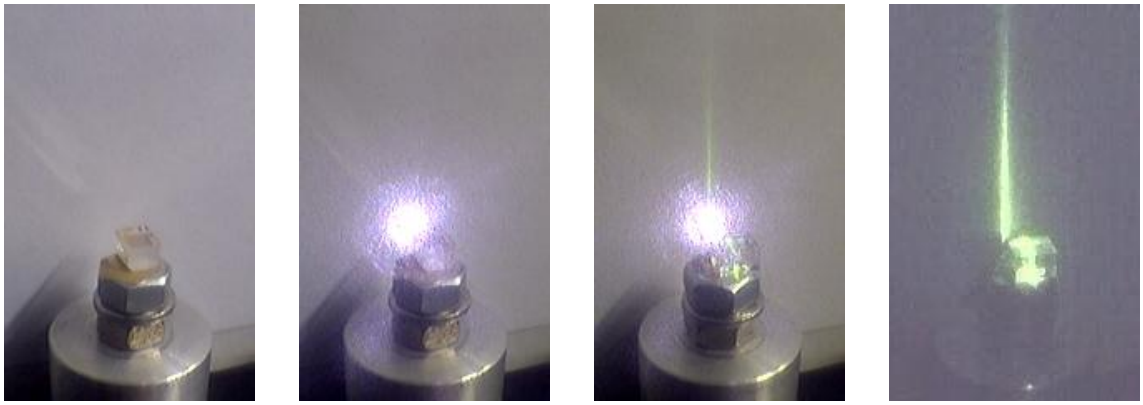

Figure 57: Non-collinear scattering. Pictures from left to right: (1) SBN crystal on a rotation stage. (2) Infrared laser directed along the c-axis (visible due to the sensitivity of the video camera at 1064 nm). (3) Crystal rotated by 90 ° – infrared laser directed perpendicular to the c-axis. (4) Ditto but infrared light now suppressed by a suitable filter.

phase-matching condition can be fulfilled in SBN due to the small birefringence of the material. Therefore, no intense collinear harmonic light is generated. Instead a part of the harmonic light is scattered at the domain boundaries, and – as the domains are directed along the c-axis – this scattering occurs perpendicular to the c-axis.

7.4 Conical harmonic generation

An interesting mechanism for the generation of harmonic light is the use of higher order nonlinearities. This mechanism for *Conical Harmonic Generation* was described and experimentally verified in 2002 by Moll et al. [8]. The wave vector geometry for second-harmonic generation via this mechanism is shown in Fig. 58.

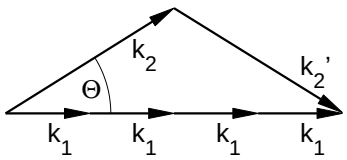

Figure 58: Wave vector diagram for conical second-harmonic generation via a 5^{th} order nonlinear interaction.

Five waves ($4 \times \mathbf{k}_1$, $\mathbf{k}_2'$) have to interact to produce a second-harmonic wave $\mathbf{k}_2$. As $\mathbf{k}_2'$ also has to be generated by the fundamental pump wave $\mathbf{k}_1$, the whole process can be regarded as parametric amplification of a signal and an idler beam, $\mathbf{k}_2$ and $\mathbf{k}_2'$, respectively. In the pump mechanism an appropriate higher-order nonlinear term has to be included. As usual for parametric amplification, the theoretical description consists of three coupled equations for the three interacting waves $\mathbf{k}_1$, $\mathbf{k}_2$, $\mathbf{k}_2'$. Generally, the two generated waves may be of different frequencies, most effective amplification is achieved, however, when the frequencies of signal and idler are identical. A comprehensive treatment is given in the above cited publication.

The wave vector geometry in Fig. 58 shows that for the generation of the second-order harmonic a 5^{th} order nonlinear interaction is responsible. This can be generalized: radiation at the mth order harmonic can be generated through the use of a $(2m{+}1)$-order nonlinearity. The tensor of the corresponding nonlinear susceptibility is of rank $(2m{+}2)$, i. e., always of even rank. Thus this process allows for the generation and amplification of both odd- and even-order harmonics in all materials, even in isotropic ones. Additionally, this process can always be phase matched in normal-dispersion materials without the use of birefringence. From the wave vector diagram we can derive

$$\cos\Theta = n(\omega)/n(2\omega) \tag{7.6}$$

or – for the generation of the mth order harmonic –

$$\cos\Theta = n(\omega)/n(m\omega)\ . \tag{7.7}$$

Both equations can always be fulfilled for normal dispersion as in this case $n(m\omega) > n(\omega)$. In isotropic materials these conditions for Θ lead to circular cones of generated harmonic light. Fig. 59 shows the experimental results for third-harmonic generation in sapphire.

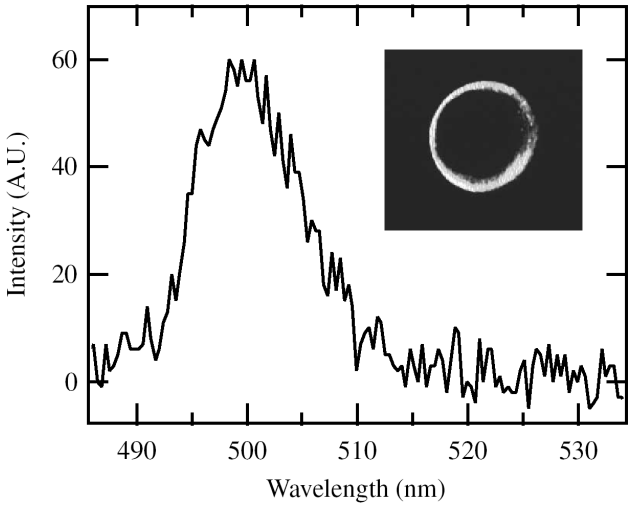

Figure 59: Experimental spectrum of conical third-harmonic emission from sapphire and the corresponding photograph of the output ring (inset) for the case in which the wavelength of the input pulse is centered at 1500 nm. The spectral width results from the bandwidth of the fundamental pulse. The cone angle is ≈12° and the conversion efficiency is ≈10^{-6} (taken from Ref. [8]).

7.5 Domain-Induced Non-Collinear SHG

A new non-collinear mechanism for the generation of second-harmonic light has been recently found in strontium barium niobate (SBN) [9]. A circular cone of second-harmonic light is generated when a fundamental beam of intensive laser light is directed along the crystallographic c-axis. The corresponding ring projected onto a screen is shown in Fig. 60 (it's the second image of Fig. 57 but now with the infrared light suppressed).

The nonzero elements of the SHG tensor of strontium barium niobate derived in section 4.7 show that no second harmonic wave in c-direction can be expected, no *collinear* SHG is possible for a fundamental beam along the c-axis. The light polarization in the ring is radial, the polarization

Figure 60: SHG ring in strontium barium niobate. The fundamental laser beam is directed along the crystallographic c-axis. In this direction, no SHG light is visible, instead a circular cone of green light is visible. The image shown corresponds to the second image of Fig. 57, the infrared light is suppressed by an appropriate filter.

direction points to the center of the ring (Fig. 61). And it is independent from the polarization of the fundamental beam. Both facts – radial polarization and no influence of the fundamental beam's polarization – conform with the fourfold symmetry around the c-axis.

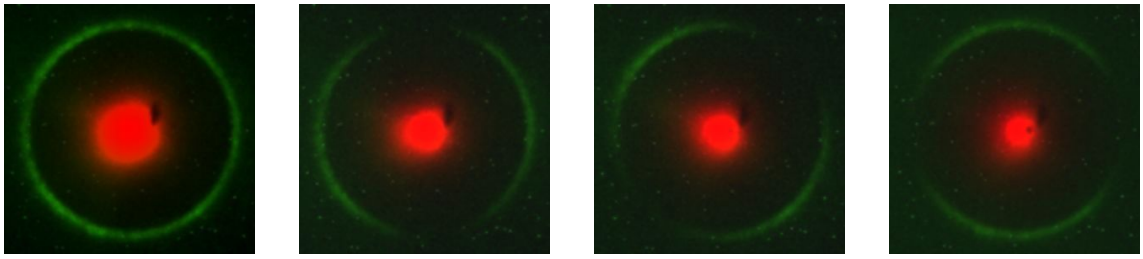

Figure 61: Polarization of the SHG ring in strontium barium niobate. From left to right: (1) without analyzer, (2) analyzer horizontal, (3) analyzer diagonal, (4) analyzer vertical.

Several authors have demonstrated that micrometer-sized needlelike domains play an important role for light scattering and for the type of the phase transition in SBN [7, 10, 11, 12]. These domains are in antiparallel order, the ferroelectric polarization is parallel or antiparallel to the crystallographic c-direction. To prove whether these domains also are responsible for the non-collinear second-harmonic process, a sample was poled by cooling it down from the high-temperature paraelectric phase with an electric field applied in c-direction. After that the ring structure had vanished. This is also a strong indication that higher nonlinearities of odd order [8], discussed in the preceding section, which are insensitive to poling and the corresponding symmetry aspects, do not contribute to the effect. Having thus proven that antiparallel ferroelectric domains are the basic cause for this non-collinear SHG effect, model calculations based on antiparallel domains were carried out to explain the ring structure.

Plane light waves propagating along the c-direction of SBN contain only electric field components perpendicular to this direction, E_1 and E_2. According to the shape of the SHG tensor for SBN, these field components produce a second order nonlinear polarization P_3. The sign of P_3 depends on the domain orientation, here indicated by arrows:

$$P_3(\Uparrow) \quad = \quad d_{31}E_1E_1 + d_{32}E_2E_2 \quad \text{and} \tag{7.8}$$

$$P_3(\Downarrow) \quad = \quad -d_{31}E_1E_1 - d_{32}E_2E_2 \quad . \tag{7.9}$$

For simplicity, all oscillatory factors have been omitted from E and P. E may be assumed to be monochromatic at frequency ω, then P accordingly is monochromatic at 2ω. The induced second-harmonic polarization P_3 acts as a source for dipolar radiation at this frequency 2ω.

The simplest nontrivial arrangement of domains contains just two antiparallel ordered ones. For the calculation, the domain sizes were assumed to be in the order of the second-harmonic wavelength. To compute the far-field behavior, the domains were replaced by suitable dipolar point sources. The angular intensity distribution due to the interference of the respective dipolar radiation fields is schematically sketched in Fig. 62 for the plane defined by the two dipole vectors.

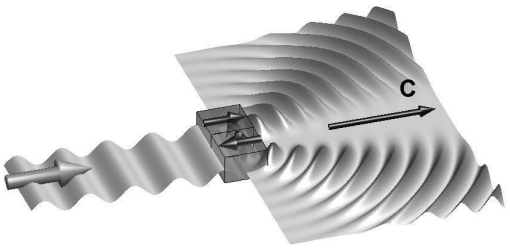

Figure 62: Angular distribution of the second-harmonic radiation originating from two antiparallel domains in SBN. The exciting wave propagates in c-direction from the left side.

No intensity in forward direction, instead a broad angular intensity distribution around two distinct angles symmetric to the c-direction is found. The dominant angles are determined by the domain sizes. Due to the oscillation direction of the dipoles, the polarization of the second-harmonic light is in the plane shown.

Increasing the number of equally sized domains leads to a narrowing of this angular distribution similar to the diffraction through an optical grating. Yet in real crystals it cannot be expected that one deals with ideal equally-sized domains. A generalization consequently has to assume a large number of domains with a random distribution of sizes. A model calculation on an arbitrarily chosen domain distribution reveals an angular dependence of the generated second-harmonic light as shown in Fig. 63.

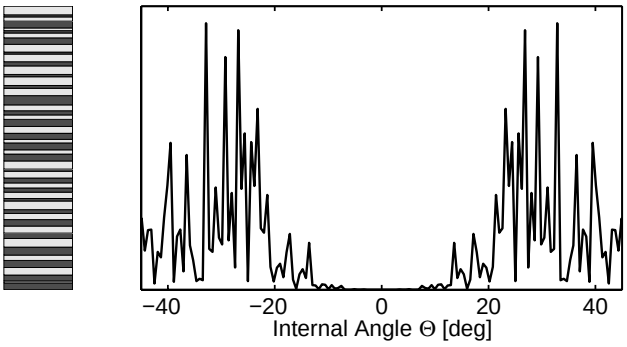

Figure 63: Angular distribution of the second-harmonic light intensity arising from a planar array of 200 randomly-sized antiparallel ordered domains in SBN. A part of the domain arrangement is sketched on the left side: c-direction is horizontal, dark domains are polarized parallel, light ones antiparallel to this direction, the exciting wave propagates in c-direction.

Again, the polarization of the second-harmonic light is *in-plane*. Varying the random distribution of the domain widths varies the random fine structure of the intensity distribution; the common

features, however – no intensity in forward direction and a broad angular distribution starting a approximately 10°– are maintained. Extending the model to an arrangement of needle-like *long* domains means that, in addition to the calculated angular distribution of Fig. 63, strong momentum conservation has to be obeyed, yielding

$$\mathbf{k}_2 = \mathbf{k}_1 + \mathbf{k}_1' + \mathbf{k}_\mathrm{g} \quad . \tag{7.10}$$

Here, $\mathbf{k}_\mathrm{g}$ represents any spatial periodicity present in the domain arrangement, $\mathbf{k}_1 = \mathbf{k}_1'$ characterizes the fundamental beam in c-direction, $\mathbf{k}_2$ one of the harmonic waves. Due to the random distribution of domain widths, $\mathbf{k}_\mathrm{g}$ shows up a corresponding reciprocal distribution. The direction of $\mathbf{k}_\mathrm{g}$, however, is strictly perpendicular to the c-axis according to the extent of the domains in c-direction. The momentum geometry for the phase-matching condition of Eq. 7.10 is sketched in Fig. 64.

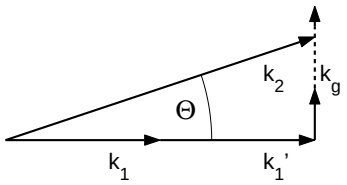

Figure 64: Wave vector diagram for Eq. 7.10. $\mathbf{k}_1$ *and* $\mathbf{k}_1'$ *are in c-direction,* $\mathbf{k}_\mathrm{g}$ *perpendicular to it with a distribution as indicated by the dashed line.*

The angle Θ between fundamental and harmonic wave vectors inside the crystal is defined by

$$\cos\Theta = \frac{k_1 + k_1'}{k_2} = \frac{n^o(\omega)}{n^e(\Theta, 2\omega)} \; . \tag{7.11}$$

Using the refractive index data for SBN, Eq. 7.11 yields an internal angle Θ of 17.1°, corresponding to an external angle of 44.8°. This is in excellent agreement with the measured angle of approximately 45°.

The extension of the model to a three-dimensional arrangement of needle-like long domains with randomly distributed widths is straightforward. Angular intensity distribution and phase-matching condition of Eq. 7.10 lead to a cone of second-harmonic light with internal cone angle Θ. *In-plane* polarization for all radial directions then accounts for the *radial* polarization experimentally found in the ring.

Generalization: Recently, it could be shown, that domain-induced non-collinear SHG is also the effect responsible for non-collinear scattering described in section 7.3. The mechanism is rather general, the wave vector diagram for a general geometry is depicted in Fig. 65. The fundamental beam propagates in the crystal at an angle α from the c-axis of the crystal. A cone of second harmonic light around the c-axis is generated. The cone angle β has to fulfill the condition

$$2k_1 \cos\alpha = k_2 \cos\beta \tag{7.12}$$

or – expressed in refractive indices –

$$n_1(\alpha)\cos\alpha = n_2(\beta)\cos\beta \, . \tag{7.13}$$

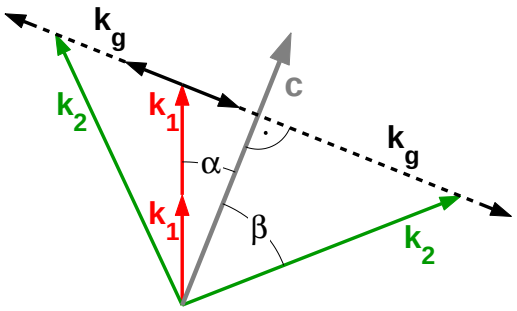

Figure 65: Wave vector diagram for domain-induced non-collinear SHG in a generalized geometry. The fundamental beam is at an arbitrary direction enclosing α with the c-axis, vectors $\mathbf{k}_g$ show a distribution as indicated but are strictly perpendicular to the c-axis, a cone angle β for the generated harmonic light $\mathbf{k}_2$ results.

For $\alpha = 0$, this results in $\beta = \Theta$, Θ of Eq. 7.11, for $\alpha = 90°$ we get the effect shown in section 7.3.

Typical cone sections, projected onto a screen behind the crystal, are shown in Fig. 66.

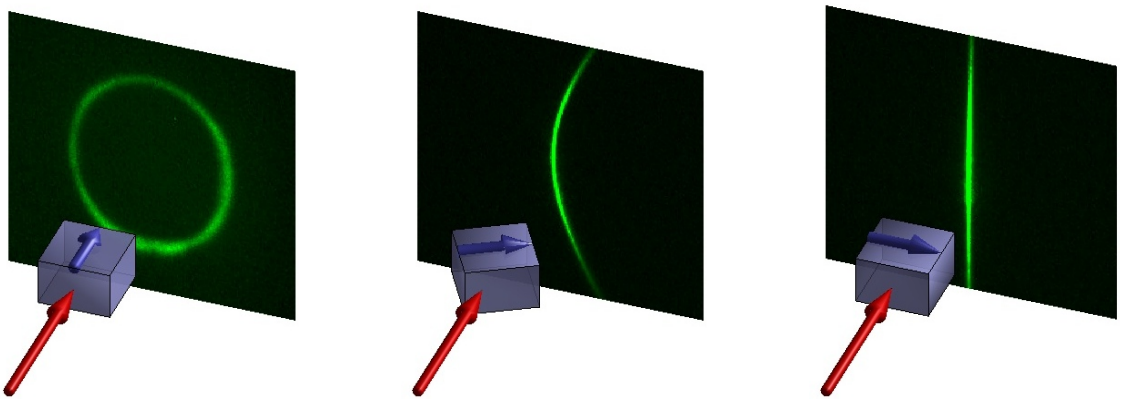

Figure 66: Cone sections for domain-induced non-collinear SHG: Circle for $\alpha = 0$ (left), line for $\alpha = 90°$ (right), ellipse or hyperbola for arbitrary α (middle).

References

[1] A. Reichert, K. Betzler. *Induced noncolinear frequency doubling: A new characterization technique for electrooptic crystals*. J. Appl. Phys. **79**, 2209–2212 (1996).

[2] U. Schlarb, K. Betzler. *Influence of the defect structure on the refractive indices of undoped and Mg–doped lithium niobate*. Phys. Rev. B **50**, 751 (1994).

[3] U. Schlarb, K. Betzler. *A generalized Sellmeier equation for the refractive indices of lithium niobate*. Ferroelectrics **156**, 99 (1994).

[4] K. Kasemir, K. Betzler, B. Matzas, B. Tiegel, T. Wahlbrink, M. Wöhlecke, B. Gather, N. Rubinina, T. Volk. *Influence of Zn/In dodoping on the optical properties of lithium niobate*. J. Appl. Phys. **84**, 5191 (1998).

[5] K.-U. Kasemir, K. Betzler. *Characterization of photorefractive materials by spontaneous noncolinear frequency doubling*. Appl. Phys. **B 68**, 763 (1999).

[6] K.-U. Kasemir, K. Betzler. *Detecting Ellipses of Limited Eccentricity in Images with High Noise Levels*. Image & Vision Computing Journal **21**, 221–227 (2003).

[7] Satoru Kawai, Tomoya Ogawa, Howard S. Lee, Robert C. DeMattei, Robert S. Feigelson. *Second-harmonic generation from needlelike ferroelectric domains in $Sr_{0.6}Ba_{0.4}Nd_2O_6$ single crystals*. Appl. Phys. Lett. **73**, 768 (1998).

[8] K. D. Moll, D. Homoelle, Alexander L. Gaeta, Robert W. Boyd. *Conical Harmonic Generation in Isotropic Materials*. Phys. Rev. Lett. **88**, 153901 (2002).

[9] Arthur R. Tunyagi, Michael Ulex, Klaus Betzler. *Non-collinear optical frequency doubling in Strontium Barium Niobate*. Phys. Rev. Lett. **90**, 243901 (2003).

[10] Y. G. Wang, W. Kleemann, Th. Woike, R. Pankrath. *Atomic force microscopy of domains and volume holograms in $Sr_{0.61}Ba_{0.39}Nd_2O_6$:$Ce^{3+}$*. Phys. Rev. B **61**, 3333–3336 (2000).

[11] W. Kleemann, P. Licinio, Th. Woike, R. Pankrath. *Dynamic light scattering at domains and nanoclusters in a relaxor ferroelectric*. Phys. Rev. Lett. **86**, 6014–6017 (2001).

[12] P. Lehnen, W. Kleemann, Th. Woike, R. Pankrath. *Ferroelectric nanodomains in the uniaxial relaxor system $Sr_{0.61-x}Ba_{0.39}Nd_2O_6$:$Ce_x^{3+}$*. Phys. Rev. B **64**, 224109 (2001).

8 Continuous wave solid-state laser systems with intra-cavity second harmonic generation [1, 2, 3, 4]

8.1 Fundamentals

We will at first recall the key aspects of the laser process. The basic principle of amplification of a light wave transmitting through a laser medium is shown in Fig. 67, where u_{in} and u_{out} denote the incoming and outgoing photon flux of the light wave with the relation $u_{out} >> u_{in}$. The phenomenon of amplification and its efficiency result from light interaction processes with the laser medium shortly summarized in the following.

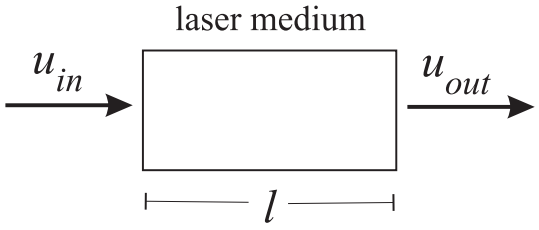

Figure 67: Basic Principle of light amplification. u_{in} and u_{out} denote the incoming and outgoing flux of the light wave with the relation $u_{out} >> u_{in}$

8.1.1 Absorption

Resonant excitation of electrons from the ground state E_1 into an excited atomic state E_2 of the laser medium occurs if the energy of the incoming photon $E_{ph} = \hbar\omega$ reaches the energetic difference between both states $E_{ph} = \Delta E = E_2 - E_1$ as sketched in Fig. 68a). Here, $N_{1,2}$ denote the

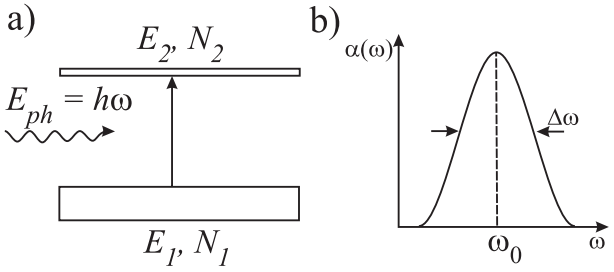

Figure 68: a) Energy model of the absorption process. Resonant excitation of electrons from the ground state E_1 into an excited atomic state E_2 occurs if the energy of the incoming photon $E_{ph} = \hbar\omega$ reaches the energetic difference between both states $E_{ph} = \Delta E = E_2 - E_1$. b) Absorption band centered at the resonance frequency ω_0 with the full width at half maximum $\Delta\nu$.

number of atoms in the energy state $E_{1,2}$ per cm^3. As a result of the resonant excitation process

the intensity of the transmitted light wave decreases, i.e., absorption occurs at the resonance frequency ω_0 with a finite full width at half maximum of the absorption band $\Delta\nu$ (Fig. 68b). The number of absorbed photons is given by:

$$Z_a = N_1 \cdot u_{in} \cdot B_{12} \cdot f(\omega) \tag{8.1}$$

with the Einstein (or probability) coefficient B_{12} and the function $f(\omega)$ taking the frequency dependence into account. Thus the number of transmitted photons Z_t can be expressed with the total number of incoming photons Z_0 via $Z_t = Z_0 - Z_a$.

8.1.2 Spontaneous emission

Assuming a finite number of atoms in the electronic state E_2, i.e., $N_2 \neq 0$, the process of spontaneous emission occurs (Fig. 69a). It is a result of the limited lifetime of excited atoms, which is reciprocally proportional to the bandwidth of the absorption band $\tau \sim 1/\Delta\omega$. Typical values are $\tau \sim 10^{-8}$s. The transition of atoms $E_2 \rightarrow E_1$, and thus $N_2 \rightarrow N_1$, is accompanied by the emission of a photon with energy ΔE. A characteristic feature of this process is the emission of photons into all directions of space. The number of spontaneously emitted photons is described via $Z_s = N_2 \cdot A$ with the Einstein coefficient $A \sim 1/\tau$. The fraction of the Einstein coefficients for absorption and spontaneous emission is expressed by:

$$\frac{A}{B_{12}} = \frac{2}{\pi}\frac{\hbar\omega}{c^3} \tag{8.2}$$

with c the speed of light in vacuum.

8.1.3 Induced emission

Induced emission occurs if there is a finite number of atoms in the electronic state E_2, i.e., $N_2 \neq 0$, and a resonant photon is present (Fig. 69b). In this case a photon $E_{ph}^{ie} = \Delta E$ is emitted. In contrast to spontaneous emission the induced emission of a photon occurs in the same direction as the incoming photon. Thus the photon flux of the incoming wave can be amplified:

$$Z_t = Z_0 + Z_i = Z_0 + N_2 \cdot U_{in} \cdot B_{21} \cdot f(\omega) \tag{8.3}$$

The energetic balance of a photon flux exposed to a laser medium with $N_1, N_2 \neq 0$ thus results to:

$$Z_t = Z_0 + Z_i - Z_a = \Delta N \cdot u_{in} \cdot B_{12} \cdot f(\omega) \tag{8.4}$$

with $\Delta N = N_2 - N_1$. Obviously three cases can be distinguished:

- $N_2 < N_1 : \Delta N < 0$, i.e. depletion of the incoming light wave
- $N_2 = N_1 : \Delta N = 0$, i.e. unaffected transmission of the light wave

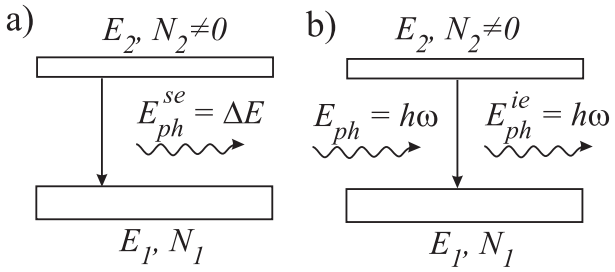

Figure 69: a) Spontaneous emissions of a photon $E_{ph}^{se} = \Delta E$ due to relaxation processes of excited atoms. b) Induced emission of a photon $E_{ph}^{ie} = \Delta E$ by an incoming photon. In both cases $N_2 \neq 0$ is required.

- $N_2 > N_1 : \Delta N > 0$, i.e. amplification of the incoming light wave.

The latter case commonly is denoted as *occupation inversion*. In the thermal equilibrium the occupation of the excited state depends on the temperature T according to $N_2 = N_1 \exp(-\Delta E/k_B T)$, with the Boltzmann constant k_B. Note that $N_2 \approx 0$ at room temperature since $k_B T << \Delta E$. For very high temperatures ($T \to \infty$) $N_2 = N_1$ can be reached resulting in an unaffected transmission of a light wave through the laser medium. Thus an occupation inversion can not be realized in the thermal equilibrium at any temperature. In order to overcome this problem laser media offering an energetic 3- or 4-level system are required.

8.1.4 3-level system

The energetic scheme of a 3-level system, e.g. of a ruby laser, is shown in Fig. 70. An occupation

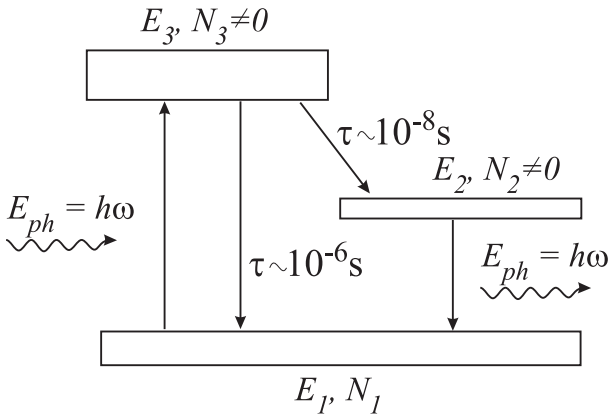

Figure 70: Energetic scheme of a 3-level system.

inversion $\Delta N = N_2 - N_1$ is reached under intense illumination with light of $E_{ph}^{p} = E_3 - E_1$, so

that light of $E_{ph} = E_2 - E_1$ can be amplified. Population of N_2 occurs via de-excitation of the optically excited atomic state $E_3 \rightarrow E_2$. Thus this process is commonly called *optical pumping*. However, the population of each state and especially the occupation inversion is very sensitive to the intensity W of the pump light as shown in Fig 71. Several characteristic population ratios can

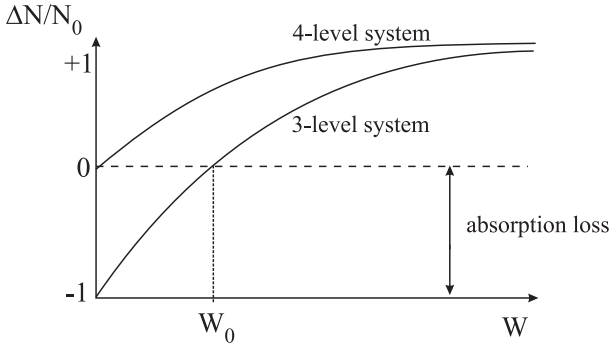

Figure 71: Dependence of the ratio $\Delta N/N_0$ on the intensity of the pump light for a 3- and 4-level system.

be distinguished depending on the intensity:

- $W = 0 : N_2 = 0 \Rightarrow \Delta N/N_0 = -1$
- $W < W_0 : N_1 > N_2 \Rightarrow \Delta N/N_0 < 0$
- $W = W_0 : N_1 = N_2 \Rightarrow \Delta N/N_0 = 0$
- $W > W_0 : N_2 > N_1 \Rightarrow \Delta N/N_0 > 0$
- $W \gg W_0 : N_1 \approx 0 \Rightarrow \Delta N/N_0 = 1$

It is obvious that the occupation inversion $\Delta N/N_0 > 0$ occurs for intensities $> W_0$. In contrast, absorption processes dominate the transmission of the light wave for intensities $< W_0$.

8.1.5 4-level system

The scheme of a 4-level system, e.g. Nd-YAG laser, is shown in Fig. 72. The key feature of the 4-level system is that E_1 is empty in the thermal equilibrium, i.e. occupation inversion is present as soon as $N_2 \neq 0$. This feature is connected with a comparable small lifetime of the atomic states in E_1. As a result there is no threshold behavior of the ratio $\Delta N/N_0$ on the intensity as shown in Fig. 71.

The efficiency of amplification further depends on the interaction length of the light wave in the laser media by:

$$I_{out} = I_{in} \exp\left(\frac{B_{12}\Delta N}{c} \cdot l\right) \tag{8.5}$$

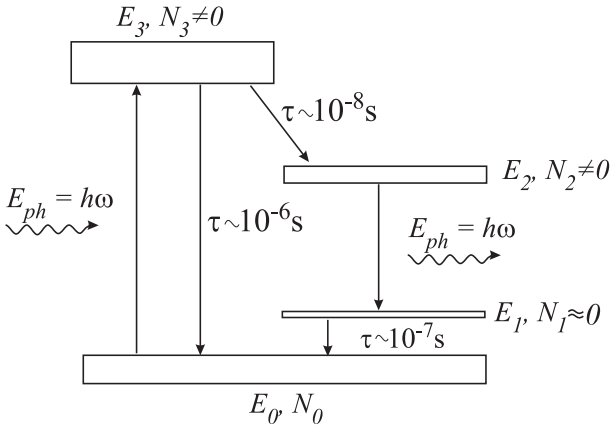

Figure 72: energetic scheme of a 4-level system.

It should be noted, that N_2 reaches saturation with increasing intensity of the amplified light wave and that there is a non-linear dependence of the amplified intensity on the pump intensity as well as on the interaction length. The gain $\Gamma = I_{out}/I_{in}$ is introduced as measure for the amplification.

8.1.6 Optical resonator

An enhancement of the gain can be reached by using an optical resonator consisting of two mirrors M as shown schematically in Fig. 73. The incoming light wave is focused by the lenses L into the laser medium in order to enhance the intensity of the incoming fundamental wave. In dependent

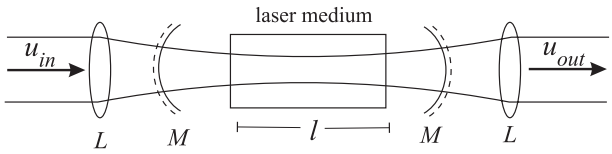

Figure 73: Optical resonator by two mirrors M with the laser medium. The incoming light wave is focused to enhance the incoming intensity of the fundamental wave.

on the reflectivity of the mirrors M the light wave passes by $1/(1-R)$ times through the laser medium, e.g. with a reflectivity of R = 0.95 an enhancement by a factor of 20 is reached by the use of the optical cavity.

8.1.7 Pump processes

- *Optical pumping*. Absorption of (laser) light in the laser medium. Typically found in solid state and liquid laser systems.

- *Electrical pumping*. Gas recharging in gas- and semiconductor lasers
- *Chemical pumping*. $A + B \rightarrow AB*$ (AB*: excited molecule) or dissociative: $AB + h\nu \rightarrow A + B*$ (B*: excited atom)

Fig. 74 displays three common configurations for optical pumping using lamps: a) *helix*-configuration, b) *elliptic cavity* and c) *close coupling*. For an efficient optical pumping the spectrum of the pump

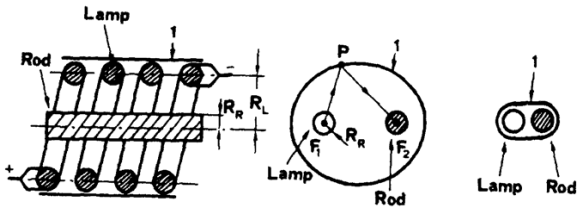

Figure 74: Optical pumping with lamps a) helix-configuration, b) eliptic cavity and c) close coupling.

source (lamp or laser) should be matched to the absorption spectrum of the laser medium. As an example Fig. 75a shows the emission spectrum of a Kr-high pressure lamp and 75b the absorption spectra of the laser media Nd:YAG and Nd:Glass. Absorption bands of the Nd-center occur in the near-infrared region at about 800 nm and show a broad absorption band when embedded in glass. Here, the exposure to light of the Kr-high pressure lamp will ensure efficient optical pumping, whereas light of a semiconductor laser with λ = 808 nm is preferable in Nd:YAG.

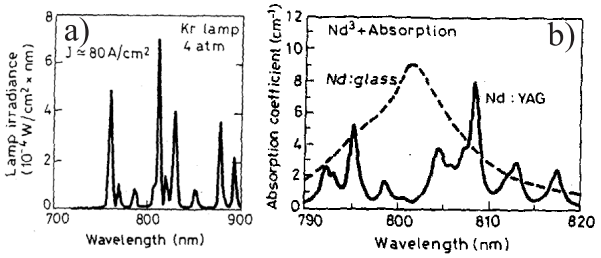

Figure 75: a) Emission spectrum of a Kr-high pressure lamp, b) Absorption spectra of the laser media Nd:YAG and Nd:Glass.

8.2 Cavity design

8.2.1 Optical resonator

In the following we will focus on a 4-level laser system of a Nd:YAG laser medium optically pumped using a semiconductor laser. Such systems are widely used and designated as *diode-pumped solid-state laser*. A typical scheme illustrating a corresponding cavity design is shown

in Fig. 76. The divergent light of a Ga-Al-As-semiconductor laser (λ = 808 nm)is focused via a lens into the Nd:YAG laser rod. As a remarkable feature the optical cavity is realized by dielectric mirrors coated onto the entrance surfaces of the laser rod. A difference in the reflectivity of 99.9 % and 99.8 % ensures high and low reflector properties such that the emission of laser light occurs into a preferred direction. According to the energetic scheme of the Nd:YAG 4-level system light of wavelength λ = 1064 nm is emitted. Typical system specifications are a pump power of 1 - 2 W and infrared light of several 100 mWs. It is noteworthy that this cavity design enforces high

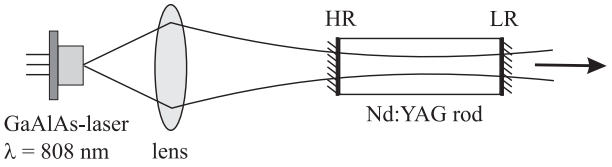

Figure 76: Schematic setup of a diode-pumped Nd:YAG laser cavity. The divergent light of a Ga-Al-As-semiconductor laser (λ = 808 nm) is focused via a lens into the Nd:YAG laser rod. The optical cavity is realized by dielectric mirrors coated onto the entrance surfaces of the laser rod with different reflectivity.

demands to the polishing of the laser rod and to the parallelism of the two entrance surfaces to each other. Other possibilities for a compact cavity design are the *prism* and *spherical resonator* (confocal as well as concentric) as shown in Fig. 77a and 77b. *Open resonators* are of advantage to get linearly polarized light. E.g. in Fig. 77c the entrance faces of the laser rod are cut corresponding to Brewsters law. Internal reflections are suppressed in the *in-line configuration* by dielectrically coated surfaces (77d). Further, it is possible to influence the laser light by e.g. diaphragms, modulators, filters, optical switches, etc. .

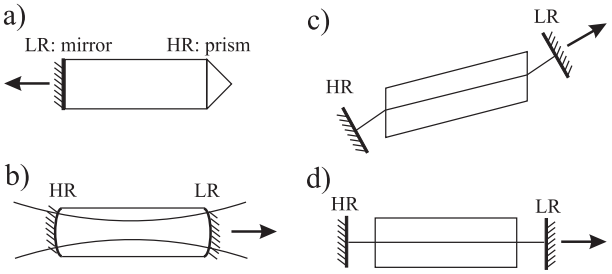

Figure 77:

8.2.2 Laser medium

In addition to the optical cavity great demands are required from the Nd:YAG laser-rod itself. Beyond the most important are:

- high optical quality: no striations, high optical homogeneity in the refractive index and absorption coefficient, perfect surfaces
- high optical damage threshold: e.g. cw-laser light up to 1 kW IR at a diameter of 100 μm.
- high conversion efficiency: Nd:YAG e.g. 1-2 $\%$
- high heat flow in order to avoid thermal lens effects
- good preparation and growth conditions in order to get high quality and to reduce costs

8.2.3 Losses

One of the key aspects in the cavity design is the balance between the light amplification Γ and its losses L. For an efficient laser process the condition $\Gamma > l$ has to be fulfilled with the threshold condition $\Gamma - L = 0$. Losses are distinguished from 1) the laser rod:

- scattering in the volume or on the surface of the laser rod
- absorption in the volume of the laser rod
- reflection losses at the laser rod entrance faces
- beam distortion due to refraction or diffraction processes at refractive index inhomogeneities

and b) the laser cavity:

- reflection losses and scattering at the mirrors
- absorption losses in the surrounding medium
- coupled-out intensity
- filters, switches, modulators, diaphragms.

8.2.4 Dimensions of the laser rod

The dimensions of the laser rod, i.e. the length l and the diameter $d = 2 \cdot r$ with $l \gg r$, are related via the Fresnel number:

$$F = \frac{n \cdot r^2}{\lambda \cdot l}. \tag{8.6}$$

In order to reduce losses by diffraction the condition $F \gg 1$ has to be fulfilled. Typical values are $5 < l < 20.0$ mm. On the other hand the volume of the rod is decisive for the efficiency of optical pumping, which is described by the *Schawlow-Townes relation* for a 4-level system:

$$P = \frac{P_0}{P_{(\Gamma - L = 0)}} \cdot \frac{V}{B_{12} \cdot \tau_{21} \cdot \tau_c}, \tag{8.7}$$

whereby τ_c denotes the lifetime of the photons in the laser cavity and P_0 the pump power. Typical values of $\zeta = P_0/P_{(\Gamma - L=0)}$ are ~ 1000 for Nd:YAG and ~ 30 for ruby (3-level system).

8.2.5 Estimation of the cavity parameter τ_c

The measure τ_c is strongly dependent on the cavity losses and of importance a) to determine laser losses in order to optimize the cavity design and b) to determine the optimum pump power. However, τ_c can not be measured inside the laser cavity. A widely used experimental procedure is the optical pumping of the laser process with a single light pulse and the subsequent detection of the kinetics of the out-coupled intensity. The value τ_c is then determined from the periodicity and the damping of the retrieved signal as described in the following.

Optical pumping with pulsed light leads to a temporal development of the number of atoms N_2 in the energy level E_2 of the Nd:YAG 4-level system and thus of the number of photons Q within the optical cavity. The laser rod contributes via

$$\frac{dN_2}{dt} = P - \frac{B_{12}NQ}{V} - \frac{N}{\tau_{21}} \tag{8.8}$$

with τ_{21} the characteristic lifetime of the spontaneous emission $N_2 \rightarrow N_1$. The second and third terms of equation (8.8) account for induced and spontaneous emission, respectively. The temporal development of the number of photons in the cavity follows

$$\frac{dQ}{dt} = \frac{B_{12}NQ}{V} + \frac{N}{M\tau_{21}} - \frac{Q}{\tau_c} \tag{8.9}$$

and is enlarged by induced and spontaneous emission (1st and 2nd terms) and is minimized by the restricted lifetime of photons. The measure M accounts for photons which participate in the eigenmode of the optical cavity. The equation system is solved with the linear approximation:

$$\begin{aligned} N &= N_0 + \epsilon; \qquad N_0 = \frac{V}{B_{12}\tau_c} \\ Q &= Q_0 + \eta; \qquad Q_0 = M - P\tau_c \end{aligned} \tag{8.10}$$

where ϵ and η are small fluctuations of N_0 and Q_0. Here, the power P inside the laser cavity and the pump power are connected by $P = \zeta \cdot P_0 = \zeta \cdot N_0/\tau_{21}$. Solution of eq. (8.8) and (8.9) yields:

$$\left.\begin{matrix} \eta \\ \tau \end{matrix}\right\} \sim \exp\left(-\frac{\zeta t}{2\tau_{21}}\right) \begin{matrix} \sin \\ \cos \end{matrix} \sqrt{\frac{\zeta - 1}{\tau_{21}\tau_c}} \tag{8.11}$$

which represents a harmonic oscillation of period

$$T^2 = 4\pi^2 \frac{\tau_c \tau_{21}}{\zeta - 1} \tag{8.12}$$

and a damping constant

$$\tau_d = \frac{2\tau_{21}}{\zeta} \tag{8.13}$$

In the approximation $\zeta \approx 1$ we get : $T^2 = 2\pi^2 \tau_c \tau_d$, so that τ_c can be determined by the periodicity T and the damping constant τ_d of the detected laser intensity.

8.2.6 Reduction of unwanted Eigenmodes

The suppression of unwanted longitudinal Eigenmodes is related with a cavity of high mechanical stability. This can be realized using a temperature controlled cavity where all optical elements including the laser rod are stabilized thermally. Further materials with extreme low extension coefficients are commonly used (super invar). Unwanted transversal Eigenmodes are suppressed by introducing diaphragms inside the optical cavity. A birefringence filter, i.e. a combination of polarizer and retarder wave-plate, is commonly used to get linear polarized laser light with an extremely small bandwidth. Fig. 78 shows the setup of an optical resonator with a temperature controlled base plate and laser rod, a birefringence filter BF and a diaphragm D. Note the specific

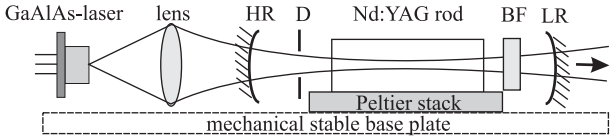

Figure 78: Setup of an optical resonator with a temperature controlled base plate and laser rod, a birefringence filter BF and a diaphragm D.

demands for the dielectric coatings of the laser rod (low reflection coating for λ = 1064 nm and λ = 808 nm) and for the transmission of the high reflector (high transmission for λ = 808 nm, high reflection for λ = 1064 nm). Typical specifications of such laser systems are a single pass power of 20-40 mW of infrared light (λ = 1064 nm) with a pump power of $P(\lambda = 808\,nm)$ = 2 W and dimensions of the laser rod of 10 mm length and 3 $\times$ 3 mm^1 surface area. An optimum cavity design leads to an intra-cavity power of 20 - 50 W and of $\approx$ 500 mW extra-cavity.

8.2.7 Cavity design with intra-cavity second harmonic generation

The next step is the design of a Nd:YAG laser system with intra-cavity second harmonic generation to get intense continuous-wave laser light of wavelength λ = 532 nm. The demands for the design of an optical cavity with intra-cavity second harmonic generation (SHG) are

- Two independent adjustable beam waists, one localized in the laser rod and one in the non-linear crystal for SHG. The dimensions of the beam waist in the laser rod has to be adapted for the beam waist of the laser light for optical pumping. The beam waist within the non-linear crystal should be optimized for a high intensity under consideration of the crystal length.
- A high mechanical stability of the optical cavity over a long timescale.
- Linear polarized laser light.

Further the redesign of the Nd:Yag optical cavity should account for the following aspects

- losses due to the non-linear crystal, especially losses due to SHG
- dielectric coatings for the non-linear crystal (λ = 1064 nm and λ = 532 nm)
- transmission of the low reflector (high transmission at λ = 532 nm)
- refractive index of the non-linear crystal influences the beam waist intra-cavity.

With respect to these demands and aspects it should be stressed that intra-cavity second harmonic generation is inevitably necessary to get intense continuous wave laser light. The power of the frequency doubled beam is $\sim I_{1064}^2$ and $I_{1064}^{\mathrm{ic}} >> I_{1064}^{\mathrm{ec}}$, where ic and ec denote intra- and extra-cavity, respectively. In contrast, SHG with pulsed laser light is commonly realized in an extra-cavity configuration.

The disadvantage of intra-cavity SHG is two-folded: a) a more complicated design of the optical cavity is enforced and an exchange of the non-linear crystal is impossible, e.g. for purposes of optimization, b) the demands to the non-linear crystal are enormous especially due to the extremely high power of the fundamental wave (high risk for optically induced mechanical damage). Fig. 79

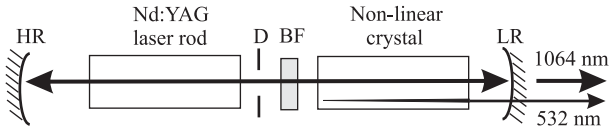

Figure 79: principle setup for an optical cavity with intra-cavity SHG.

shows the principle setup for an optical cavity with intra-cavity SHG. All laser properties are restricted for the generation of infrared light at λ = 1064 nm, i.e., the cavity does not amplify light of λ = 532 nm. The emission of the frequency doubled laser light occurs in both directions, but is blocked by the polarizer of the birefringence filter (the orientation of the electric field vector for type I and type II phase matching are different to the electric field vector of the fundamental wave). The intensity of the visible light is comparable small in such systems, e.g., with a pump power of 2 W and an intra-cavity power of 10 - 50 W a laser beam with $\approx$ 150 mW at λ = 532 nm is generated in the output.

8.2.8 Losses by the non-linear crystal

As already mentioned intra-cavity SHG represents an additional loss and thus the demand for a large SHG coefficient is questionable. The condition for the threshold of the laser process with intra-cavity SHG now follows the connection: $\Gamma - L - (K \cdot P_{1064})$ with $P_{532} = K \cdot P_{1064}^2$ and the non-linear coupling coefficient

$$K = K_{IR} \cdot l_i \cdot k_{IR} \cdot h(\sigma, \zeta) \cdot 10^7 \tag{8.14}$$

Here, $k_{IR} = 2\pi n_{IR}/\lambda_{IR}$ denotes the wave vector of the infrared laser beam, l_i the interaction length of the fundamental and harmonic waves and K_{IR} is a material specific constant, e.g. $K_{IR} = 128\pi^2\omega^2/c^3 n_{IR}^2 n_{VIS} \cdot d_{32}$ for $Ba_2NaNb_5O_{15}$. The function $h(\sigma, \zeta)$ is given by the theory of Boyd and Kleinmann and takes diffraction, double refraction and absorption processes into account. Here $\sigma = 1/2b\Delta K$ is connected to the phase matching parameter ΔK and $\zeta = l_i/b$ to the confocal parameter $b = \omega_0^2/k_{IR}$ with the beam waist ω_0. The dependencies of P_{SHG} on the coupling coefficient and of the coupling coefficient on the beam waist are shown in Fig. 80.

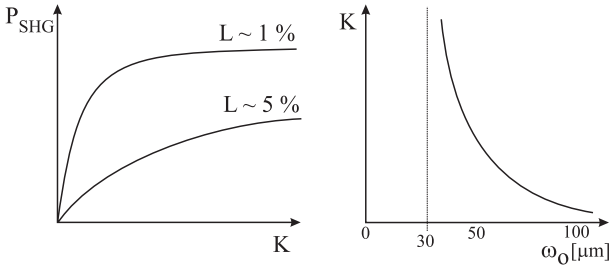

Figure 80: P_{SHG} as a function of the coupling coefficient K and of K on the beam waist ω_0.

8.2.9 Selection of the non-linear crystal

The selection of an adequate non-linear crystal is restricted by

- a large SHG coefficient
- the refractive index and the dispersion
- the optical transmission range
- the phase matching properties
- the optical damage threshold
- the optically induced mechanical damage threshold
- the optical homogeneity of refractive index and absorption coefficient
- the hardness, chemical stability.

Some of the commonly used non-linear crystals are given in tab. 6.

$KTiOPO_4$ is widely used for intra-cavity second harmonic generation of cw-laser light. An important feature is its pronounced birefringence, which is used in combination with a polarizer as birefringence filter.

	Transparency range (nm)	Damage threshold (GW/cm^2)	FOM
β-BaB_2O_4	198-3300	10	15
$Ba_2NaNb_5O_{15}$		0.001	
KH_2PO_4	200-1500	0.5	1
LiB_3O_5		2	1
$LiNbO_3$		0.02	
$LiIO_3$	300-5500	0.05	50
$KTiOPO_4$	350-4500	1	215
$KNbO_3$	410-5000	0.35	1755
CsD_2AsO_4	1660-2700	0.5	1.7
$(NH)_2CO$	210-1400	1.5	10.6
LAP	220-1950	10	40
m-NA	500-2000	0.2	60
MgO-$LiNbO_3$	400-5000	0.05	105
POM	414-2000	2	350
MAP	472-2000	3	1600
COANP	480-2000		4690
DAN	430-2000		5090
PPLiNbO_3	400-5000	0.05	2460

Table 6: Properties of non-linear crystals. FOM is determined by $(d^2/n^3)(EL/\lambda)\Delta\theta^2$. LAP: L-arginine phosphate monohydrate, m-NA: meta nitroaniline, POM: 3-methyl-4-nitropyridine N-Oxide, MAP: methyl (2,4-diinitrophenyl) aminopropanoate, COANP: 2N-cyclooctylamino-5-nitropyridine

References

[1] O. Svelto. *Principles of Lasers*. Plenum Press, New York und London, 1998.

[2] A. E. Siegmann. *Lasers*. Unversity Science Books, Mill Valley, California, 1986.

[3] W. Koechner. *Solid State Engineering*. Springer Verlag, New York, 1998.

[4] A. Yariv. *Quantum Electronics*. John Wiley and Sons, New York, 1967.

A Matrices for symmetry operations

selection of matrices for point group operations in orthogonal systems

at origin [0 0 0]

$1(E)$	$\begin{pmatrix} 1 & 0 & 0 \\ 0 & 1 & 0 \\ 0 & 0 & 1 \end{pmatrix}$	$\bar{1}(i)$	$\begin{pmatrix} -1 & 0 & 0 \\ 0 & -1 & 0 \\ 0 & 0 & -1 \end{pmatrix}$

along [1 0 0]

$2(C_2)$	$\begin{pmatrix} 1 & 0 & 0 \\ 0 & -1 & 0 \\ 0 & 0 & -1 \end{pmatrix}$	$\bar{2} = m$	$\begin{pmatrix} -1 & 0 & 0 \\ 0 & 1 & 0 \\ 0 & 0 & 1 \end{pmatrix}$
$4(C_4)$	$\begin{pmatrix} 1 & 0 & 0 \\ 0 & 0 & 1 \\ 0 & -1 & 0 \end{pmatrix}$	$\bar{4} = (S_4^3)$	$\begin{pmatrix} -1 & 0 & 0 \\ 0 & 0 & -1 \\ 0 & 1 & 0 \end{pmatrix}$
$4^2(C_4^2) = 2(C_2)$		$\bar{4}^2(S_4^2) = 2(C_2)$	
$4^3(C_4^3)$	$\begin{pmatrix} 1 & 0 & 0 \\ 0 & 0 & -1 \\ 0 & 1 & 0 \end{pmatrix}$	$\bar{4}^3 = (S_4)$	$\begin{pmatrix} -1 & 0 & 0 \\ 0 & 0 & 1 \\ 0 & -1 & 0 \end{pmatrix}$

along [0 1 0]

$2(C_2)$	$\begin{pmatrix} -1 & 0 & 0 \\ 0 & 1 & 0 \\ 0 & 0 & -1 \end{pmatrix}$	$\bar{2} = m$	$\begin{pmatrix} 1 & 0 & 0 \\ 0 & -1 & 0 \\ 0 & 0 & 1 \end{pmatrix}$
$4(C_4)$	$\begin{pmatrix} 0 & 0 & -1 \\ 0 & 1 & 0 \\ 1 & 0 & 0 \end{pmatrix}$	$\bar{4} = (S_4^3)$	$\begin{pmatrix} 0 & 0 & 1 \\ 0 & -1 & 0 \\ -1 & 0 & 0 \end{pmatrix}$
$4^2(C_4^2) = 2(C_2)$		$\bar{4}^2(S_4^2) = 2(C_2)$	
$4^3(C_4^3)$	$\begin{pmatrix} 0 & 0 & 1 \\ 0 & 1 & 0 \\ -1 & 0 & 0 \end{pmatrix}$	$\bar{4}^3 = (S_4)$	$\begin{pmatrix} 0 & 0 & -1 \\ 0 & -1 & 0 \\ 1 & 0 & 0 \end{pmatrix}$

along [0 0 1]

$2(C_2)$ $\begin{pmatrix} -1 & 0 & 0 \\ 0 & -1 & 0 \\ 0 & 0 & 1 \end{pmatrix}$ $\bar{2} = m$ $\begin{pmatrix} 1 & 0 & 0 \\ 0 & 1 & 0 \\ 0 & 0 & -1 \end{pmatrix}$

$4(C_4)$ $\begin{pmatrix} 0 & -1 & 0 \\ 1 & 0 & 0 \\ 0 & 0 & 1 \end{pmatrix}$ $\bar{4} = (S_4^3)$ $\begin{pmatrix} 0 & 1 & 0 \\ -1 & 0 & 0 \\ 0 & 0 & -1 \end{pmatrix}$

$4^2(C_4^2) = 2(C_2)$ $\bar{4}^2(S_4^2) = 2(C_2)$

$4^3(C_4^3)$ $\begin{pmatrix} 0 & 1 & 0 \\ -1 & 0 & 0 \\ 0 & 0 & 1 \end{pmatrix}$ $\bar{4}^3 = (S_4)$ $\begin{pmatrix} 0 & -1 & 0 \\ 1 & 0 & 0 \\ 0 & 0 & -1 \end{pmatrix}$

along [1 1 0]

$2(C_2)$ $\begin{pmatrix} 0 & 1 & 0 \\ 1 & 0 & 0 \\ 0 & 0 & -1 \end{pmatrix}$ $\bar{2} = m$ $\begin{pmatrix} 0 & -1 & 0 \\ -1 & 0 & 0 \\ 0 & 0 & 1 \end{pmatrix}$

along [1 0 1]

$2(C_2)$ $\begin{pmatrix} 0 & 0 & 1 \\ 0 & -1 & 0 \\ 1 & 0 & 0 \end{pmatrix}$ $\bar{2} = m$ $\begin{pmatrix} 0 & 0 & -1 \\ 0 & 1 & 0 \\ -1 & 0 & 0 \end{pmatrix}$

along [0 1 1]

$2(C_2)$ $\begin{pmatrix} -1 & 0 & 0 \\ 0 & 0 & 1 \\ 0 & 1 & 0 \end{pmatrix}$ $\bar{2} = m$ $\begin{pmatrix} 1 & 0 & 0 \\ 0 & 0 & -1 \\ 0 & -1 & 0 \end{pmatrix}$

along [1 $\bar{1}$ 0]

$2(C_2)$ $\begin{pmatrix} 0 & -1 & 0 \\ -1 & 0 & 0 \\ 0 & 0 & -1 \end{pmatrix}$ $\bar{2} = m$ $\begin{pmatrix} 0 & 1 & 0 \\ 1 & 0 & 0 \\ 0 & 0 & 1 \end{pmatrix}$

along [$\bar{1}$ 0 1]

$2(C_2)$ $\begin{pmatrix} 0 & 0 & -1 \\ 0 & -1 & 0 \\ -1 & 0 & 0 \end{pmatrix}$ $\bar{2} = m$ $\begin{pmatrix} 0 & 0 & 1 \\ 0 & 1 & 0 \\ 1 & 0 & 0 \end{pmatrix}$

along [0 1 $\bar{1}$]

$2(C_2)$ $\begin{pmatrix} -1 & 0 & 0 \\ 0 & 0 & -1 \\ 0 & -1 & 0 \end{pmatrix}$ $\bar{2} = m$ $\begin{pmatrix} 1 & 0 & 0 \\ 0 & 0 & 1 \\ 0 & 1 & 0 \end{pmatrix}$

along [1 1 1]

$3(C_3)$ $\begin{pmatrix} 0 & 0 & 1 \\ 1 & 0 & 0 \\ 0 & 1 & 0 \end{pmatrix}$ $\bar{3}(S_6^5)$ $\begin{pmatrix} 0 & 0 & -1 \\ -1 & 0 & 0 \\ 0 & -1 & 0 \end{pmatrix}$

$3^2(C_3^2)$ $\begin{pmatrix} 0 & 1 & 0 \\ 0 & 0 & 1 \\ 1 & 0 & 0 \end{pmatrix}$ $\bar{3}^5(S_6)$ $\begin{pmatrix} 0 & -1 & 0 \\ 0 & 0 & -1 \\ -1 & 0 & 0 \end{pmatrix}$

$\bar{3}^2(S_6^4) = 3^2(C_3^2)$
$\bar{3}^3(S_6^3) = \bar{1}(i)$
$\bar{3}^4(S_6^2) = 3(C_3)$

along [$\bar{1}$ 1 1]

$3(C_3)$ $\begin{pmatrix} 0 & -1 & 0 \\ 0 & 0 & 1 \\ -1 & 0 & 0 \end{pmatrix}$ $\bar{3}(S_6^5)$ $\begin{pmatrix} 0 & 1 & 0 \\ 0 & 0 & -1 \\ 1 & 0 & 0 \end{pmatrix}$

$3^2(C_3^2)$ $\begin{pmatrix} 0 & 0 & -1 \\ -1 & 0 & 0 \\ 0 & 1 & 0 \end{pmatrix}$ $\bar{3}^5(S_6)$ $\begin{pmatrix} 0 & 0 & 1 \\ 1 & 0 & 0 \\ 0 & -1 & 0 \end{pmatrix}$

$\bar{3}^2(S_6^4) = 3^2(C_3^2)$
$\bar{3}^3(S_6^3) = \bar{1}(i)$
$\bar{3}^4(S_6^2) = 3(C_3)$

along [1 $\bar{1}$ 1]

$3(C_3)$ $\begin{pmatrix} 0 & -1 & 0 \\ 0 & 0 & -1 \\ 1 & 0 & 0 \end{pmatrix}$ $\bar{3}(S_6^5)$ $\begin{pmatrix} 0 & 1 & 0 \\ 0 & 0 & 1 \\ -1 & 0 & 0 \end{pmatrix}$

$3^2(C_3^2)$ $\begin{pmatrix} 0 & 0 & 1 \\ -1 & 0 & 0 \\ 0 & -1 & 0 \end{pmatrix}$ $\bar{3}^5(S_6)$ $\begin{pmatrix} 0 & 0 & -1 \\ 1 & 0 & 0 \\ 0 & 1 & 0 \end{pmatrix}$

$$\bar{3}^2(S_6^4) = 3^2(C_3^2)$$
$$\bar{3}^3(S_6^3) = \bar{1}(i)$$
$$\bar{3}^4(S_6^2) = 3(C_3)$$

along [1 1 $\bar{1}$]

$3(C_3)$ $\begin{pmatrix} 0 & 1 & 0 \\ 0 & 0 & -1 \\ -1 & 0 & 0 \end{pmatrix}$ $\bar{3}(S_6^5)$ $\begin{pmatrix} 0 & -1 & 0 \\ 0 & 0 & 1 \\ 1 & 0 & 0 \end{pmatrix}$

$3^2(C_3^2)$ $\begin{pmatrix} 0 & 0 & -1 \\ 1 & 0 & 0 \\ 0 & -1 & 0 \end{pmatrix}$ $\bar{3}^5(S_6)$ $\begin{pmatrix} 0 & 0 & 1 \\ -1 & 0 & 0 \\ 0 & 1 & 0 \end{pmatrix}$

$$\bar{3}^2(S_6^4) = 3^2(C_3^2)$$
$$\bar{3}^3(S_6^3) = \bar{1}(i)$$
$$\bar{3}^4(S_6^2) = 3(C_3)$$

B A tiny group theory primer

*D*efinition 1: Group
A group $\mathcal{G}$ is a set of elements together with a binary composition called a product such that

(i) the product of any two elements in the group is defined and is a member of the group: if $A, B \in \mathcal{G}$ then $A \cdot B \in \mathcal{G}$

(ii) the product is associative: $A \cdot (B \cdot C) = (A \cdot B) \cdot C$ for all $A, B, C \in \mathcal{G}$,

(iii) there exists a unique identity E in the group: $E \cdot A = A \cdot E = A$ for all $A \in \mathcal{G}$, and

(iv) every element has a unique inverse element: given $A \in \mathcal{G}$ there exists a unique element A^{-1} such that $A \cdot A^{-1} = A^{-1} \cdot A = E$.

*D*efinition 2: Order of a group
The number $|g|$ of elements in a group, $\mathcal{G}$, is called the order of the group.

*D*efinition 3: Order of an element
The order of an element $A \in \mathcal{G}$ is the least positive integer s such that $A^S = E$.

The full information of a group is given by its multiplication table that means a quadratic table of all products of two elements with all elements in the first row and the first column. Usually not all $|g|$ elements are needed to construct the multiplication table. There exist relations between several elements. For example some elements are simply formed by operations like those in definition 3. In general, if every element of $\mathcal{G}$ is expressible as a product of a smaller number of distinct elements, we call those elements generating elements (generators) of $\mathcal{G}$. The choice of generators is not unique!

*D*efinition 4: Abelian group
If $\mathcal{G}$ is a group and $G_1 \cdot G_2 = G_2 \cdot G_1$ für alle $G_1, G_2 \in \mathcal{G}$ then it is called an Abelian group.

*D*efinition 5: Cyclic group
If all elements of $\mathcal{G}$ can be expressed by products of one distinct element, then it is called a *c*yclic group. All cyclic groups are Abelian groups.

*D*efinition 6: Conjugate elements
Two elements $G_1, G_2 \in \mathcal{G}$ are said to be *c*onjugate if there exists an element $G \in \mathcal{G}$ such that $G_2 = G \cdot G_1 \cdot G^{-1}$.

*D*efinition 7: Subgroup
A subset $\mathcal{H}$ of a group $\mathcal{G}$ that is itself a group is called a subgroup of $\mathcal{G}$

*D*efinition 8: Invariant subgroup
If $\mathcal{H}$ is a subgroup of $\mathcal{G}$ such that , for all $G \in \mathcal{G}$ and for all $H \in \mathcal{H}$, $G \cdot H \cdot G^{-1} \in \mathcal{H}$, then $\mathcal{H}$ is said to be an *invariant* subgroup of $\mathcal{G}$.

*D*efinition 9: Direct product of groups
Let $\mathcal{G}$ be a group with subgroups $\mathcal{H}$ and $\mathcal{K}$ such that

(i) if $H \in \mathcal{H}$, $K \in \mathcal{K}$ then $H \cdot K = K \cdot H$

(ii) all $G \in \mathcal{G}$ can be expressed in the form $G = H \cdot K$

(iii) and if the intersection $\mathcal{H} \cap \mathcal{K}$ consists only of the identity, then $\mathcal{G}$ is called the direct product of $\mathcal{H}$ and $\mathcal{K}$ and we write $\mathcal{G} = \mathcal{H} \times \mathcal{K} = \mathcal{K} \times \mathcal{H}$. This product is sometimes called the outer direct product.

*D*efinition 10: Matrix representation
Let $\mathcal{G}$ be a finite group of order $|g|$ with elements $g \in \mathcal{G}$, and let a square matrix D(g) be associated

with each group element g. If the matrices satisfy

$$D(g_i)\, D(G_j) = D(G_k)$$

for the corresponding relation of the group elements $g_i g_j = g_k$, then the set of matrices is called a representation. The dimension of the representation is equal to the dimension of the matrix.

*D*efinition 11: Direct sum of representation
With two representations $D^{(1)}$ and $D^{(2)}$ of a group $\mathcal{G}$, a larger representation, the direct sum, is constructed according to

$$D(g) = \begin{bmatrix} D^{(1)}(g) & 0 \\ 0 & D^{(2)}(g) \end{bmatrix}$$

If no equivalence transformation exists which allows to construct a block-diagonal structure with elements of smaller dimension, then $D(g)$ is called an irreducible representation , otherwise a reducible one .

*D*efinition 12: Trace and character
The trace of a matrix D is the sum of its diagonal elements, often written $tr\, D$. The character of a matrix group D is the function χ defined on all elements $D(g)$ such that $\chi(D(g)) = tr\,(D(g))$.

C Some completions for point groups

The Table 7 of the appendix C contains 32 point groups with their notation (Schönflies and International). In addition the classes of symmetry elements and a suggestion for generators are given.

The figures 81 and 82 show objects which reflect the symmetry of each point group.

Int. short	Int. full	Schönflies	symmetry-operation	generating elements	pace-groups
triclinic					
1	1	C_1	E	E	1
$\bar{1}$	$\bar{1}$	$S_2\ (C_i)$	$E\ i$	i	2
monoclinic					
2	2	C_2	$E\ C_2$	C_2	3 - 5
m	m	$C_{1h}\ (C_s)$	$E\ \sigma_h$	σ_h	6 - 9
$2/m$	$\frac{2}{m}$	C_{2h}	$E\ C_2\ i\ \sigma_h$	$i\ C_2$	10 - 15
orthorhombic					
222	222	$D_2\ (V)$	$E\ C_2\ C_2'\ C_2''$	$C_2\ C_2'$	16 - 24
$mm2$	$mm2$	C_{2v}	$E\ C_2\ \sigma_v\ \sigma_v'$	$C_2\ \sigma_v$	25 - 46
mmm	$\frac{2}{m}\frac{2}{m}\frac{2}{m}$	$D_{2h}\ (V_h)$	$E\ C_2\ C_2'\ C_2''\ i\ \sigma_h\ \sigma_v'\ \sigma_v''$	$i\ C_2\ C_2'$	47 - 74
tetragonal					
4	4	C_4	$E\ 2C_4\ C_2$	C_4	75 - 80
$\bar{4}$	$\bar{4}$	S_4	$E\ 2S_4\ C_2$	S_4^3	81 - 82
$4/m$	$\frac{4}{m}$	C_{4h}	$E\ 2C_4\ C_2\ i\ 2S_4\ \sigma_h$	$i\ C_4$	83 - 88
422	422	D_4	$E\ 2C_4\ C_2\ 2C_2'\ 2C_2''$	$C_2\ C_4$	89 - 98
$4mm$	$4mm$	C_{4v}	$E\ 2C_4\ C_2\ 2\sigma_v\ 2\sigma_d$	$C_4\ \sigma_v$	99 - 110
$\bar{4}2m$	$\bar{4}2m$	$D_{2d}\ (V_d)$	$E\ C_2\ 2C_2'\ 2\sigma_d\ 2S_4$	$C_2\ S_4^3$	111- 122
$4/mmm$	$\frac{4}{m}\frac{2}{m}\frac{2}{m}$	D_{4h}	$E\ 2C_4\ C_2\ 2C_2'\ 2C_2''$ $i\ 2S_4\ \sigma_h\ 2\sigma_v\ 2\sigma_d$	$C_2'\ C_4$	123 - 142
trigonal (rhombohedral)					
3	3	C_3	$E\ 2C_3$	C_3	143 - 146
$\bar{3}$	$\bar{3}$	$S_6\ (C_{3i})$	$E\ 2C_3\ i\ 2S_6$	$i\ C_3$	147 - 148
32	32	D_3	$E\ 2C_3\ 3C_2'$	$C_2'\ C_3$	149 - 155
$3m$	$3m$	C_{3v}	$E\ 2C_3\ 3\sigma_v$	$\sigma_v\ C_3$	156 - 161
$\bar{3}m$	$\bar{3}\frac{2}{m}$	D_{3d}	$E\ 2C_3\ 3C_2'\ i\ 2S_6\ 3\sigma_d$	$i\ C_2'\ C_3$	162 - 167
hexagonal					
6	6	C_6	$E\ 2C_6\ 2C_3\ C_2$	$C_2\ C_3$	168 - 173
$\bar{6}$	$\bar{6}$	C_{3h}	$E\ 2C_3\ \sigma_h\ 2S_3$	$C_3\ \sigma_h$	174
$6/m$	$\frac{6}{m}$	C_{6h}	$E\ 2C_6\ 2C_3\ C_2$ $i\ 2S_3\ 2S_6\ \sigma_h$	$i\ C_2\ C_3$	175 - 176
622	622	D_6	$E\ 2C_6\ 2C_3\ C_2\ 3C_2'\ 3C_2''$	$C_2\ C_2'\ C_3$	177 - 182
$6mm$	$6mm$	C_{6v}	$E\ 2C_6\ 2C_3\ C_2\ 3\sigma_v\ 3\sigma_d$	$C_2\ \sigma_v\ C_3$	183 - 186
$\bar{6}m2$	$\bar{6}m2$	D_{3h}	$E\ 2C_3\ 3C_2'\ \sigma_h\ 2S_3\ 3\sigma_v$	$C_2\ \sigma_h\ C_3$	187 - 190
$6/mmm$	$\frac{6}{m}\frac{2}{m}\frac{2}{m}$	D_{6h}	$E\ 2C_6\ 2C_3\ C_2\ 3C_2'\ 3C_2''$ $i\ 2S_3\ 2S_6\ \sigma_h\ 3\sigma_v\ 3\sigma_d$	$i\ C_2'\ C_2\ C_3$	191 - 194
cubic					
23	23	T	$E\ 8C_3\ 3C_2$	$C_2\ C_3$	195 - 199
$m\bar{3}$	$\frac{2}{m}\bar{3}$	T_h	$E\ 8C_3\ 3C_2\ i\ 8S_4\ 3\sigma_h$	$i\ C_2\ C_3$	200 - 206
432	432	O	$E\ 8C_3\ 3C_2\ 6C_2'\ 6C_4$	$C_3\ C_4$	207 - 214
$\bar{4}3m$	$\bar{4}3m$	T_d	$E\ 8C_3\ 3C_2\ 6\sigma_d\ 6S_4$	$C_3\ S_4^3$	215 - 220
$m\bar{3}m$	$\frac{4}{m}\bar{3}\frac{2}{m}$	O_h	$E\ 8C_3\ 3C_2\ 6C_2'\ 6C_4$ $i\ 8S_4\ 3\sigma_h\ 6\sigma_d\ 6S_4$	$i\ C_3\ C_4$	221 - 230

Table 7: Notation and symmetry elements of the 32 point groups

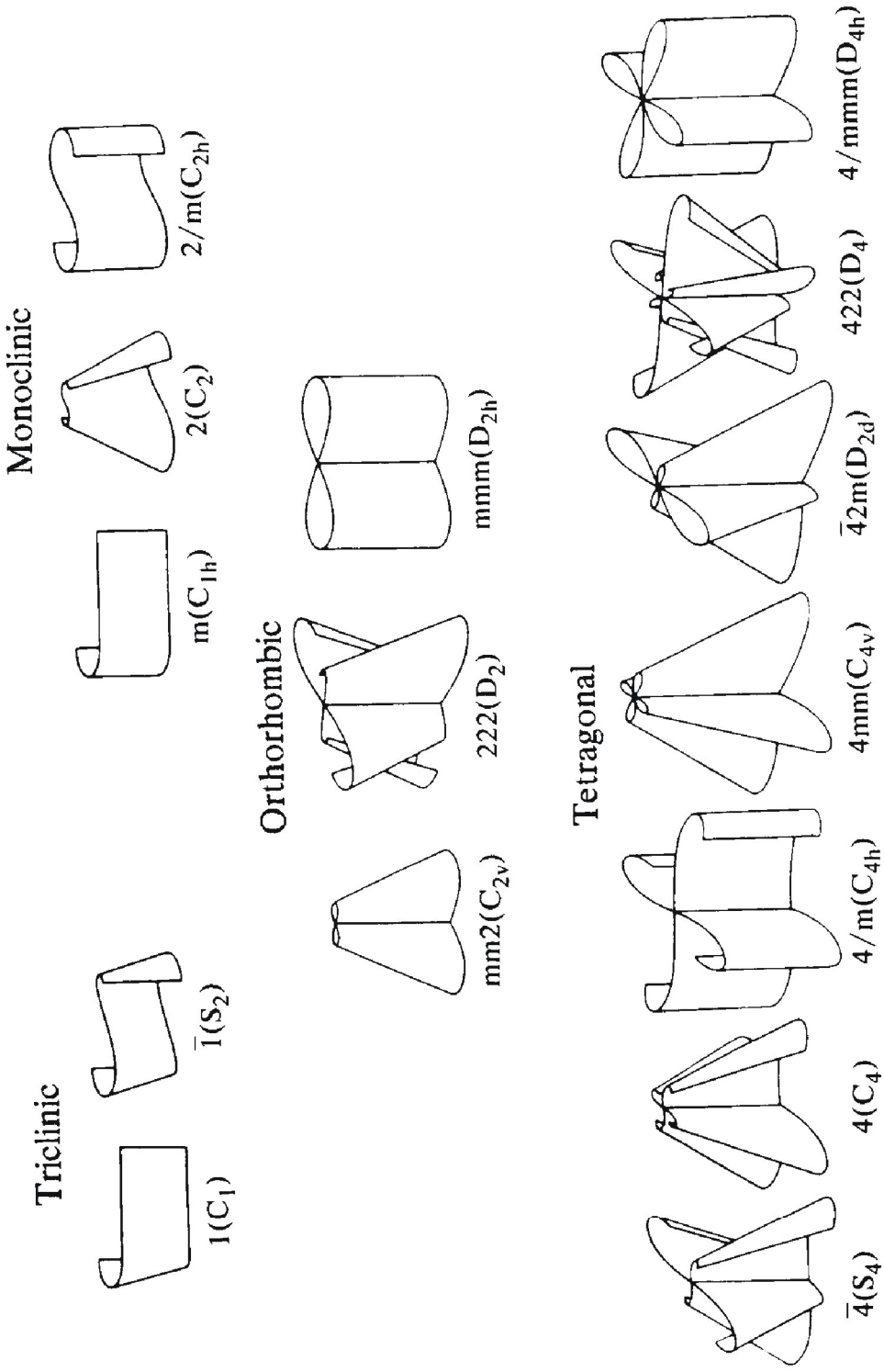

Figure 81: Part 1 of the objects of the 32 point groups

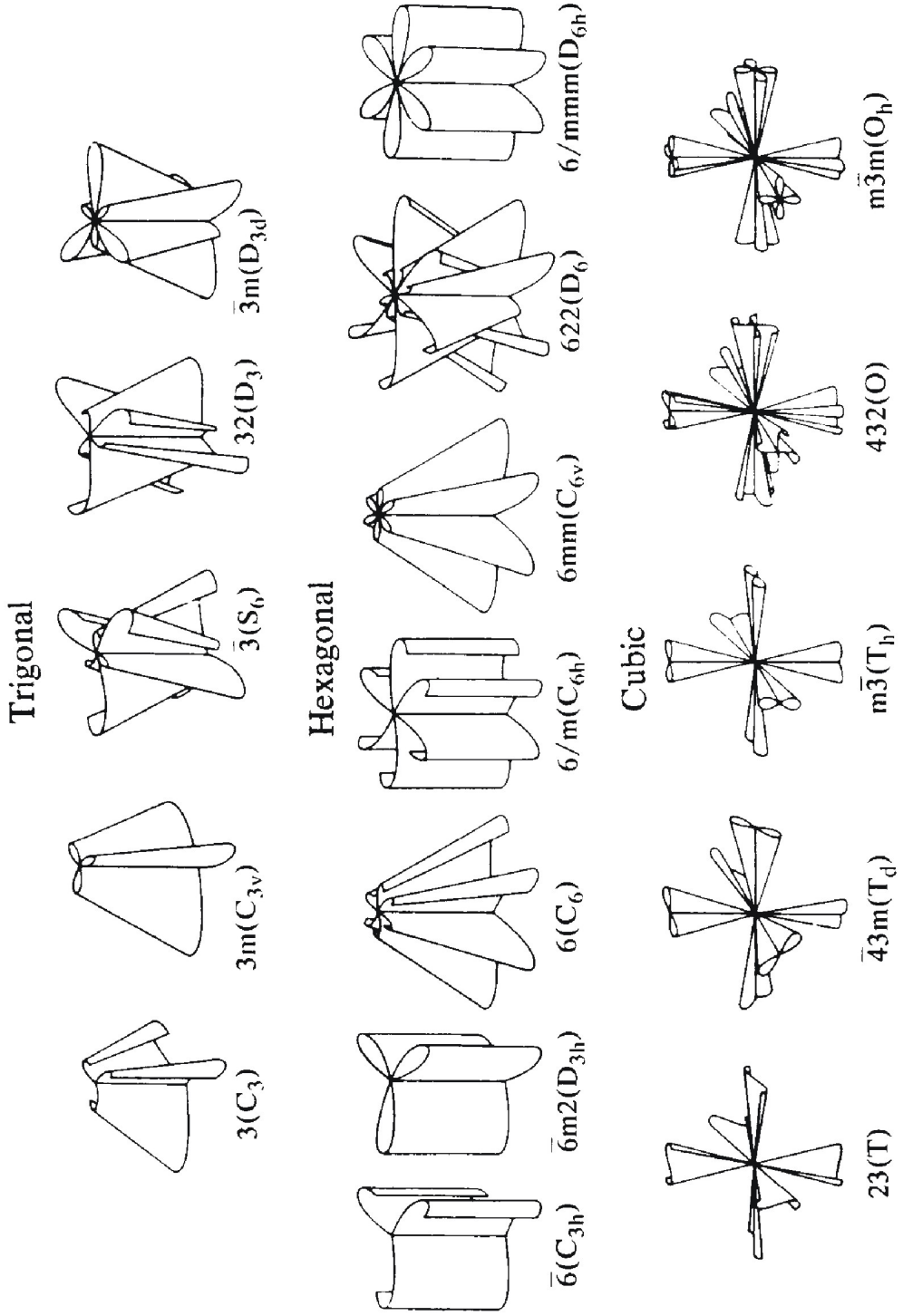

Figure 82: Part 2 of the objects of the 32 point groups

D Some completions for space groups

In this part of appendix D we collect some useful information on notations and conventions.

crystal system	direction of symmetry element		
	primary	secondary	tertiary
triclinic	none		
monoclinic	[010]		
orthorhombic	[100]	[010]	[001]
tetragonal	[001]	[100] / [010]	[110]
hexagonal / trigonal	[001]	[100] / [010]	[120] / [1$\bar{1}$0]
cubic	[100] / [010] / [001]	[111]	[110]

Table 8: Conventions for directions of symmetry elements in the seven crystal systems

We give some more information on conventions and some examples.

Cubic - The secondary symmetry symbol will always be either 3 or $\bar{3}$ (i.e. Ia3, Pm3m, Fd3m)

Tetragonal - The primary symmetry symbol will always be either 4, $\bar{4}$, 4_1, 4_2 or 4_3 (i.e. P$4_1 2_1 2$, 14/m, P4/mcc)

Hexagonal - The primary symmetry symbol will always be a 6, $\bar{6}$, 6_1, 6_2, 6_3, 6_4 or 6_5 (i.e. P6mm, P6_3/mcm)

Trigonal - The primary symmetry symbol will always be a 3, $\bar{3}$, 3_1 or 3_2 (i.e P31m, R3, R3c, P312)

Orthorhombic - All three symbols following the lattice descriptor will be either mirror planes, glide planes, 2-fold rotation or screw axes (i.e. Pnma, Cmc2_1, Pnc2)

Monoclinic - The lattice descriptor will be followed by either a single mirror plane, glide plane, 2-fold rotation or screw axis or an axis/plane symbol (i.e. Cc, P2, P2_1/n)

Triclinic - The lattice descriptor will be followed by either a 1 or a $\bar{1}$.

Textbooks on Nonlinear Optics

G. C. Baldwin. *An Introduction to Nonlinear Optics*. Plenum Press, New York, 1969.

P. N. Butcher and D. Cotter. *The Elements of Nonlinear Optics*. Cambridge University Press, Cambridge, 1991.

N. Bloembergen. *Nonlinear Optics*. Benjamin, New York, 1965.

R. W. Boyd. *Nonlinear Optics*. Academic Press, Boston, 1992.

P. Meystre and M. Sargent III. *Elements of Quantum Optics*. Springer, Berlin/Heidelberg, 1991.

Herbert Rabin and C. L. Tang, editors. *Quantum Electronics, Volume I: Nonlinear Optics*. Academic Press, Inc., 1975.

Y. R. Shen. *The Principles of Nonlinear Optics*. John Wiley & Sons, Inc., 1984.

A. Yariv. *Quantum Electronics*. John Wiley and Sons, New York, 1967.

Frits Zernike and John E. Midwinter. *Applied Nonlinear Optics*. John Wiley & Sons, Inc., 1973.

Index